Coordinated spatiotemporal reorganization of interstitial fluid is required for axial mesendoderm migration in zebrafish gastrulation

by

Karla Huljev

April, 2021

A thesis presented to the
Graduate School
of the
Institute of Science and Technology Austria, Klosterneuburg, Austria
in partial fulfillment of the requirements
for the degree of
Doctor of Philosophy

The dissertation of Karla Huljev, titled *Coordinated spatiotemporal reorganization of interstitial fluid is required for axial mesendoderm migration in zebrafish gastrulation*, is approved by:

Supervisor: Carl-Philipp Heisenberg, IST Austria, Klosterneuburg, Austria

Signature: _____

Committee Member: Eva Benkova, IST Austria, Klosterneuburg, Austria

Signature: _____

Committee Member: Daniel J. Müller, ETH, Zurich, Switzerland

Signature: _____

Exam Chair: Maximilian A. Jösch, IST Austria, Klosterneuburg, Austria

Signature: _____

signed page is on file

IST Austria Thesis, ISSN: 2663-337X
[ISBN: Please contact IST Library library@ist.ac.at if you want to register an ISBN]

I hereby declare that this dissertation is my own work and that it does not contain other people's work without this being so stated; this thesis does not contain my previous work without this being stated, and the bibliography contains all the literature that I used in writing the dissertation.

I declare that this is a true copy of my thesis, including any final revisions, as approved by my thesis committee, and that this thesis has not been submitted for a higher degree to any other university or institution.

I certify that any republication of materials presented in this thesis has been approved by the relevant publishers and co-authors.

Signature: _____

Karla Huljev

May 18, 2021

signed page is on file

Abstract

Accumulation of interstitial fluid (IF) between embryonic cells is a common phenomenon in vertebrate embryogenesis. Unlike other model systems, where these accumulations coalesce into a large central cavity – the blastocoel, in zebrafish, IF is more uniformly distributed between the deep cells (DC) before the onset of gastrulation. This is likely due to the presence of a large extraembryonic structure – the yolk cell (YC) at the position where the blastocoel typically forms in other model organisms. IF has long been speculated to play a role in tissue morphogenesis during embryogenesis, but direct evidence supporting such function is still sparse. Here we show that the relocalization of IF to the interface between the YC and DC/epiblast is critical for axial mesendoderm (ME) cell protrusion formation and migration along this interface, a key process in embryonic axis formation. We further demonstrate that axial ME cell migration and IF relocalization engage in a positive feedback loop, where axial ME migration triggers IF accumulation ahead of the advancing axial ME tissue by mechanically compressing the overlying epiblast cell layer. Upon compression, locally induced flow relocalizes the IF through the porous epiblast tissue resulting in an IF accumulation ahead of the leading axial ME. This IF accumulation, in turn, promotes cell protrusion formation and migration of the leading axial ME cells, thereby facilitating axial ME extension. Our findings reveal a central role of dynamic IF relocalization in orchestrating germ layer morphogenesis during gastrulation.

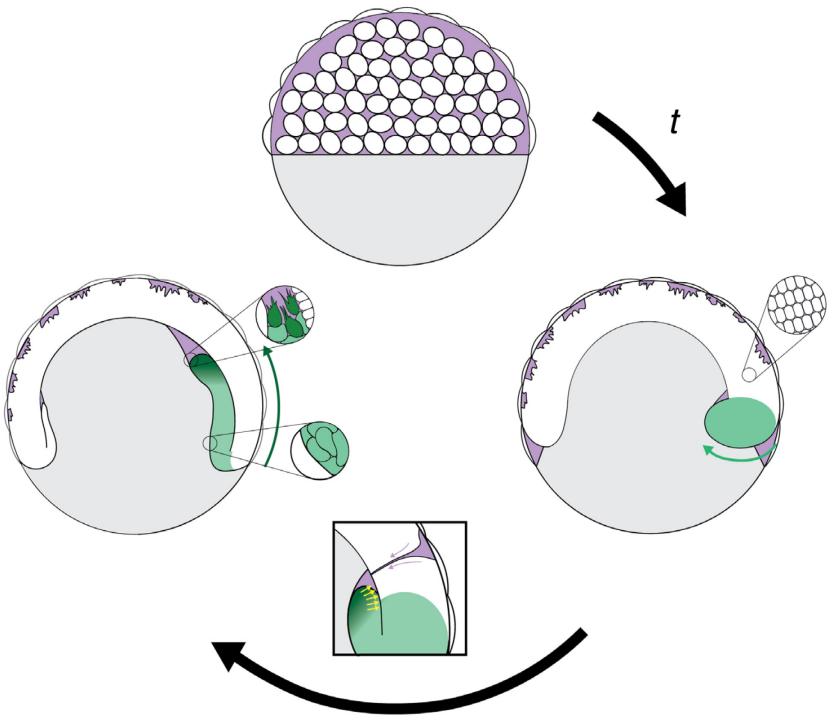

Acknowledgments

I want to acknowledge and thank every amazing person who played an important role in making my PhD journey an exciting and memorable experience. I want to thank my supervisor, CP Heisenberg, for his continuous support and individual approach, which gave me sufficient freedom to explore various directions during my PhD – a mentoring style that has positively resonated with me ever since I joined the group. We hit it off in the “beer hour” as well, and I genuinely had loads of fun during our group activities. I want to thank Eva Benkova, who actively helped and supported me to find my research interest and direction from the beginning of my journey at IST. Eva played an important role by directly teaching and inspiring me to pursue my interest in Developmental biology despite no formal biology training as a Chemical engineering undergraduate. I would like to thank my External advisor, Daniel Müller, for his constructive feedback during Progress review meetings.

During my PhD, I had many opportunities to engage in hands-on practical and theoretical workshops where I had the chance to network and build connections with exceptional scientists who shaped the course of my research. An example of such is a collaboration and friendship with Friedrich Preusser, whom I met at an EMBO imaging workshop and soon after started collaborating on 3D image reconstruction, which is presented in this Thesis. I would also like to thank his supervisor, Stephan Preibisch, for showing enthusiasm and supporting our collaboration, and ensuring fun times during my visit to the BIMSBI, Berlin. I would like to thank Andrea Pauli, who supported my light-sheet imaging endeavors at the IMP, Vienna, as well as for very nice discussions during our joint meetings.

A huge thanks to my collaborators in this study Shiny, Diana, and Alex – you rock! I enjoyed discussing the analysis and doing the experiments with you guys! Along with all the previously mentioned people, I am very grateful to my friends and colleagues in the lab from whom I learned so much and had much fun with: Feyza, Silvia, Ste, Madison, Gayathri, Nikhil, Suyash, Xin, Irene, Koni, Nicoletta, Conny, Peng, Jana, Matt, Michy, Hitoshi, Roland. Big thanks to the Bioimaging and Fish facilities, especially Verena, for her continuous support.

Special thanks to my parents, who always supported me in my adventures. Finally, the enormous THANK YOU goes to Hannes, my boyfriend, for always being there for me – I am so lucky to have you in my life!

About the Author

Karla Huljev completed a BA in Environmental Engineering and an MA in Chemical engineering with honors (*Cum laude*) at the Faculty of Chemical Engineering and Technology, University of Zagreb, Croatia, before joining IST Austria in September 2014. During her PhD studies, Karla has worked on the research project “Coordinated spatiotemporal reorganization of interstitial fluid is required for axial mesendoderm migration in zebrafish gastrulation” in the Heisenberg group at IST Austria. She presented her work in progress at several conferences, such as ISDB Congress, EMBO symposia, and the Gordon Conference. Besides scientific engagements, Karla showed a great interest in communication and leadership by attending numerous personal development workshops and representing the Graduate Student Association (GSA) in 2015 – 2017.

Nulla dies sine linea

(“Not a day without a line”)

Apelles – Greek painter

Table of Contents

List of Figures

List of Abbreviations

AQP	Aquaporin
BCR	Blastocoel roof
BMP	Bone morphogenetic protein
cas	Casanova
CM	Chordamesoderm
cyc	Cyclops
DC	Deep cells
DD	Dorsal determinants
E-Cad	E-Cadherin
ECM	Extracellular matrix
EMT	Epithelial to mesenchymal transition
EVL	Enveloping layer
FGF	Fibroblast growth factor
flh	Floating head
FN	Fibronectin
gsc	Goosecoid
HA	Hyaluronic acid
HGF	Hepatocyte growth factor
ICM	Inner cell mass
ID	Inner diameter
IF	Interstitial fluid
LEM	Leading-edge mesendoderm
MBT	Mid-blastula transition
***MZ*oep**	Maternal/zygotic one-eye-pinhead
N-Cad	N-Cadherin
ndr1/2	Nodal-related-protein 1/2
NTC	Notochord tip cell
ntl	No tail
OD	Outer diameter
oep	One-eye-pinhead
pam	Posterior axial mesendoderm
ppl	Prechordal plate
RGD	Arginine, glycine, aspartic acid peptide
ROI	Region of interest
Shh	Sonic hedgehog
sqt	Squint
TE	Trophectoderm
TRP	Transient receptor potential channel
TST	Tissue surface tension
Vrtn	*Vertebrate development associated transcription repressor*
WMISH	Whole mount in situ hybridization
Xbra	Xenopus Brachyury
YC	Yolk cell
YSL	Yolk syncytial layer
β-cat	Beta catenin

1 INTRODUCTION

1.1 Morphogenesis in development

The big-picture goal of developmental biology is to understand how it is possible that out of a single fertilized cell of few hundreds of micrometers in diameter and simple geometry, do we get animals and plants of various shapes and sizes performing complex biophysical and chemical processes. During early developmental stages, the cells forming the future organism increase in number by cell division and proliferation, they communicate with each other and their environment to acquire diverse cell fates in the process of differentiation, and they undergo a series of morphogenetic events leading to a formation of their final shape. The *emergence* (γενντση- gennisi) *of shape* (μορφη- morphi), or *morphogenesis* is precisely orchestrated by the control of fate, function, and form and it is laid out by a genetically encoded program of development. Via genetic analyses, the central signalling pathways, a small number of which controlling the vast majority of developmental processes, taking part in cell communication and differentiation have been elucidated.

Understanding morphogenesis through genetic approaches only was shown to be tricky as not many known gene-mutations specifically affect shape formation[1]. On the one hand, this might be due to gene regulatory networks often being redundant so that deletion of a single gene can be functionally compensated by the activity of another or by maternally supplied products buffering the phenotype. Apart from a certain level of robustness, a prerequisite for reaching the final form is that all the underlying processes such as cell division orientation, changes in cell shapes, and cell migration occur without interruptions.

On the other hand, the pre-patterned genetic makeup was shown to be dramatically modulated and fine-tuned by mechanical forces resulting in changes in cell size, shape, number, position, and gene expression[2]. These forces, exerted and perceived by the cells and their environment, were demonstrated to act on all scales, from molecular and cellular to the tissue level, spanning the whole organism. When studying the formation of shape, it is therefore critical to consider the developing organism as a whole, with its cellular and extracellular constituents. Biophysical processes during development, through local or global force generation, often result in feedback response following energy conservation laws. In my doctoral thesis, I will discuss one such feedback loop during gastrulation in zebrafish, where force generated by a cluster of cells is required to enable their migration via local interstitial fluid relocalization. These results shed light on the interplay between interstitial fluid dynamics in combination with cell-induced mechanical force generation in controlling large-scale morphogenetic movements required for optimal germ layer positioning in gastrulation – a prerequisite for subsequent development.

1.1.1 Zebrafish embryogenesis

Zebrafish, *Danio rerio*, is a fresh-water fish whose embryonic development occurs externally, surrounded by a medium of very low salinity. Due to its external development, transparency, and rather large size (0.7 mm), zebrafish is an excellent model organism to study morphogenesis. It is accessible to culture the embryos under the microscope for extended imaging of dynamic movements and cellular rearrangements.

During oogenesis, an acellular eggshell, the chorion, forms and surrounds the embryo throughout early development[3]. The chorion contains a funnel-like structure, the micropyle, which allows the sperm entry during fertilization[4] (Fig. 1.1.1.1).

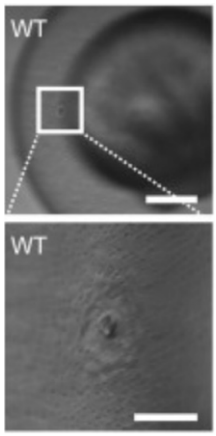

Fig.1.1.1.1 – Zebrafish micropyle morphology and localization in the chorion. Low-magnification (top) and high-magnification bright-field images (bottom) of the micropyle region (boxed area at the top) within the chorion of an embryo. Scale bars, 200 μm (top) and 50 μm (bottom). From[5]

Before fertilization, the embryo is already intrinsically asymmetric, although it is essentially a mixture of cytoplasm and yolk. Upon fertilization, this asymmetry amplifies in the process of cytoplasmic streaming, where bulk actin polymerization wave accumulates the cytoplasm at the animal pole and concentrates the yolk at the vegetal pole, defining the animal-vegetal or future anterior-posterior axis of the embryo[6,7] (Fig. 1.1.1.2).

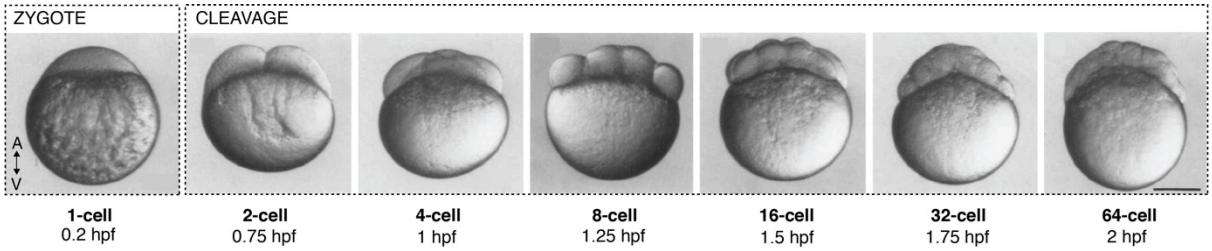

Fig.1.1.1.2 – Early stages of zebrafish embryonic development. The zygote period: One-cell stage embryo within the elevated chorion, few minutes after fertilization. Yolk-free cytoplasm has begun to segregate to the animal pole by a process of cytoplasmic streaming. A-V (animal-vegetal axis). The cleavage period: Two-cell stage (0.75 hours post fertilization, hpf), Four-cell stage (1 hpf), Eight-cell stage (1.25 hpf), Sixteen-cell stage (1.5 hpf), Thirty-two cell cell stage (1.75 hpf), and Sixty-four cell stage (2 hpf). Marginal blastomeres are continuous with the yolk cell due to incomplete (meroblastic) cleavages. Scale bar = 250 pm. Adapted from[7]

The first cleavages are synchronous, with a 15-minute period, and occur only in the cytoplasmic domain at the animal pole, the blastoderm, while the yolk cell (YC) never divides. The cleavages are planar and incomplete or meroblastic, leaving the early blastomeres continuous with the YC via cytoplasmic bridges[8] (Fig. 1.1.2). At the 16-cell stage, the four central blastomeres enclose entirely, while the marginal cells remain continuous with the YC. From the 32- to the 64-cell stage, there is a change in cleavage plane, and the embryo is now composed of two tiers of blastomeres, the inner ones referred to as deep cells (DC) and surface ones the enveloping layer (EVL)[7] (Fig. 1.1.1.3). At this stage, the surface cells display epithelial polarization, and under their basolateral sides, the first interstitial fluid (IF) pockets can be seen, characterized for the first time in this study (*discussed in **4 Results** section of this thesis*).

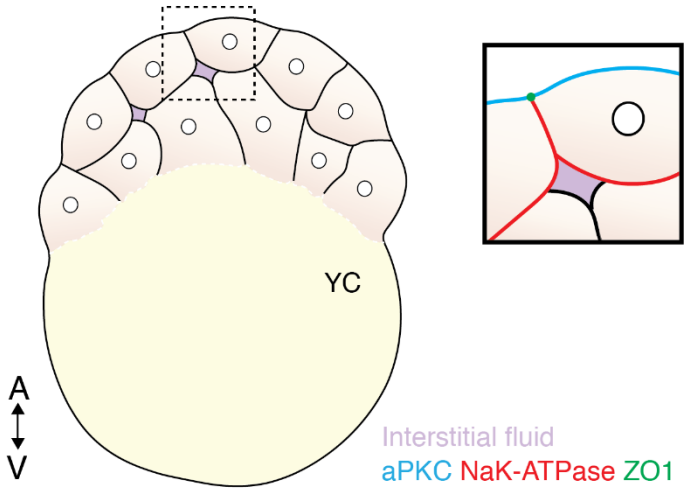

Fig.1.1.1.3 – The onset of interstitial fluid accumulation in the 64-cell stage zebrafish embryo. Schematic illustrating a cross-section through a 64-cell stage zebrafish embryo, highlighting the onset of interstitial fluid (purple) accumulation between the blastomeres and epithelial polarization of the surface cells. A-V (animal-vegetal axis), yolk cell (YC).

After the 128-cell stage, the embryo is considered a blastula, or more appropriately "stereoblastula," due to the absence of the central fluid-filled cavity, the blastocoel, and the presence of the large YC at the position of the blastocoel in other "non-yolky" vertebrate embryos[7] (*discussed in **1.2** section of this thesis*). Unlike, e.g., mouse blastula, which is permeable to the outside medium until the maturation of tight junctions, the zebrafish embryo is already sealed off early on with the expression of tight junction components ZO-1 and ZO-3 at surface cell-cell junctions at 8- and 64-cell stage, respectively[9,10]. In the fish, junctions are impermeable to small molecular tracers, as seen from the exclusion of interstitial fluid labelling when bathed in the tracer-containing medium throughout the entire early development[10]. It comes as no surprise, knowing that the zebrafish medium is of very low salinity and could potentially induce cell swelling if it would freely perfuse the DCs, unlike the isotonic oviduct fluids in the mouse[11].

During the 512-cell stage, the zygotic gene transcription starts, which marks the mid-blastula transition (MBT). Concomitantly, cell cycles lengthen and lose their synchrony[12]. This is also the stage during which the yolk syncytial layer (YSL) forms.

It was proposed that the YSL forms due to most marginal EVL cells fusing with the yolk cell and giving their nuclei and cytosol into the syncytium[13,14]. The YSL plays an essential role during gastrulation, where it induces the specification of germ layers by secreting Nodal ligands[13].

At about 4 hpf, the embryo resembles a perfect sphere with the blastoderm or the embryo-proper on the upper hemisphere and the YC on the lower hemisphere (Fig. 1.1.1.4). From this point on, the embryo undergoes large-scale morphogenetic changes, which eventually establish the dorsoventral axis.

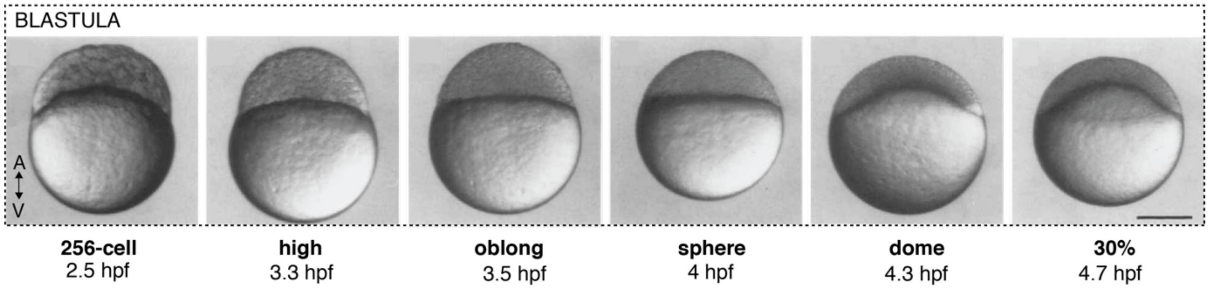

Fig.1.1.1.4 – Zebrafish embryonic development during the blastula period. 256-cell stage (2.5 hpf), high stage (3.3 hpf), transition between the high and oblong stages (3.5 h), transition between the oblong and sphere stages (3.8 hpf). Onset of morphogenesis: dome stage (4.3 h), 30%-epiboly stage (4.7 h). A-V (animal-vegetal axis). Scale bar = 250 pm. Adapted from[7]

The first of the morphogenetic movements is the epiboly or spreading of the blastoderm towards the vegetal pole, engulfing the YC[15]. In parallel with the epiboly movements, the DC radially intercalate, thinning the blastoderm and generating a characteristic dome-like shape of the blastoderm-YC interface at the onset of morphogenesis[16,17] (Fig. 1.1.1.4). It was demonstrated that the formation of this characteristic dome shape results from the release in EVL surface tension by unbalancing the forces at the blastoderm-YC contact line[17]. Moreover, the different blastoderm thinning rates between the central and marginal tissue can be explained through mitotic cell rounding-dependent cell-cell contact disassembly within the central blastoderm, leading to local tissue fluidization. Within the marginal tissue, this phenomenon is disabled due to non-canonical Wnt signalling that locally increases cell cohesion[18]. The following developmental staging reflects the rate of epiboly progression. Therefore, as the spreading has reached the equator, at 50% epiboly, it marks the onset of gastrulation[7] (Fig. 1.1.2.1).

1.1.2 Zebrafish gastrulation

Up until this point, the fate and morphology of the DC were seemingly uniform within the multi-layered blastoderm. During gastrulation, the DCs differentiate and give rise to three distinct germ layers: (1) **ectoderm** – forming the epidermis and nervous system, (2) **mesoderm** – giving rise to muscle, connective tissue, bone, urogenital and circulatory systems, and (3) **endoderm** – forming the gastrointestinal tract. Gastrulation is controlled by key signalling pathways (Nodal, Wnt) and large-scale cell rearrangements, which ensure proper positioning of the germ layers and give rise to

the body plan of the future animal.

Gastrulation starts with the internalization of mesoderm and endoderm (mesendoderm) progenitors at the germ ring margin, specifically pronounced at the dorsal side of the gastrula, defining the dorsoventral axis[7,19] (Fig. 1.1.5). The thickening of the dorsal margin, known as the embryonic shield in zebrafish, serves as the organizer known to induce differentiation of distinct germ layer progenitors and is analogous in function to the Hansen`s node in avian and Spemann-Mangold`s organizer in amphibian embryos[20].

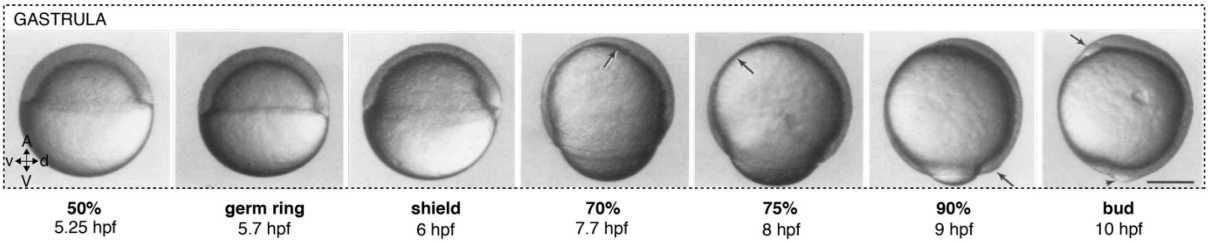

Fig.1.1.2.1 – Zebrafish embryonic development during the gastrula period. Lateral view of the embryo at the onset of gastrulation. 50%-epiboly (5.25 hpf), germ ring (5.7 hpf), shield stage (6 hpf), 70%-epiboly stage (7.7 hpf) highlighting the prechordal plate, ppl (arrow), 75%-epiboly stage (8 hpf) highlighting the thin evacuation zone on the ventral side (arrow), 90%-epiboly stage (9 hpf) highlighting the tail bud (arrow) and bud stage (10 hpf) highlighting the polster (arrow) and the tail bud (arrowhead). A-V (animal-vegetal axis), v-d (dorsoventral axis). Scale bar = 250 pm. Adapted from[7]

Once internalized, axial mesendoderm progenitors on the dorsal side migrate away from the germ ring margin towards the animal pole, confined between the YC and the overlying DCs/epiblast, and together with the lateral progenitors eventually converge to the dorsal side[7,19,21,22]. Cells on the ventral side, soon after internalization, change direction and move vegetally, eventually ending up in the tail region[7]. During this migration, mesendoderm progenitors further differentiate into the mesoderm and endoderm and exhibit distinct cell motility modes. Unlike endodermal cells, which initially display random motion, mesodermal cells migrate directly towards the animal pole[19,21,23]. At about 70% epiboly, DCs initiate convergence to the dorsal side, narrowing of the embryo and lengthening of the body axis. The anterior-posterior axis further extends by cells squeezing between each other via mediolateral intercalations[19,24,25]. The gastrulation has completed as the blastoderm had entirely engulfed the YC (100% epiboly), germ layers had specified and correctly positioned – visible by the correct position of head and tail structures at this stage[7].

1.1.2.1 Germ layer specification

As hinted in the previous chapter, germ layer specification is associated with establishing the dorsoventral axis of the future animal. Interestingly, this asymmetry dates back to the early cleavages, when dorsal determinants (DD), namely components of the canonical Wnt signalling pathway, are differentially distributed by microtubules marking the future dorsal side of the embryo[26,27] (Fig. 1.1.2.1.1). Following DD relocalization, ventralizing agents, namely members of the Bone morphogenetic protein family (BMPs), accumulate to ventrolateral regions of the

embryo. Their activity is counteracted in the region by the BMP regulator *Vertebrate development associated transcription repressor* (Vrtn), shaping the prospective ventralizing BMP gradient[28].

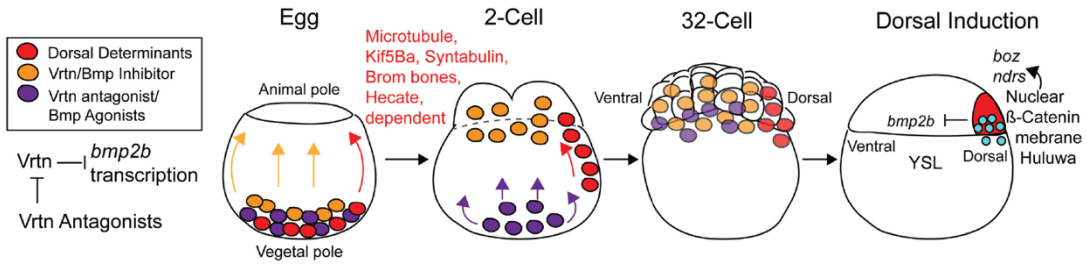

Fig.1.1.2.1.1 – Maternal factors in dorsal-ventral axis determination. Maternally deposited dorsal determinants (DD), ventral agonists and inhibitors reside at the vegetal pole of the unactivated zebrafish egg. Upon egg activation, DDs and Bmp regulator Vrtn move to the animal pole (AP) in a microtubule dependant manner. The antagonists of Vrtn (Bmp agonists) are translocated to the AP with a delay and together with Vrtn they shape the bmp2b expression domain. From[29]

As DDs reach the prospective dorsal side, they promote shield formation, as seen by nuclear β-Catenin (β-cat) accumulation and membrane localization of Huluwa protein at the dorsal side[30,31]. This leads to the activation of dorsal-specific genes, *bozozok* and Nodal-related proteins 1/2, kick-starting the Nodal signalling pathway, essential for mesendoderm specification and subsequent patterning[32,33]. Additionally, Nodal signalling also induces dorsal expression of BMP antagonists, such as Chordin, sinking the BMP gradient dorsally[34]. This is how the dorsal organizer, the shield, ensures dorsal identity, prechordal plate and axial mesoderm differentiation in the ventralizing environment dominated by the BMPs[29,35–38].

1.1.2.1.1 Mesendoderm patterning

Mesendoderm patterning in zebrafish is induced by Nodal/TGF-β ligands, specifically Ndr1 (Squint, Sqt) and Ndr2 (Cyclops, Cyc)[32,33,39]. Additional TGF-β ligand, Growth differentiation factor 3 (Gdf3/Dvr1/Vg1) was shown to be associated with the Nodal ligands and essential for mesendoderm specification[40–42]. Nodal signals are perceived through a triple receptor complex, Activin type I and II receptors and the One-Eyed-Pinhead (Oep) co-receptor[33]. Activation of the receptor complex triggers Smad2/3 phosphorylation and association with Smad4, leading to induction of target gene expression such as Goosecoid (Gsc) and No tail (Ntl) – required for mesoderm and Casanova (Cas/Sox32) – for endoderm specification[43–46].

Nodal ligands are thought to function as morphogens, molecules that are able to induce cell fate specification in a dose-dependent manner. For instance, low levels of Nodal signaling were shown to induce the expression of notochord-inducing genes like Ntl and Floating head (Flh), while higher doses induce endoderm and anterior axial mesendoderm (prechordal plate, *ppl*) genes like Sox32 and Goosecoid (Gsc)[47–50]. Additionally, extended Nodal signalling favours *ppl* specification on the expense of endoderm cells[51].

Furthermore, Nodal signalling can induce the expression of Nodal ligands themselves, as well as their inhibitors Lefty1/2[52,53] (Fig. 1.1.2.1.1.1A). Following that concept, it was proposed that the Nodal signalling domain is established by a reaction-diffusion system, where an activator-inhibitor pair with differential diffusivity can give rise to pattern formation[52,54–56]. In favour of this mechanism, it was demonstrated that Nodal, secreted from a localized source, can activate the expression of target genes in the surrounding tissue, while the expression of Lefty limits its range[54,55,57]. As for their reach, it was shown that Ndr2 displays lower diffusivity than Ndr1, while Lefty1/2 diffuses faster than both Nodal ligands[56].

An additional mechanism, where Nodal ligands activate their expression in the neighboring cells, the so-called relay-based mechanism, was shown to contribute to the expansion of the Nodal signalling domain. It was shown that the secretion of Ndr1/2 from the YSL promotes Nodal signalling in the marginal blastomeres[58,59] (Fig. 1.1.2.1.1.B). As Nodals and Leftys are co-expressed in cells with active Nodal signalling, it was proposed that the expression of a microRNA miR-430 transiently delays Nodal-induced Lefty1/2 production, thereby delaying the inhibitory effect and, together with the relay-based mechanism, predicts the size of the Nodal signalling domain[60]. However, Lefty1/2 double mutants do not show a dramatic expansion of the Nodal signalling domain[61].

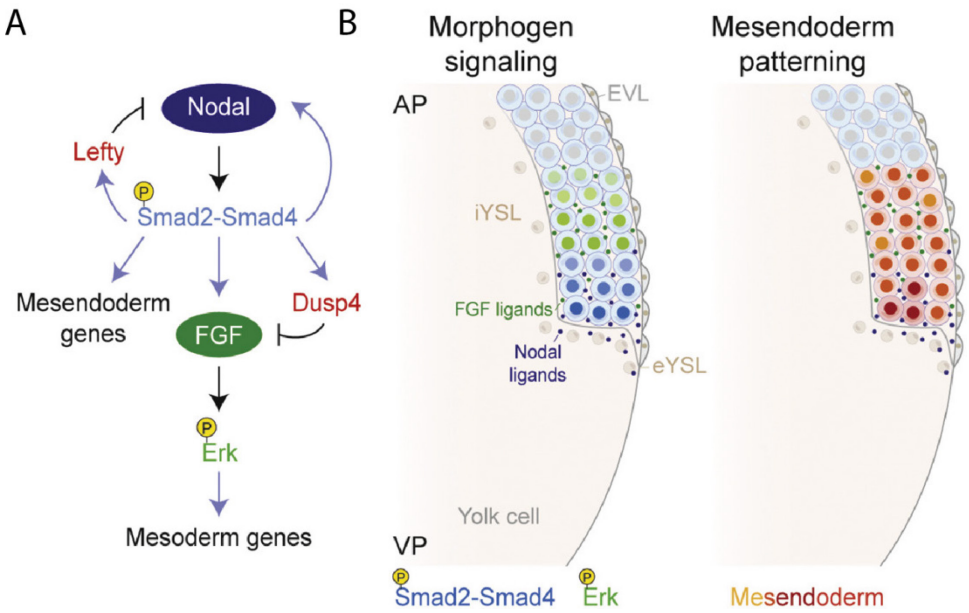

Fig.1.1.2.1.1.1 – Mesendoderm induction and patterning in zebrafish embryos. (**A**) Schamatic diagram highlighting the main signaling pathway responsible for mesendoderm cell fate specification in zebrafish gastrulation. Nodal signaling starts by interaction of Nodal ligands with its receptors which triggers a cascade of events leading to Smad2 phosphorilation and association with Smad4. Activated Smad2/4 complexes accumulate in the nucleus, where they interact with other transcription factors to induce transcription of Nodal and FGF ligands, as well as inducing genes directly implicated in mesendodermal cell specification (e.g. Gsc, Sox32). Nodal activity is regulated by Lefty1/2 antagonists. FGF signaling is established at a distance from the germ ring margin, due to the short-range activity of its inhibitor Dusp4. Upon FGF activation, phosphorylated Erk (P-Erk) results in expression of mesodermal genes. (**B**) Schematic illustrating a cross-section of a zebrafish embryo at 50% epiboly highlighting the Nodal and FGF signaling gradients and resulting mesendoderm patterning. Nodal

signaling (nuclear accumulation of P-Smad2, blue) near the margin. FGF signaling (nuclear accumulation of P-Erk, green) further away from the margin. AP (animal pole), VP (vegetal pole), D (dorsal side), V (ventral side), EVL (enveloping layer), YSL (yolk syncytial layer, *i* internal, *e* external. From[43]

Moreover, the findings that FGF signalling can activate Nodal target genes beyond the Nodal signalling domain suggest a secondary relay-mechanism with a longer range[45,62–64]. In line with this, Nodal was shown to induce the expression of Fgf8/3 ligands, which were able to induce the expression of Ntl further away from the germ margin[65] (Fig. 1.1.2.1.1.1.A-B). On the other hand, Nodal can also limit short-range FGF signalling by inducing the expression of the FGF inhibitor Dusp4, which could potentially affect the scope of mesendoderm segregation[62] (Fig. 1.1.2.1.1.1.A-B).

Taken together, differential diffusivity of Nodal/Lefty pair, long-range FGF signalling, and auto-regulation are all likely to cooperate to establish the correct Nodal signalling gradient at the dorsal margin of the blastoderm.

1.1.2.1.2 Ectoderm specification

The ectoderm specification is thought to be a default cell fate as the absence or reduction in Nodal signalling results in the expansion of the ectoderm domain[33,66–68]. Interestingly, although initially all the cells have the capacity to respond to Nodal signalling and specify mesendoderm-like cell fates, prospective ectoderm cells lose this competence over time by progressively downregulating the *Oep* co-receptor during gastrulation, as shown recently[69,70]. However, overexpression of *Oep* does not render the cells irresponsive to Nodal, suggesting a need for an additional mechanism for ectoderm specification[70].

1.1.2.2 Mesendoderm internalization cues

The onset of internalization marks the beginning of gastrulation in zebrafish, coinciding with the first cell fate specification and the onset of cell motility. Together with positioning the tissues in the interior of the embryo, internalization also entails the animal-pole-directed migration required for arranging distinct domains within the developing embryo. How internalization is initiated, which molecular or mechanical factors tune, direct and enable the underlying cell migration are some of the key open questions in the study of morphogenesis in development. As they internalize, mesendoderm progenitors move over the margin, below the non-internalizing ectoderm cells, to find their way towards the interior of the embryo. The mode of internalization is zebrafish is referred to as “synchronized cell ingression”, accounting for the possibility of single cell ingression but taking into account the cohesion and coordination between the internalizing progenitors[19,43,71–73]. At the dorsal side, for instance, the mesendoderm cells internalize as a compact tissue, unlike the ventrolateral progenitors which exhibits rather low cohesion while still maintaining coordination during internalization.

What triggers and guides the onset of internalization is still an open question. Mesendoderm cells innately tend to internalize and reach the surface of the yolk cell despite the margin, as seen from the animal pole transplants recapitulating the same behavior[73]. It was first proposed that the difference in tissue surface tension (TST) between distinct progenitor cell types could drive the cell sorting process and thereby accordingly position the germ layers. Although differential TST was sufficient to drive progenitor cell sorting *in vitro*, *in vivo* it did not display a significant role[74–79]. A more likely hypothesis for driving germ layer segregation is the directed migration of mesendoderm progenitors. In line with this, affecting the protrusion formation via Arp2/3 or Rac inhibition was shown to impair mesendoderm internalization[78,80,81].

The contribution of Nodal signalling in this process is thought to be rather permissive and not instructive, since inhibition on Nodal signalling at shield stage does not impact mesendoderm specification nor internalization, arguing that it likely plays a role in setting the stage before the onset of gastrulation[50,81]. However, Nodal signalling promotes cell-cell contact formation by inducing and regulating the expression of adhesion receptors or upregulating contractility, suggesting that it might contribute to driving internalization indirectly by controlling the cell-cell contact formation[75,76,80,82,83]. Nevertheless, downregulation of E-Cad in transplants and N-Cad mutants did not exhibit internalization defects[80,84,85]. The possibility that distinct levels of cell-cell adhesion coordinate internalization dynamics and tune the cell polarization remains to be experimentally tested[43].

As internalizing cells exert polarized protrusions towards the YSL/YC surface, some signals originating from the YSL likely attract the cells towards the interior. However, YSL RNAse injections did not affect the internalization of induced endoderm transplants, suggesting that YSL does not directly polarize the internalizing cells, or maybe the attractant is not encoded by mRNAs[43,80]. The other extraembryonic tissue, the EVL, might also play a role, for instance, in limiting the protrusive activity and therefore directing protrusions towards the YSL/YC[43].

1.1.2.3 Animal pole-directed migration

Once internalized on the dorsal side, axial mesendoderm progenitors continuously migrate away from the germ ring margin towards the animal pole, confined between the YC and the overlying DCs/epiblast, and together with the lateral progenitors eventually converge to the dorsal side[7,19,21,22] (Fig.1.1.2.3.1). Cells on the ventral side, soon after internalization, change direction and move vegetally, eventually ending up in the tail region[7].

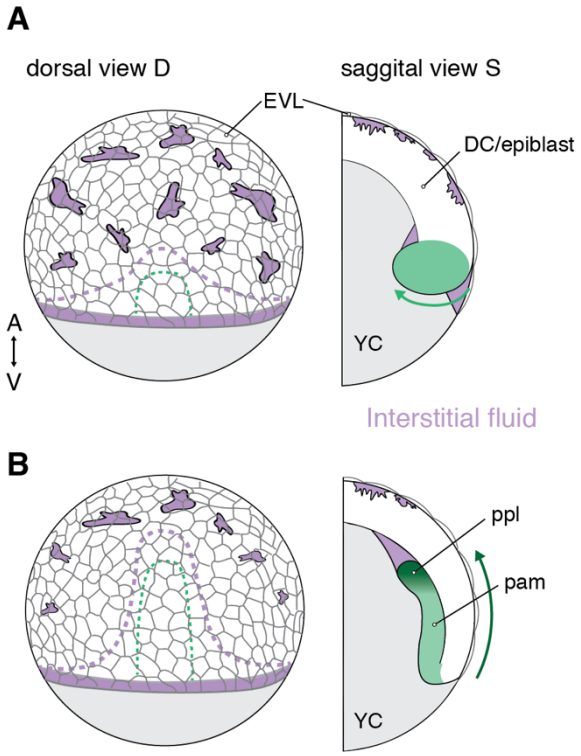

Fig.1.1.2.3.1 – Axial mesendoderm internalization and animal pole-directed migration. (**A**) Schamatic illustrating the internalization of axial mesendoderm at the dorsal side of the zebrafish gastrula (light green arrow). (**B**) Animal pole-directed migration of axial mesendoderm (dark green arrow). Animal-vegetal axis (A-V), enveloping layer (EVL), deep cells (DC), yolk cell (YC), prechordal plate (ppl), posterior axial mesendoderm (pam).

As different mesendoderm progenitors display different migratory trends, they are likely to be driven by distinct underlying mechanisms. The ventrolateral mesendoderm progenitors migrate towards the animal pole during early stages of gastrulation as a non-confluent monolayer[19,86]. It was shown that a secreted peptide, Toddler (Apela/Elabela), promotes their motility, but how it regulates mesendoderm migration remains unclear[23,86,87].

Unlike the ventrolateral, dorsal mesendoderm progenitors migrate towards the animal pole as a cohesive, multicell-layered structure, composed of the leader anterior axial mesendoderm (prechordal plate, *ppl*), the notochord tip cells (NTCs), and the trailing posterior axial mesendoderm (notochord, *pam*)[19,20,22,88]. In zebrafish, *ppl* cells remain cohesive and migrate as a cluster of mesenchymal cells displaying uniform, animal-pole directed cell polarization and directed motion, suggesting that these cells are actively migrating towards the animal pole[19,21,89]. Their motion displays collective cell migration traits since E-Cad mediated cell-cell contacts are required for protrusion orientation and coordination between the neighboring cells[20,21,89].

The initial hint for the signalling pathways involved in dorsal mesendoderm migration came from the non-canonical Wnt signaling characterization[90]. It was shown that Wnt/PCP ligand mutants, *wnt11/silberblick*, as well as receptor Frizzled 7 mutants, *fz7*

display slower and less directed *ppl* migration[90–92]. However, uniform Wnt11 overexpression was shown to rescue the *ppl* migration in *wnt11* mutants[90]. Additionally, light-induced uniform activation of Fz7 rescued the phenotype *fz7* mutants[91]. These obeservations suggest that Wnt/PCP signalling is likely to function permissively rather than instructivly enabling *ppl* migration.

Although ECM components play a critical role in guiding *ppl* migration during frog gastrulation, in zebrafish, this does not seem to be the case as there is little or non of it deposited during early *ppl* migration[89,93,94]. Additionally, interfering with Integrin α5 showed no significant effect on *ppl* migration[95].

Recently, downregulation of a Torc2 component Sin1 was shown to affect both directionality and speed of the *ppl* cell, opening a possibility that the Torc2 complex is the key regulator[96].

As the *ppl* migrates towards the animal pole, it was shown to exert friction forces onto the overlying DC/epiblast (ectoderm), thereby positioning the neural anlage[89]. Apart from friction forces, we characterized additional mechanical interactions of the *ppl* with the overlying DCs. Following that idea, in this **Thesis**, we will discuss a potential feedback mechanism between *ppl* induced interstitial fluid relocalization and its requirement for proper cell polarization and migration, shedding light on a yet functionally unknown player in gastrulation movements – the interstitial fluid.

1.2 Interstitial fluid accumulations in embryonic development

It is of great importance to observe the developing organism as a system, shaped by a multilevel control arising from the pre-set genetic canvas, finely tuned and orchestrated by the physical and chemical cues ensuring optimal development. An ever-present and often unacknowledged interface within the developing organism is the extracellular or interstitial fluid that baths cells, tissues, and organs, so it comes as no surprise to speculate about its role in orchestrating developmental processes.

1.2.1 The impact of blastocoel in gastrulation

Interstitial fluid accumulations, namely the blastocoel, have long been thought to play a critical role in gastrulation movements across different species where the onset of gastrulation occurs either within the blastocoel or around it, as seen in, e.g., avian and amphibian embryos, respectively. In the following chapters, we will review a few such examples. Additionally, we will discuss the structural relevance and the evolutionary loss of yolk in amniote embryos, speculating a functional compensation by the evolution of the blastocyst.

1.2.1.1 Amphibian gastrulation – internalization around the blastocoel

Like zebrafish, the frog egg also contains a large amount of yolk concentrated at one pole (vegetal hemisphere) as opposed to the animal hemisphere that contains the nucleus and the majority of the cytoplasm. Unlike in zebrafish, the cleavages are holoblastic or complete and unequal already after the second round[97]. The initiation of blastocoel formation dates to the first cleavage in the Xenopus embryo, where the widening of the cleavage furrow creates an initial cavity sealed off by the tight junctions[98] (Fig. 1.2.1.1.1).

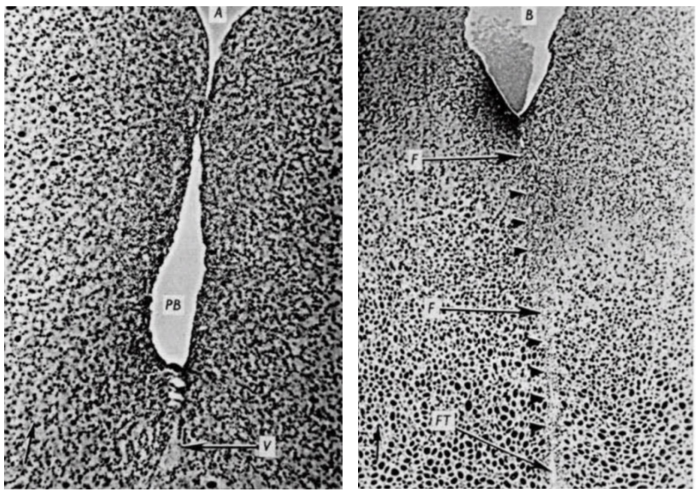

Fig.1.2.1.1.1 – Blastocoel origin in Xenopus embryos. (*Left*) Brightfield phase micrograph of the animal pole (A) furrow 90' after fertilization. The presumptive blastocoel cavity (PB) has been formed by the closing of the furrow. Several vacuoles (V) are seen beneath the furrow tip. Magnification 250x. (*Right*) Brightfield phase micrograph of the lower animal pole furrow region 60' after fertilization. The furrow (F) extends from the floor of the blastocoel (B) The furrow is indicated by arrowheads. Magnification 250x. From[98]

At the third cleavage (8-cell stage embryo), the central cavity formation at the animal hemisphere can be clearly seen[99] (Fig.1.2.1.1.2). This cavity is slightly upward-shifted from the equatorial plane of the embryo due to the presence of a larger cytoplasmic domain in that region and to relatively less yolk, which generally resists the cleavage forces[97].

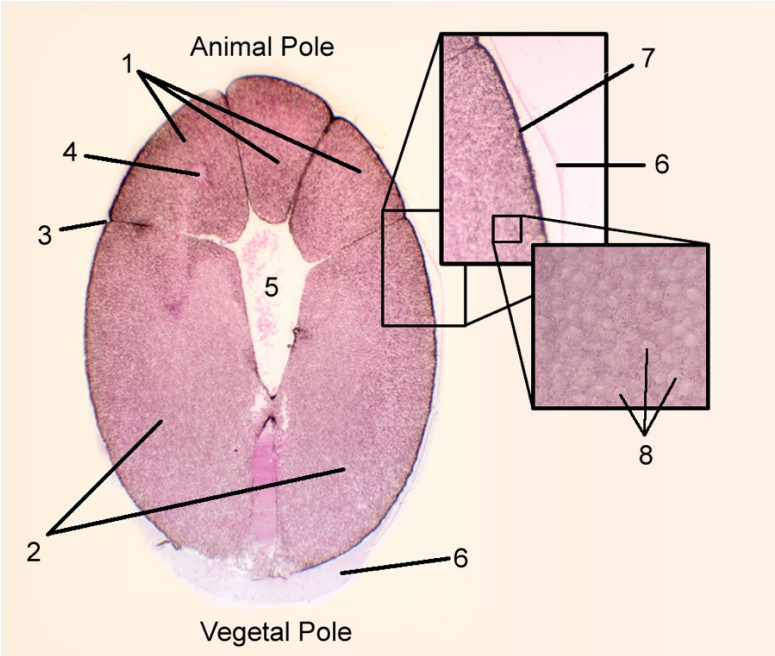

Fig.1.2.1.1.2 – Xenopus embryo morphology at the 8-cell stage. (1) micromeres at the animal hemisphere (2) macromeres at the vegetal hemisphere with evident cleavage furrows (3) (4) nucleus (5) blastocoel (6) fertilization envelope (7) cortical pigment (8) yolk composition - golgi-derived yolk platelets. From[99]

With each of the early cleavages, the cavity is enlarged, and at the early gastrula stage, the embryo is about 20% larger than at the early blastula stage[100] (Fig. 1.2.1.1.3).

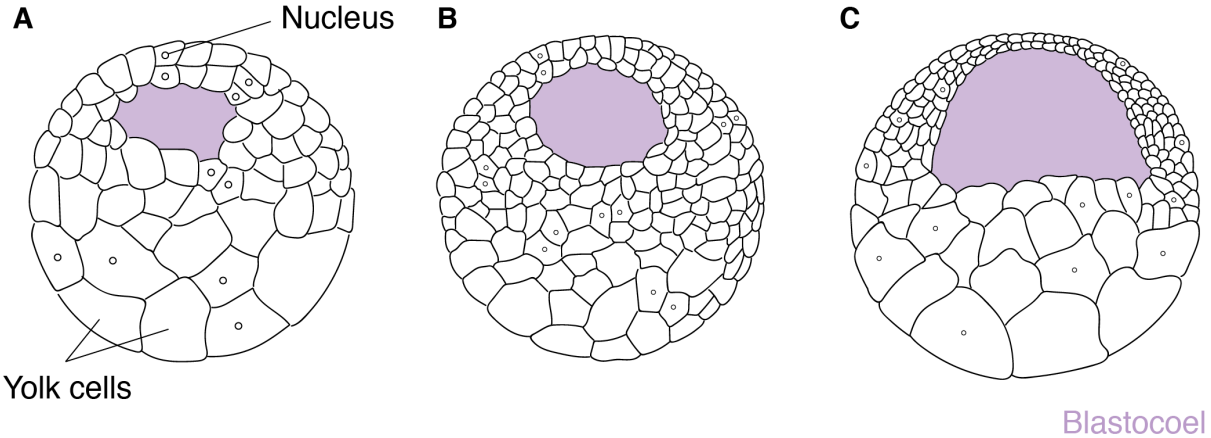

Fig.1.2.1.1.3 – The blastocoel expansion in frog embryos. (A) Early blastula (B) midblastula (C) late blastula. Adapted from[97]

The blastocoel is filled with protein- and polysaccharide-rich fluid, such as the hyaluronic acid (HA), arising from the surrounding cells[97,101–104], and it contains common extracellular ions $[Na^+]_B$ 101,8±10,2 mM, $[K^+]_B$ 3,7 ± 0,8 mM, $[Ca^{2+}]_B$ 1,40 ±

0,51 mM and $[Cl^-]_B$ 61,2 ± 9,9 mM, as measured in the Xenopus and Axolotl embryos during blastula and early gastrula stages with the interstitial pH in the range of 8,42 ± 0,22[105].

The blastocoel will remain in its position beneath the animal hemisphere until it is later displaced by the development of other cavities. Prior to gastrulation, the blastocoel wall consists of an epithelial sheet surrounding several layers of inner cells. It forms a thin blastocoel roof (BCR) in the animal hemisphere (ectoderm), a middle marginal zone with an intermediate thickness (mesoderm), with a portion of cells at the vegetal hemisphere (endoderm)[106–108].

At the onset of Xenopus gastrulation, a few surface cells, called bottle cells, move into the interior of the embryo, followed by the mesendoderm cells[109]. On the dorsal side, the mesoderm is composed of the Xenopus Brachyury (Xbra) expressing chordamesoderm (CM), the Goosecoid (Gsc) expressing prechordal mesoderm (PCM), and the Xhex expressing leading-edge mesendoderm (LEM)[110,111] (Fig.1.2.1.1.4). Shortly after initial involution, a slit-like spacing forms between the mesendoderm and ectoderm, continuous with the blastocoel, and is referred to as the gastrular slit or the Brachet's cleft[112] (Fig.1.2.1.1.4).

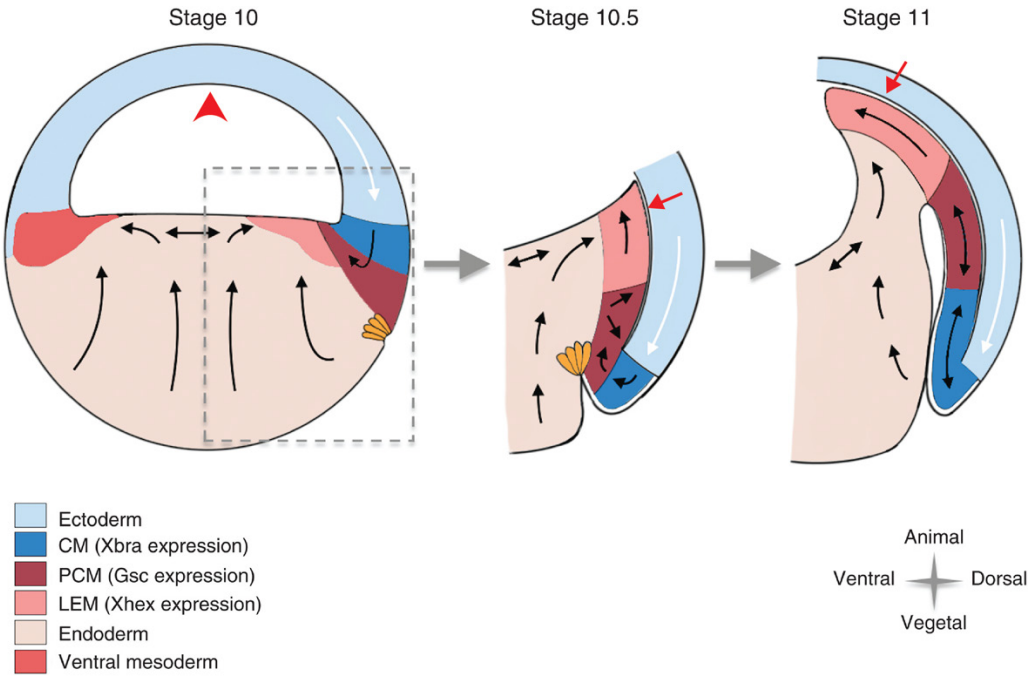

Fig.1.2.1.1.4 – Positioning of the tissues during Xenopus gastrulation. Schematic illustrating the embryo at the onset of gastrulation (stage 10), at early (stage 10.5) and middle stage of gastrulation (stage 11). Active cell movement (black arrows), passive cell movement (white arrows), blastocoel roof (BCR, ectoderm) (red arrowhead), Brachet`s cleft (red arrow), bottle cells (orange), leading edge mesendoderm (LEM), prechordal mesoderm (PCM), chordamesoderm (CM). Adapted from[108]

The anterior and posterior parts of the cleft are formed by distinct morphogenetic processes. The former is generated by the movement of endodermal cells towards the BCR before the formation of the blastopore and the latter by the involution of the

mesoderm through the dorsal blastopore lip[113]. Maintenance of Brachet's cleft requires two distinct cellular processes, the separation behavior of the involuting mesendoderm and repulsion behavior of the presumptive ectoderm, which prevent mixing of mesendoderm with the differentiating ectodermal cells. To discriminate between these two processes, BCR assay, where the cells of distinct tissue types are tested for separation and repulsion behavior, can be used[112]. The BCR assay revealed that endoderm cell aggregates display separation behavior already at the blastula stage, while the dorsal mesoderm acquires this capacity only at gastrula stages, during involution. In parallel, ectodermal animal cap cells develop the capacity for repulsion behavior[114]. In order to understand what determines the tissue separation at the Brachet's cleft, several scenarios were considered, amongst which the impact of cell adhesion molecules[115,116], Rho signalling pathway[117], ectopic induction of mesendoderm cell fate specification factors[114,118], as well as the Eph/Ephrin signalling in generating adhesion and repulsion cycles in mesodermal cell aggregates when they are in contact with ectodermal BCR substrate[119,120].

Brachet's cleft and the whole BCR are lined with the components of the extracellular matrix (ECM), especially fibronectin (FN). It was proposed that the interaction of mesendodermal cells with the FN matrix is necessary for the formation of lamellipodia-like protrusions in mesoderm cells, enabling them to migrate towards the animal pole[121]. Nevertheless, involution and gastrulation still proceed in the presence of FN inhibitors arguing for additional factors apart from FN. This migration can be blocked by an RGD (arginine, glycine, aspartic acid) peptide which competes with FN for interaction with the cellular integrin receptors that facilitate cell migration. However, even in the presence of RGD peptide, tissue separation at the Brachet's cleft was not affected[112,122–124].

The early studies sought to address the relevance of the Xenopus blastocoel in gastrulation movements. Specifically, a study tested if the puncture of the blastocoel and complete removal of the BCR, which thereby eliminates the pressure within the blastocoel and exposes the deep cells to the external media, affect morphogenetic processes during gastrulation[125]. They found that both perturbations did not significantly affect the rate of blastopore closure. Interestingly, they also found that convergence and extension of axial mesoderm, which occurs by cell intercalation, was largely independent of the BCR. In contrast, removing the BCR, the substrate of migratory mesodermal cells, resulted in those cells not being able to spread out to form a thin layer on the inner surface of the animal pole as they would in normal development[126,127].

As the mesendoderm migrates of the BCR, the ectoderm undergoes epiboly and extends around the embryo surface. This mesendodermal migration also serves to enlarge the second, newly forming fluid-filled cavity – the archenteron, which inflates on the expanse of the blastocoel collapse and becomes the only embryonic cavity as the gastrulation completes[128] (Fig. 1.2.1.1.5).

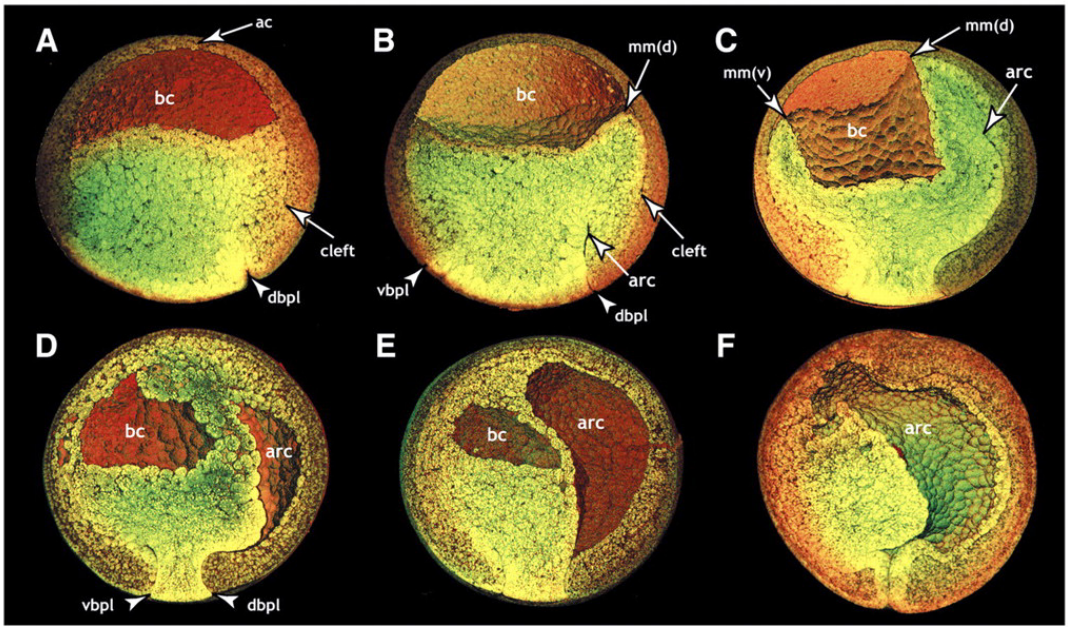

Fig.1.2.1.1.5 – Internal events during frog gastrulation. (**A**) Blastopore groove formation, (**B**) archenteron formation, (**C**) archenteron elongation, (**D-F**) archenteron inflation. Blastocoel (bc), animal cap (ac), dorsal blastopore lip (dbpl), Brachet`s cleft, ventral blastopore lip (vbpl), archenteron (arc), mesodermal mantle (mm), ventral (v), dorsal (d). From[128]

1.2.1.2 Avian gastrulation – ingression into the blastocoel

In birds, fertilization is internal, and it occurs within the oviduct before the albumen (egg white), and the shell is secreted, and the egg is laid. Like the fish, the bird embryo is also telolecithal, with the blastodisc sitting atop a large yolk. The proportion of yolk to blastodisc is about 100:1. For that reason, cell cleavages are meroblastic, as in the fish embryo, and occur only within the blastodisc resulting in the development of the embryo-proper only at one pole, the animal pole[129].

Early blastomeres are held together by tight junctions, separating the interior from the exterior of the embryo[130]. In the region between the blastoderm and yolk, a fluid-filled cavity called the subgerminal cavity forms due to the blastomeres absorbing the fluid from the albumen and secreting it into the interstitial space[131] (Fig. 1.2.1.2.1).

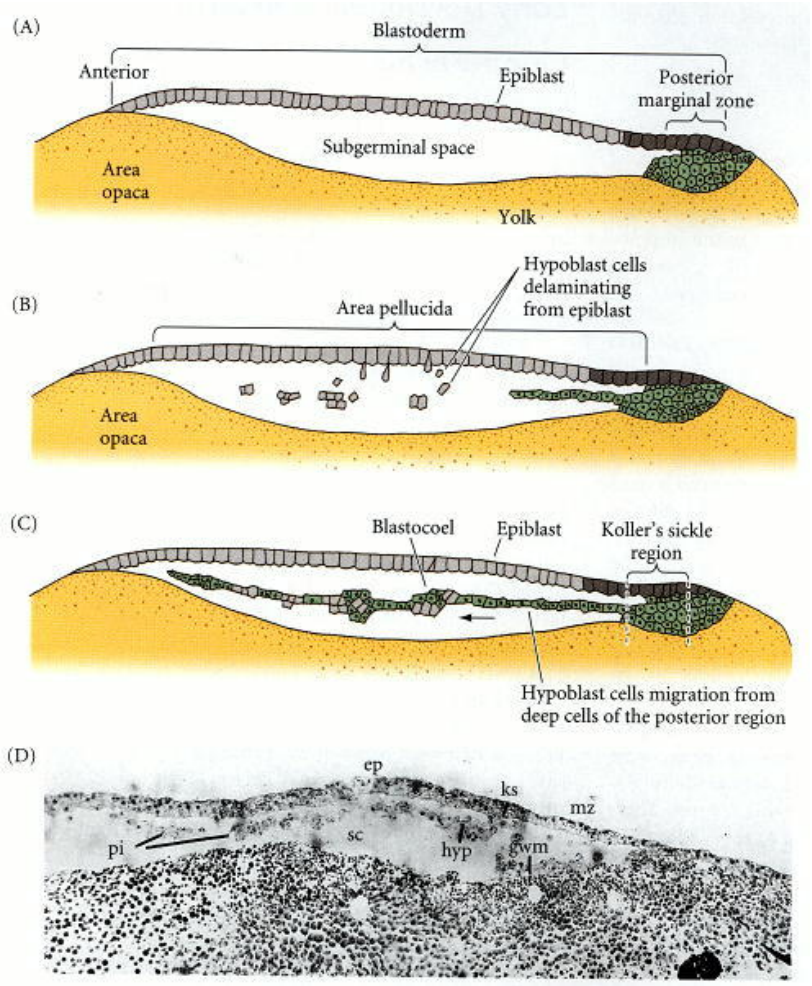

Fig.1.2.1.2.1 – Formation of the two-layered blastoderm of the chick embryo. (**A, B**) Delaminating hypoblast cells beneath the epiblast. (**C**) Hypoblast cells from the posterior margin migrate beneath the epiblast and incorporate in the polyinvagination islands. As the hypoblast moves anteriorly, epiblast cells collect at the region anterior to Koller's sickle forming the primitive streak. (**D**) This sagittal section of an embryo near the posterior margin highlighting the cells of Koller's sickle (ks), the posterior marginal zone (mz), epiblast (ep), polyinvagination islands (pi), hypoblast (hyp), secondary hypoblastic layer (sc, subgerminal cavity). From[129]

This cavity is not yet the blastocoel, which forms after the egg is laid when a sheet of cells from the posterior margin of the blastoderm migrates to form the secondary hypoblast[132]. The space between these two layers, epiblast and hypoblast, is known as the blastocoel in birds.

During gastrulation, all three germ layers of the embryo proper are formed from the epiblast cells[129]. The characteristic structure in avian, reptilian and mammalian gastrulation is the formation of the primitive streak – a thickening of the epiblast which defines the embryonic axes (Fig. 1.2.1.2.2). The primitive streak becomes visible as the epiblast cells converge and form a depression down the middle that later serves as an opening through which migrating cells can enter the blastocoel.

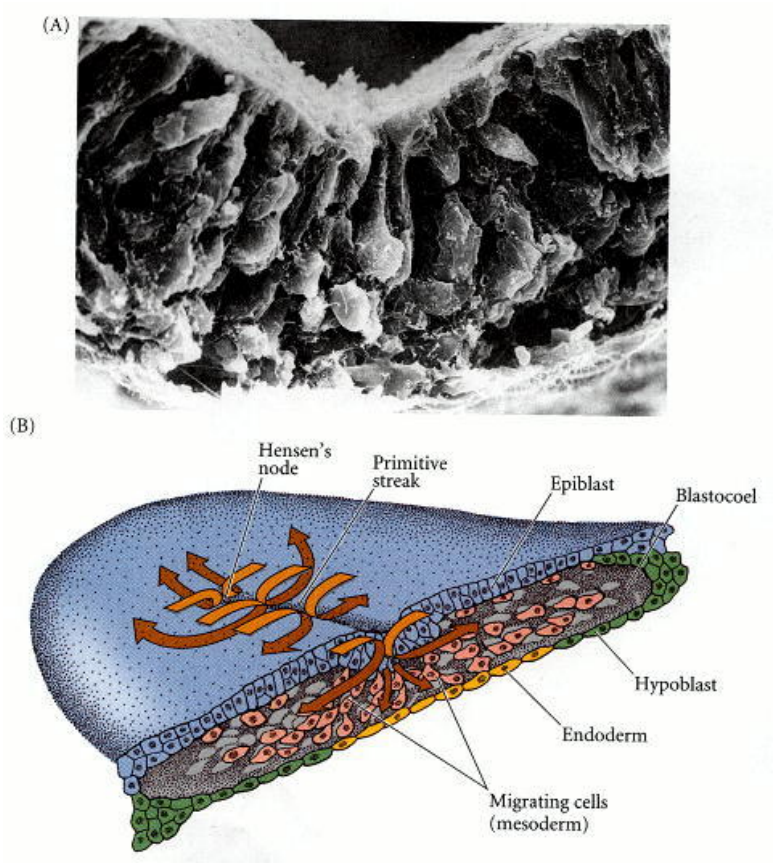

Fig.1.2.1.2.2 – Invagination of mesodermal and endodermal cells through the primitive streak. (**A**) Scanning electron micrograph shows epiblast cells passing into the blastocoel and extending their apical ends to become bottle cells. (**B**) Schamatic illustrating chick gastrulation highlighting the mesoderm and endoderm migration into the primitive streak. The lower layer becomes a mosaic of endoderm and hypoblast cellswhich eventually sort out to contribute to the yolk sac. From[129]

At the anterior end of the primitive streak there is a regional thickening of cells called the primitive knot or Hensen's node, analogous to the fish embryonic shield, through which cells can pass into the blastocoel and migrate anteriorly, giving rise to the majority of endodermal and mesodermal tissues[133] (Fig. 1.2.1.2.2).

Unlike the Xenopus mesoderm which migrates as sheets of cells into the blastocoel[108], ingressing cells in the avian embryo migrate as singles after undergoing an epithelial-to-mesenchymal transition induced by the Hepatocyte growth factor (HGF)/Scatter factor secreted by the cells themselves. Scatter factor likely converts epithelial sheets into mesenchymal cells by downregulating E-cadherin expression and interfering with its function[134,135].

1.2.1.3 Yolk vs. blastocoel – Evolutionary loss of yolk in amniotes

The amniotes consist of two major groups of vertebrate animals, the synapsids (monotreme, marsupial, and eutherians mammals) and sauropsids (reptiles and birds). There is a remarkable morphological difference at the level of early development regarding the amount of yolk substance that these embryos contain. It is

very insightful to review them individually as this distinction observed at the blastula stage of embryonic development sheds light on the evolution of the blastocyst, which goes hand in hand with the evolution of placental development and viviparity[136].

The onset of blastocyst formation is marked by the differentiation of the epithelial layer, the trophectoderm (TE), on the surface of the embryo proper that has the capacity to support the blastocyst expansion. This expansion is a key feature of mammalian development and is regarded as an infrastructural compensation for the evolutionary loss of yolk[136] (Fig. 1.2.1.3.1).

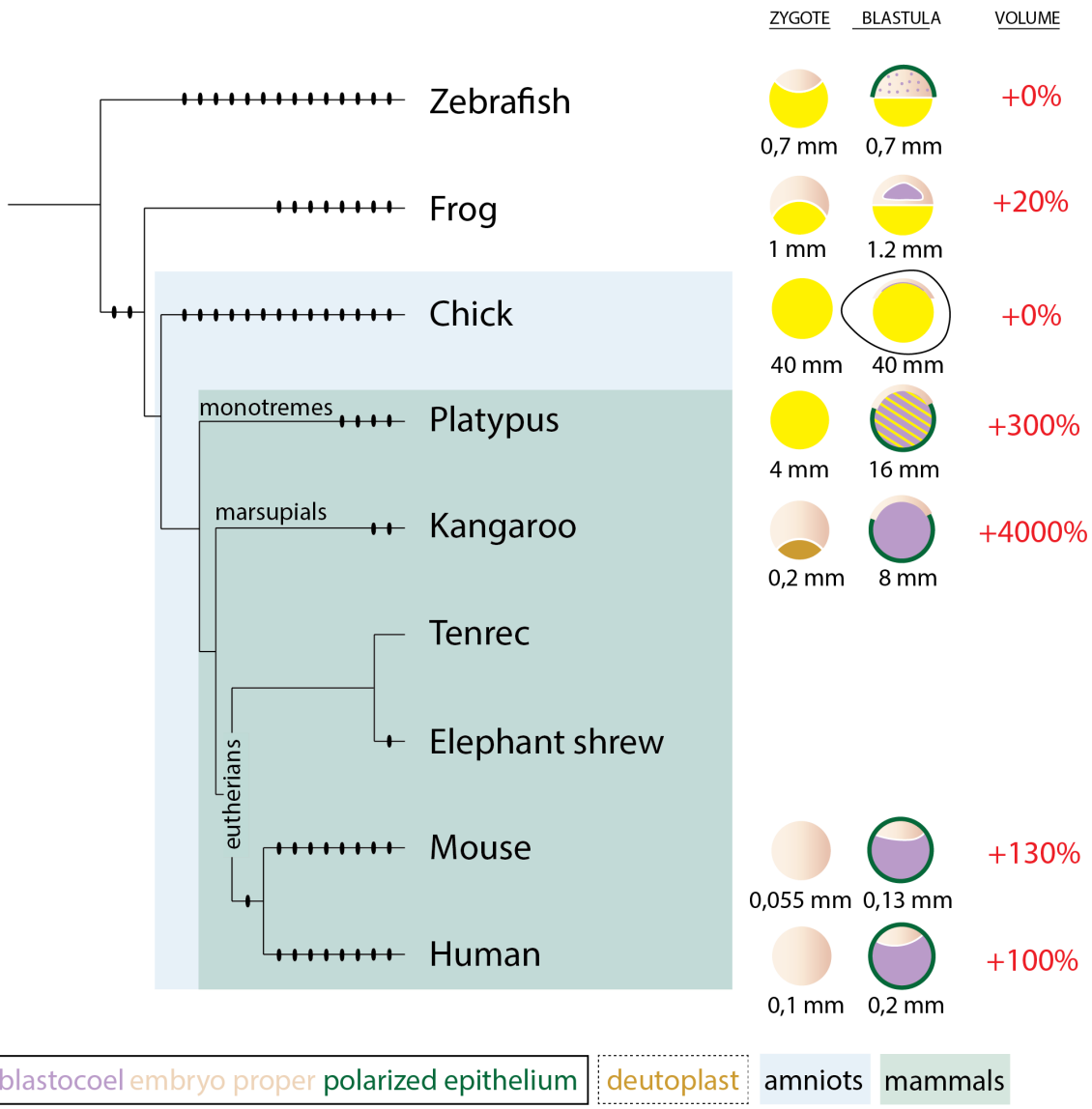

Fig.1.2.1.3.1 – Comparison of the relationship between yolk/deutoplasm content and the embryo expansion due to blastocoel inflation across the vertebrate phylogenetic tree. The tree highlights the evolutionary loss of yolk present in lower vertebrates and structural compensation by developing the blastocyst. An interesting turning point can be seen in the evolution of amniotes (blue), especially mammals (green), where in monotremes, like in birds and reptiles, there is a large amount of yolk present in the oocyte. Marsupial oocytes contain white yolk only, and the composition of marsupial white yolk differs from that in monotreme oocytes. Eutherian eggs do not have yolk in the traditional sense. Monotreme, reptilian, avian, frog, and fish blastulae have a multilayered blastoderm positioned on top of a large yolk cell (or vegetal cells containing a large amount of yolk, as seen in frogs). Eutherian

blastulae have mural trophectoderm cells surrounding the inner cell mass cells. The polar trophectoderm cell lineage is a eutherian invention but is not present in all eutherian mammals. According to[136,137]

Unlike most other vertebrates, mammals have evolved placental development, where the extraembryonic ectoderm (trophoblast) serves the role of taking up nutrients from the mother to support embryonic development, which occurs internally. The trophoblast is the first specialized cell lineage to form, and early on, it segregates from the pluriblast that will give rise to all other cell lineages[136].

The morphology of mammalian blastocysts differs significantly amongst different groups (monotremes, marsupials, and eutherians), with some of the difference conceptually related to the amount of yolk or deutoplasm present within the zygote. The marsupial eggs are relatively yolky[138,139], and the eggs of monotremes have an organization very similar to that of the birds and reptiles[140], while there is no yolk present in eutherians (Fig. 1.2.1.3.2).

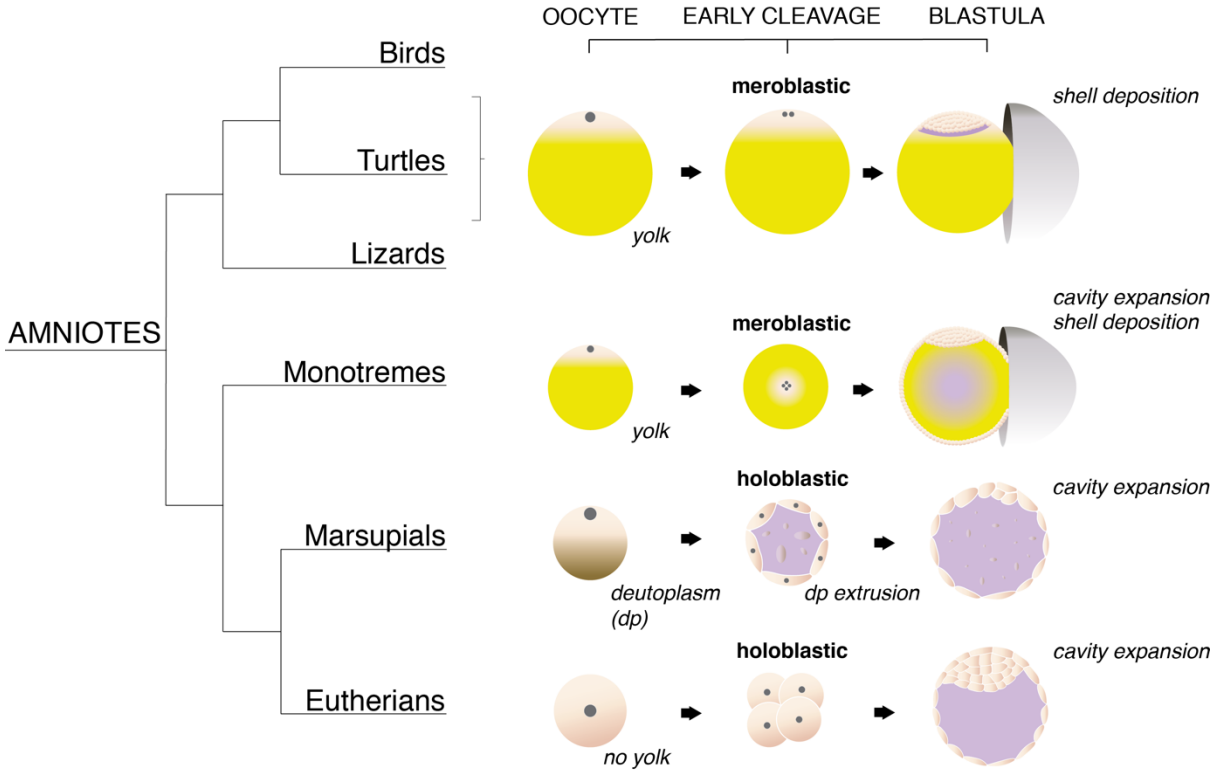

Fig.1.2.1.3.2 – Amniote phylogeny – the relationship between oocyte/embryo organization in respect to yolk content, shell deposition, and blastocoel inflation. The sauropsids (reptilian and avian) group contains birds, crocodiles, turtles, lizards, snakes, and tuatara. The Synapsida (mammalian) group contains the monotremes, marsupials, and eutherians. Three early developmental stages: mature oocyte before fertilization, early cleavage, and blastula stage. Monotremes, reptiles, and birds have similar oocyte organization, with a large amount of yolk. Marsupial eggs contain white yolk or deutoplasts, which get extruded into the central cavity. Eutherian oocytes do not contain yolk. In birds, reptiles, and monotremes, the cleavages are meroblastic due to a large amount of yolk. Cleavages in marsupial and eutherian embryos are holoblastic. In birds, reptiles, and monotremes at the blastula stage, the embryo proper is positioned on top of a large yolk cell. In marsupials, blastocysts are unilaminar, while in eutherians, the polar trophectoderm lines the blastocoel and the inner cell mass cells. According to[136,137]

Monotremes retained many ancestral features, of which the most noticeable is that they are the only oviparous mammals, where only the initial development (until somite stage) occurs within the mother after which the egg is laid[140–142]. The yolk takes up most of its oocyte and is partly homologous to the yolk of non-mammalian vertebrates, suggesting a transitional stage in the evolution of the mammalian blastocyst[136,140,142]. Like in birds, reptiles, and fish, cleavages are meroblastic, defining the embryonic-extraembryonic axis. The embryo is composed of two structures, the central multi-layered blastoderm and surrounding syncytial germ ring[140]. As the blastocyst expands, the germ ring moves to the vegetal pole and eventually completely encloses the yolk[140,141] (Fig. 1.2.1.3.2).

Marsupial oocytes contain a large number of vesicles whose contents, together with a large amount of cytoplasm, are removed into the extracellular space during cleavages, as membrane-enclosed yolk masses[143,144]. Although referred to as yolk masses, the genes encoding vitellogenin proteins are no longer functional in those oocytes, and it was suggested that they function in the formation of the extracellular matrix (ECM)[136,145,146]. For that reason, they are better termed deutoplasts[136]. Like in higher mammals, cleavages are holoblastic although this elimination of deutoplasts slightly resembles meroblastic cleavages (Fig. 1.2.1.3.2). Blastomeres are concentrated in the animal hemisphere, where they adhere to zona pellucida, a thick transparent membrane surrounding the embryo. The initial epithelium continues to divide and spread toward the vegetal hemisphere, forming a complete single-layered blastocyst that continues to expand[143]. There is some variation among marsupial blastocysts, and in some cases, they contain a single large deutoplast that remains within the blastocyst, unlike in others which usually contain multiple and rapidly fragmenting deutoplasts[136].

A characteristic feature of eutherian blastocysts distinguishing them from marsupials is the presence of the trophoblast, which entirely envelopes the pluriblast (inner cell mass, ICM)[147–149]. Oocytes contain a negligible amount of yolk/deutoplasts, and unlike in marsupials, the pronuclei show no polarized positioning within the zygote, so the embryo is spherically symmetric during early cleavages[136] (Fig. 1.2.1.3.2). Unlike in marsupials, cleaving blastomeres do not adhere to the zona pellucida but only to each other (Fig. 1.2.1.3.2).

The polar trophoblast is not a conserved structure among the eutherians. It is absent in the tenrec and elephant shrew[136,150] and formed but quickly lost in the rabbit, cattle, dog, cat and many other species[136,137,151,152]. For example, in the elephant shrew, the expansion of the blastocyst cavity occurs at the 4-cell stage, resulting in a formation of a single-layer blastocyst, with the ICM forming later by oriented divisions, randomly within the totipotent surface cells[136]. Following cell divisions, inner cells contact each other via long pseudopodium-like protrusions and eventually coalesce into an asymmetrically positioned ICM resembling the mouse blastocyst. A similar blastocyst morphogenesis process occurs in tenrecs, but unlike the elephant shrew, the ICM

formation is restricted to one pole of the blastocyst[136]. The presence of a single-layer blastocyst in elephant shrews and tenrecs suggests that this may be a basal eutherian trait as it also occurs in marsupials, although via a different mechanism[136].

Following the idea of the evolutionary loss of yolk, Pilato[153] hypothesized that the eutherian trophoblast is derived from the perivitelline syncytium (present in avian and reptilian embryos), which cellularises due to the reduction of yolk squeezed out of the blastomeres (as seen in marsupials) or out of the oocyte (as seen in eutherians), illustrated in (Fig. 1.2.1.3.3).

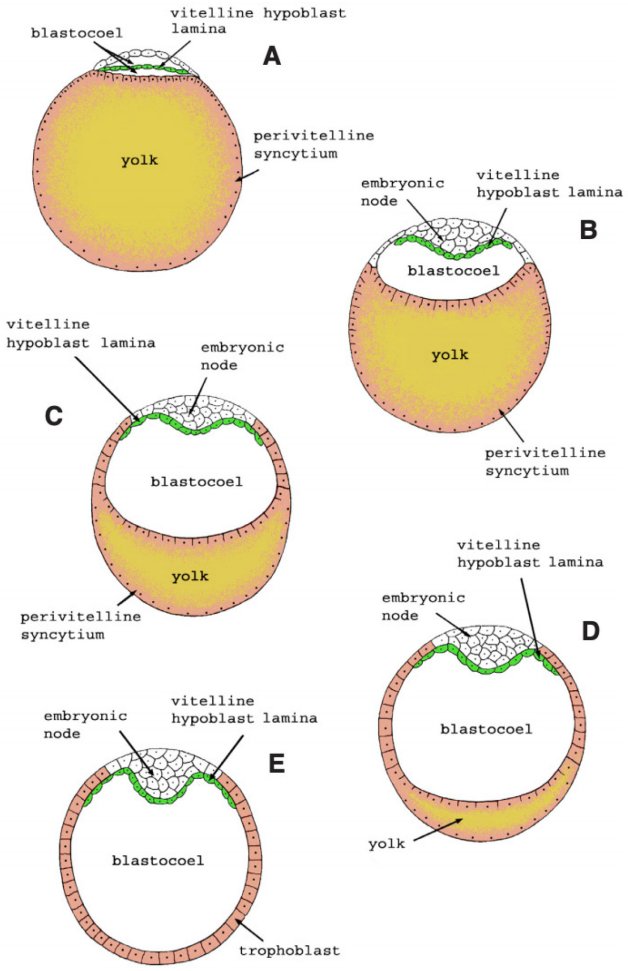

Fig.1.2.1.3.3 – Hypothetical origin of the mammalian trophoblast. A speculation that mammal blastocyst **(E)** is derived from an avian/reptilian blastula **(A)** by gradual, or sudden, reduction of the yolk. From[153]

1.2.2 Mechanism of interstitial fluid formation – lessons from the mouse blastocyst

The mechanism of blastocyst cavity formation is most studied in the context of mammalian embryos, especially the mouse[154]. Prior to cavitation, or blastocyst expansion, the blastomeres of the eight-cell stage embryo increase cell-cell contacts with their neighbours in the process referred to as compaction, coinciding with the apico-basal polarization of the surface, epithelium-like cell layer[136] (Fig. 1.2.2.1). It is this epithelialization of the surface cell-layer or the trophectoderm (TE) that is essential

for the cavity expansion[155].

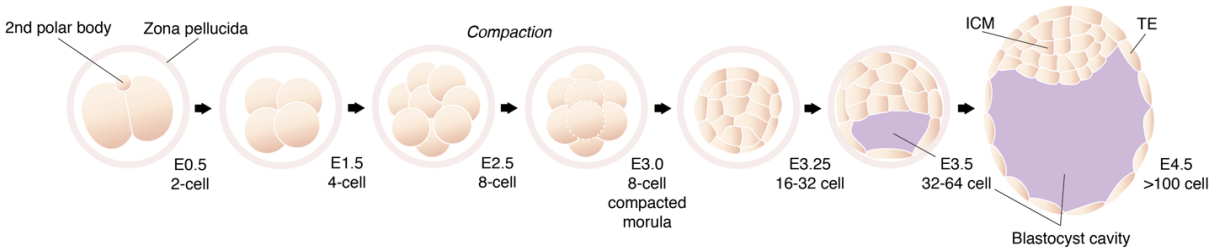

Fig.1.2.2.1 – Morphological transformation of the mouse embryo from the 1-cell stage to the blastocyst stage. Adapted from[156]

The blastocyst has the polarity of the "inverted cyst", with weakly adhesive apical membranes facing the outside of the embryo and highly adhesive basolateral sides, on the inside facing the lumen[157–159]. This configuration seems mechanically less favourable for fluid to accumulate from the outside medium. It was observed that the blastocyst cavity formation starts with the exocytosis of intracellular vesicles, or vacuoles through the basal membranes of TE cells into the extracellular space around 16- and 32-cell stage[160,161]. This results in a formation of multiple microlumens at the cell-cell contacts. These microlumens were shown to locally pressure-fracture the adhesive basolateral cell-cell contacts[158] (Fig. 1.2.2.2). Eventually these microlumens were shown to coalesce into a single dominant cavity, following the principles of Oswald ripening[158].

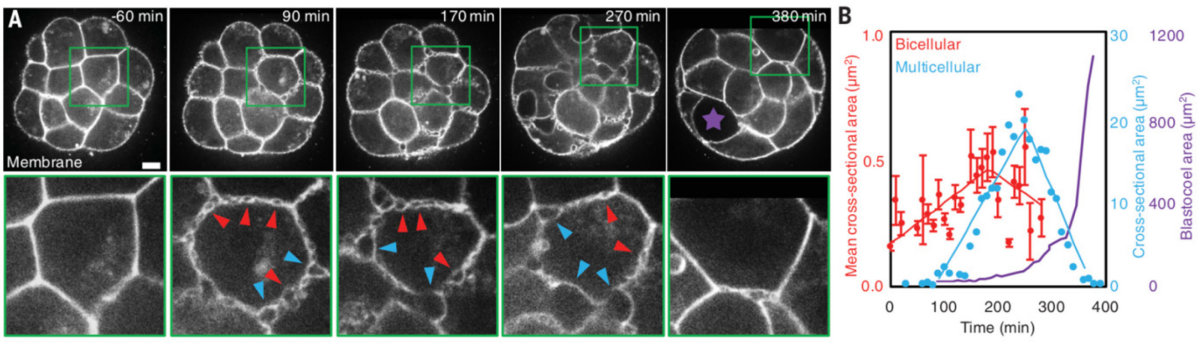

Fig.1.2.2.2. – The blastocoel forms by swelling and discharge of microlumens. (**A**) Snapshots of blastocoel formation in an embryo with membrane marker (mTmG). Microlumens form transiently at cell-cell contacts (red arrowheads) and multicellular junctions (blue arrowheads). They first swell and then shrink as the blastocoel (purple star) expands. The lower panels are 3× magnifications of the green squares in the upper panels. Scale bar, 10 mm. (**B**) Blastocoel (purple) and microlumens growth dynamics at bicellular (red) or multi- cellular (blue) junctions. For bicellular microlumens, means ± SEM of all microlumens at a cell-cell contact are shown. From[158]

In order for the cavity to further expand, osmotic forces across the TE are required to drive the water influx from the outside medium into the growing cavity. It was shown that increased sodium ion (Na^+) concentration within the microlumens is created by active Na^+ transport through transmembrane pumps localized in the TE[155,162–164]. Na^+/K^+-ATPases and Na^+/H^+ exchangers play a key role in Na^+ influx at the apical membrane and Na^+ efflux at the basal membrane, respectively[156] (Fig. 1.2.2.3).

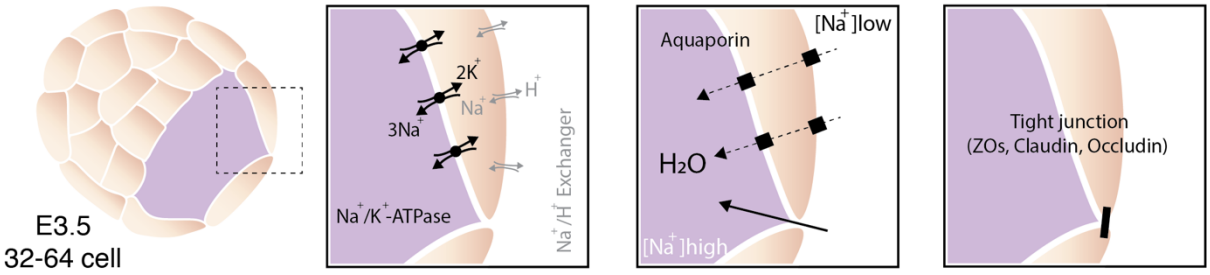

Fig.1.2.2.3 – The mechanism of blastocyst cavity expansion. Schematic illustrating the 3 critical steps in blastocyst cavity expansion and maintenance, directional Na^+ transport, water influx, and paracellular sealing. Adapted from[156]

Interesting observation pointing to the importance of the optimal culture medium came from basolaterally-enriched Na^+/K^+-ATPase (Atp1a1) null-mutant embryos, which failed to develop to the blastocyst stage when cultured *in vitro*, although *in vivo* they developed normally regardless of active Na^+ transport[156,165,166]. Chemical composition of the standard in vitro medium (KSOM) is probably much simpler then the oviduct fluid and a more complex mouse embryonic stem cell culture medium was shown to promote the expansion of the blastocyst cavity more robustly[156,167].

Active generation of an inside-out osmotic gradient favours a passive water influx into the cavity, which can occur through paracellular junctions and/or transcellularly, into the surface cells through the apical membranes and out, towards the cavity, via the basal membranes (Fig. 1.2.2.3).

In favour of transcellular water transport, various water channels, aquaporins (AQPs), were found to be expressed in TE cells with distinct spatiotemporal expression patterns, but single knockouts of individual AQP genes did not affect blastocyst expansion[156,168,169].

In order for the blastocyst to retain the water within the cavity, developmentally orchestrated paracellular sealing must be established between the TE cells. After about embryonic day 3.5 the junctional complexes are established and the blastocyst in now impermeable to its environment[10]. Tight junctions are composed of various components, such as claudins, occludins and zonula occludens proteins (ZO-1, ZO-2, and ZO-3) although none of the single knockouts interfered with the blastocyst expansion, probably due to functional compensation[170–173]. Some RNAi knockdown experiments hinted to the involvement of ZO-1 and/or ZO-2, by causing delayed cavity expansion, as well as claudins when functionally inhibited by Clostridium perfringens enterotoxin[10,174,175].

The maintenance of the blastocyst cavity is a dynamic process, where expansion is coupled with periodic blastocyst collapse resulting in leakage through the tight junctions[159]. There are many hints about the origin of such leakage, such as e.g. cell divisions, which compromise the integrity of the TE[159,176] as daughter cells need to reassemble new junctional complexes[177,178]. Additionally, material properties of the TE

cells might play a role in respect to their ability to withstand the stretch imposed by the expanding cavity[179].

1.2.3 The impact of interstitial fluid in morphogenesis

While a fluid interface could merely provide a milieu for passive diffusion of substances, it can also exert forces when conditioned to move. Furthermore, it can distribute signalling molecules and provide structural integrity and compartmentalization to the tissue due to its incompressibility.

1.2.3.1 Fluid flow in development

Fluid flow is a powerful morphogenic force, and its impact has been observed in various distinct developmental processes[180] (Fig. 1.2.3.1.1).

According to the regime in which it occurs, the flow can be either laminar or turbulent, where during laminar flow, no mixing occurs, and fluid forms a parabolic profile due to the friction with the vessel wall, while turbulent flow is characterized as irregular with chaotic mixing among the layers. Most of the interstitial flows are slow and occur in the laminar regime, while the vascular blood flow can reach turbulence[180]. Fluid flow creates a frictional force against the lumen wall, known as shear stress, that depends on the flow rate and viscosity of the fluid.

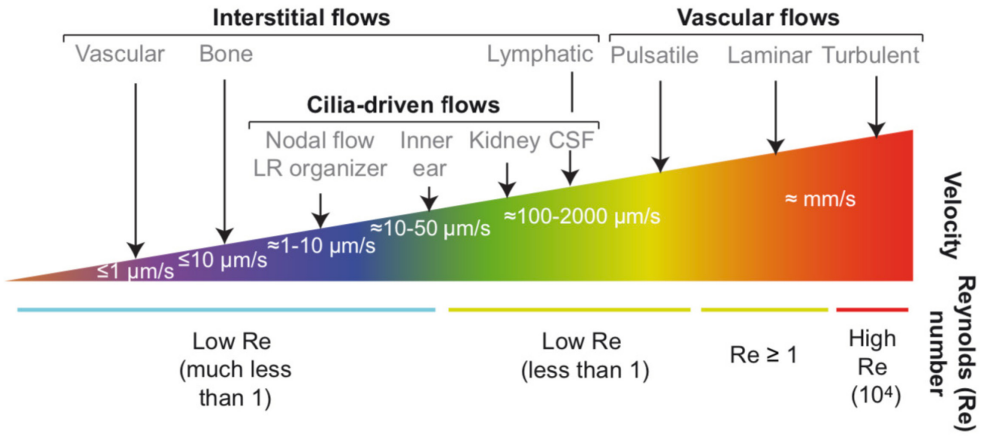

Fig.1.2.3.1.1 – Fluid flow in biological systems. Chart classifying the various types of flows encountered in vivo based on their average velocity and Reynolds number, Re: between tissues (interstitial flows); in developing body plans (cilia-driven flows); and in vascular systems (vascular flows). The chart highlights the fact that biological flows generated *in vivo* vary in location and in velocity. LR, left/right; CSF, cerebrospinal fluid. From[180]

The impact of fluid flow in development was long considered, for instance, in early studies of cardiovascular development where heart removal from a chick embryo impaired normal vascular development[181]. Wherever in development, the fluid flow was observed, a closer look revealed a functional role in the process itself. The flowing fluids demonstrated the capacity to create morphogen gradients and mechanically induce changes in gene expression and subsequent cell differentiation in development.

1.2.3.1.1 Interstitial fluid flow for morphogen distribution / mechanical stimulus

An exquisite example of fluid flow-induced morphogenesis comes from the process of left-right (LR) symmetry breaking that happens shortly after gastrulation and ensures asymmetric positioning of internal organs in vertebrates[182].

It was demonstrated that the fluid flow within the lumen of the laterality organ, the node in mouse and Kupffer's vesicle in zebrafish, causes LR patterning as the flow deficient mutants showed LR patterning defects[182–185]. The laterality organ consists of ciliated epithelial cells lining a fluid-filled cavity. Posteriorly shifted motile cilia rotate to generate a leftward fluid flow within the lumen of the organ, which is essential for its LR patterning activity[186,187]. The posterior shift is thought to be specified through PCP/Vangl2 pathway in zebrafish embryos[188,189].

For this flow to translate into distinct features of LR morphology, two mechanisms have been postulated about the role of the flow: (1) establishing a morphogen gradient or (2) through mechanosensation (Fig. 1.2.3.1.1.1).

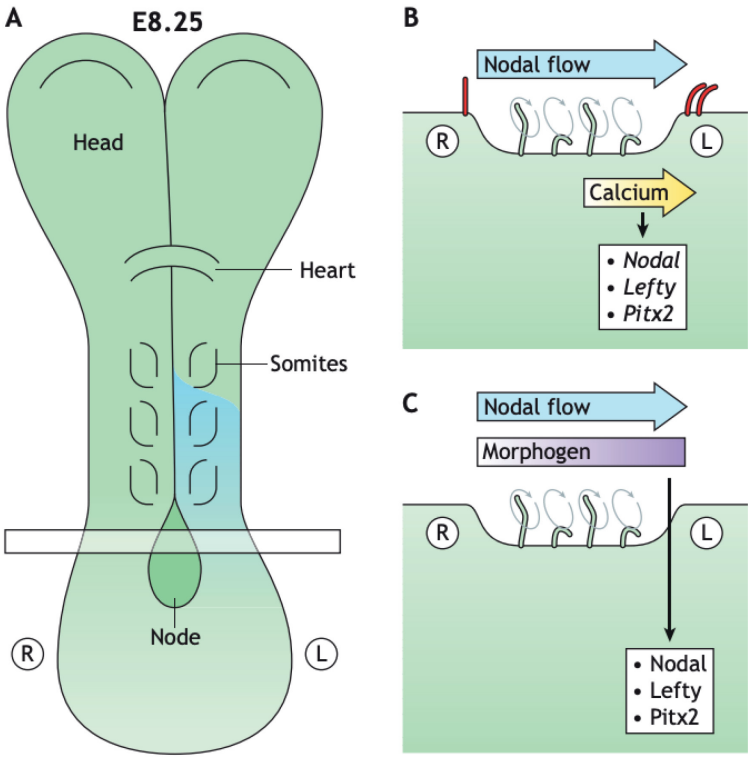

Fig. 1.2.3.1.1.1 – Mechanosensation versus chemosensation theories of nodal flow. (**A**) Schematic overview of E8.25 mouse embryo; Nodal (blue) is expressed on the left side. Horizontal box indicates the plane of the cross-section through the node displayed in B and C. (**B**) In the mechanosensation model, cilia-driven Nodal flow is sensed by immotile mechanosensitive cilia (red), which induces an intracellular Ca^{2+} increase and stimulates Nodal, Lefty and Pitx2 expression. (**C**) In the chemosensation model, cilia-driven Nodal flow creates a morphogen gradient towards the left side of the node, where receptor-based signalling induces Nodal, Lefty and Pitx2 expression. L, left; R, right. From[181]

The idea behind morphogen signalling is that the interstitial fluid (IF) flow-induced

morphogen gradient could be perceived by the receptors within the laterality organ to trigger the differentiation between the left and the right sides of the developing embryo.

Despite the identity of morphogens still being up for debate, the chemical gradient is proposed to have two shapes: a smooth gradient of fibroblast growth factor 8 (Fgf8) and Nodal, that spans the entire laterality organ and concentrates on the left side, and a steep gradient of sonic hedgehog (Shh) and retinoic acid, packed in lipid vesicles that are transported by the flow[180,185,190]. However, mathematical models suggest that nodal flow rates are insufficient to transport large vesicles and are simply too strong to create a gradient of small proteins thereby creating a symmetric distribution[191].

In favour of mechanosensation, a fraction of cilia are immotile, and it has been suggested that those could sense flow through mechanosensitive Ca^{2+} channels, such as transient receptor potential channels (TRP, PKD2)[192–194] (Fig. 1.2.3.1.1.1.A-B). Supporting that, it was shown that the flow triggers asymmetric Ca^{2+} response on the left side of the cavity, and Xenopus embryos lacking *trp2* fail to develop left-side oriented Nodal expression[192,195,196].

As the direction of the flow was shown to be critical in defining the left-right patterning, so the primary cilium is thought to either detect the flow direction (low flow) or sense their own movement and thereby amplify the asymmetry within the laterality organ[192].

1.2.3.1.2 Vascular flow-induced shear stress in cell differentiation

Fluid flow was shown to be an intrinsic part of organogenesis where it is utilized to induce morphogenesis and growth of various developing organs. In the context of cardiovascular development, the blood flow-induced shear stress appears to be instrumental in many stages of formation and maturation of the developing circulatory system within the embryo[181].

Considering the early developing embryonic heart, there is increasing evidence that the primary role of the early heart beating is not only to pump the blood for transport but also to regulate morphogenesis, contradicting the old notion that the heart begins to beat at the moment when diffusive transport is no longer efficient[197]. The role of early beating is then proposed to provide shear stress that modulates gene expression of endocardial cells – the endothelial cells lining the inside of the heart equipped with various mechanosensors that activate several signalling pathways to drive proper heart morphogenesis, vascular remodelling, and specification[181,198].

In zebrafish, the primary cilium of endocardial cells facilitates shear stress-induced *klf2a* expression, one of the principal transcription factors driving mechanotransduction, in the endocardium and subsequent *notch1b* expression[199]. Furthermore, Piezo1 Ca^{2+} channels in endocardial cells were also shown to be involved in outflow tract valve development and also induce *klf2a* expression[200].

Endocardial *klf2a* activation induces *wnt9b* expression, which stimulates cell proliferation and subsequent cardiac remodelling[201].

Blood flow pattern was also shown to impact the vascularization in the yolk sac during chick embryonic development by affecting the level of arterial-venous differentiation[202]. In perturbation experiments, when the red blood cells were blocked from entering circulation, no remodelling of the yolk sac vasculature was observed due to low shear stress levels. However, restored blood viscosity by injection of a starch solution rescued vascular remodelling, directly discriminating between the effects of shear stress and direct involvement of red blood cells themselves in this process[203].

Apart from sheer stress, fluid pressure-induced stretch is also speculated to contribute to vasculature development as blood vessels undergo periodic stretching. However, it is not trivial to disentangle the contribution of pressure from shear stress as several mechanosensitive Ca^{2+} channels, including Piezo1 and Trp2, are also activated by stretch[204,205].

1.2.3.2 Interstitial fluid pressure-driven morphogenesis

The effects of pressurized fluid or luminal pressure on surrounding tissue morphogenesis were most studied in the context of mouse blastocyst development. During compaction, the local mechanical effect of pressurized fluid was shown to fracture adhesive cell-cell contacts into hundreds of micron-size lumens, initiating blastocoel formation. These pressurized microlumens eventually coalesce following Oswald ripening principles, where larger particles are more energetically favoured than smaller ones. Following that analogy, smaller lumens give their contents to the larger ones until finally, only one dominant lumen is present, the blastocoel[158].

Following the initiation of blastocyst formation in mice, it was directly demonstrated that the pressure could act as a size-determining force. A two-fold increase in luminal pressure during blastocyst expansion induced an increase in cell cortical tension and trophectoderm (TE) tissue stiffness, leading to a mechanosensitive response and tight junction maturation in order to accommodate for the growth of the lumen (Fig. 1.2.3.2.1.A). In turn, changes in luminal pressure and size additionally affected TE cell division pattern, and consequently positioning and cell fate[159,206] (Fig. 1.2.3.2.1.B).

As expected for energetically costly tasks, biological processes during development rarely occur solemnly for their beauty but rather serve a purpose in creating an optimally functioning organism. An example of such a pressure-driven process is the blastocyst expansion which was demonstrated to promote hatching of the blastocyst from the acellular shell, the zona pellucida, so that the mouse embryo can successfully implant in the uterine wall and continue its development. In the same study, authors computationally showed that the lower blastocyst pressure due to cryopreservation

leads to delayed hatching, shedding light on the potential caveats of embryo freezing/thawing during in vitro fertilization[176].

Moreover, following implantation, it was demonstrated that the expansion of the amniotic cavity exerted forces on the epiblast, thereby promoting the notochord morphogenesis during gastrulation in mice[207].

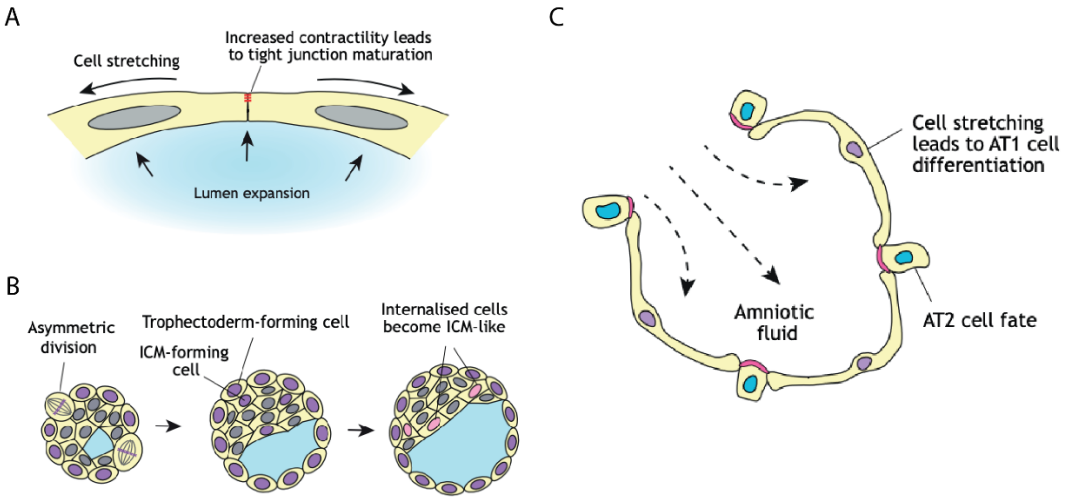

Fig.1.2.3.2.1 – Examples of lumen-mediated mechanotransduction during embryo development. (**A**) An example of hydrostatic pressure-induced trophectoderm (TE) stretching which leads to tight junction maturation. (**B**) Reduction in lumen expansion leads to changes in cell fate distribution in mouse blastocysts. Surface cells divide asymmetrically to generate a TE (purple nuclei) and an inner cell (grey nuclei) which will later become a part of the inner cell mass fate (pink nuclei). (**C**) During lung development, fluid-mediated stretching affects cell fate specification. Cells that face the amniotic fluid undergo stretching and differentiate into AT1 cell, while ones that do not undergo stretching differentiate into AT2 cells. Adapted from[208]

By exerting localized pressure, fluids were also shown to establish and fine-tune the volume of specific compartments and organs during development. An example of such is the possible impact of ocular pressure on eye development in mice. It was shown that in mutants with reduced aqueous humour, the transparent liquid in front of the lens, the intraocular pressure was lost, resulting in the formation of smaller eyes lacking normal protrusion[209]. Similar fluid-amount-dependency was seen in zebrafish brain ventricle morphogenesis, where contractility of the neuroepithelium controls the expansion of the ventricle lumen and the organ size[210].

Cell-fate specification was shown to be controlled by pressure-induced stretching in a neat example of alveolar morphogenesis in the mouse lung. There, mechanical stress induced by the uptake of amniotic fluid caused differential alveolar cell stretching due to cell-cell contact strength differences. The degree of cell stretching, in turn, triggered differential gene expression to generate distinct alveolar cell types required for proper lung function[211] (Fig. 1.2.3.2.1.C).

Fluid pressure has been shown to influence cell proliferation and division. In the chick embryonic brain, luminal pressure induces neuroepithelial cell proliferation via

symmetric cell division[212,213]. Recently, PIEZO1 has been identified as a key mechanosensor in controlling epithelial proliferation during homeostasis[214,215].

In the context of disease, interstitial fluid pressure was shown to play a role in altering the expression of genes such as Snail, vimentin, and E-cadherin that promote collective invasion associated with epithelial-to-mesenchymal transition (EMT) by modulating the motility and persistence of individual cells within the aggregates. These findings highlight the impact of fluid pressure in regulating gene expression within tissue aggregates and emphasize its relevance in tumor metastasis[216].

1.2.3.3 Fluid-filled compartment as a signalling hub

Some signaling molecules, like extracellular Bone morphogenetic protein (BMP) and Fibroblast growth factor (FGF) ligands, were shown to favor luminal accumulation, with or without establishing gradients, wherefrom they trigger their respective signaling cascades via targeted delivery or targeted compartmentalization-depended reception. Apart from their mechanical or structural role, fluid-filled cavities could serve as signaling centers, where specific biologically important molecules could act in order to enable and ensure proper patterning during morphogenesis.

FGF was shown to favour signalling from local microluminal structures, thereby spatially restricting its signalling activity. During zebrafish lateral line development, migrating primordium generates mechanosensitive, rosette-like structures enclosing a microlumen containing trapped FGF. Microlumen inhibition and laser micropuncture experiments have revealed the function of microlumens in compartmentalizing the signalling response to participating cells as a function of FGF signaling[217] (Fig. 1.2.3.3.1.A).

Another example of luminal FGF signalling affects the cell fate segregation process during mouse blastocyst expansion. There, the secretion of FGF4 carrying cytoplasmic vesicles into the interstitial space was shown to promote epiblast segregation from primitive endoderm and partially rescue the reduced specification in blastocysts with smaller cavities, thereby highlighting the impact of luminally deposited signalling molecules in cell differentiation and patterning[161] (Fig. 1.2.3.3.1.B).

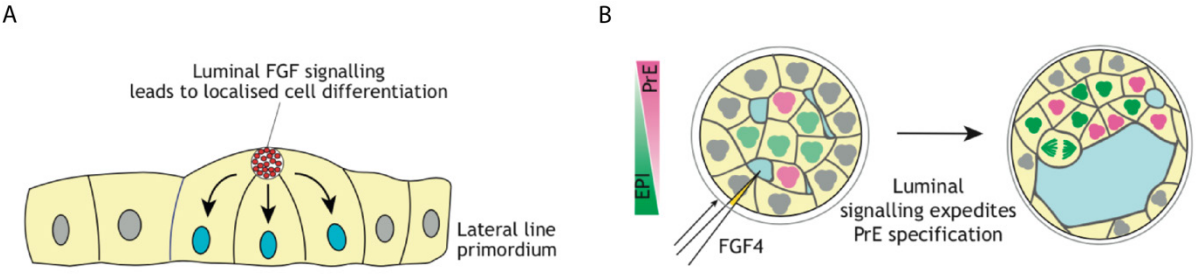

Fig.1.2.3.3.1 – Examples of lumen-mediated biochemical signalling during embryo development (**A**) Restricted fibroblast growth factor (FGF) signalling in cells neighbouring the FGF-containing microlumens during zebrafish lateral line morphogenesis. (**B**) During mouse blastocyst development, luminal FGF signalling promotes primitive endoderm fate specification in the inner cell mass. Modified

from[208]

Signalling molecules, such as morphogens and chemokines, are sometimes confined within specific compartments, as seen in the examples above, but they are also freely diffusing within the interstitial fluid, bathing the cells and tissues of the developing organism. Sometimes, the localized perception of these molecules, due to the asymmetric distribution of signalling receptors, drives restricted downstream effects.

An interesting example of such comes from the studies of BMP/TGFβ signalling in BMP4 differentiated human embryonic stem cell gastruloids in culture. There, the apical side faces the medium, as it would be facing the pre-amniotic cavity *in vivo*. Interestingly, the high cell density at the center of the colony relocalizes the TGFβ receptors to lateral sides, rendering them irresponsive to the apically applied ligand while maintaining apical localization of receptors at the edge. The laterally localizing receptors were responsive to basally presented ligands suggesting that the embryo geometry and receptor localization play a key role in tissue patterning[218]. Following these findings, a study of gastrulating mouse embryos tackled the establishment of the BMP signalling gradient *in vivo*. They showed that restricted localization of BMP receptors and ligands creates a signalling gradient that is buffered against fluctuations. Additionally, they showed that the mislocalization of receptors to the apical membranes results in ectopic BMP signalling in the epiblast shedding light on the importance of compartmentalization in tuning biochemical signalling and tissue patterning[219] (Fig. 1.2.3.3.2).

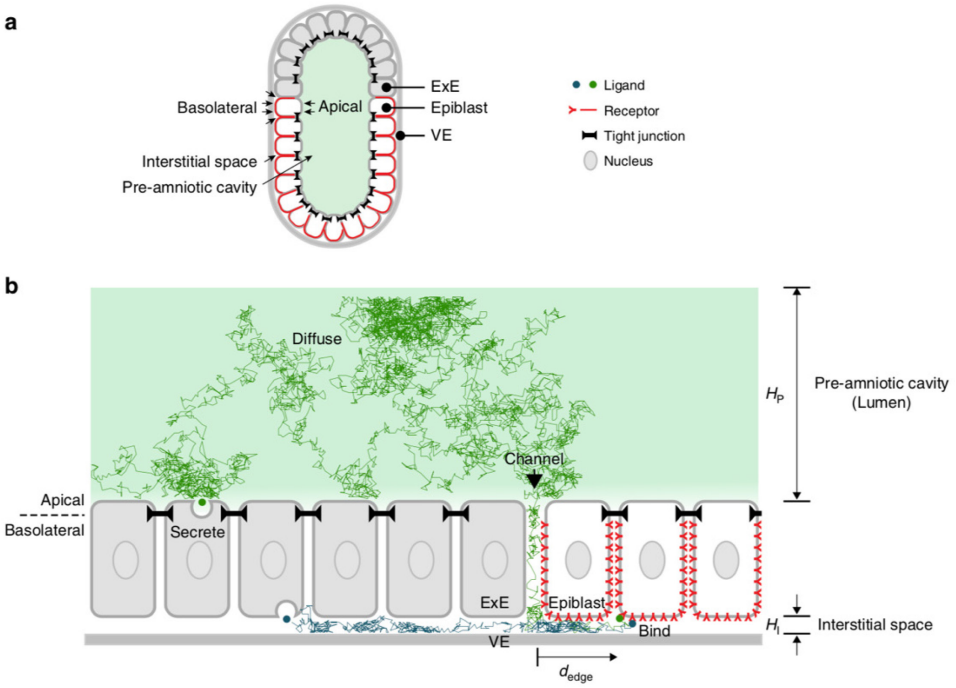

Fig.1.2.3.3.2 – Receptor localization facilitates the formation of a robust signalling gradient in early mouse embryo. (**A**) Schematic illustrating a pre-gastrulation mouse embryo. Epiblast (white), extraembryonic ectoderm (ExE, light gray) and the pre-amniotic cavity (green). Apical membranes of epiblast cells face the pre-amniotic cavity, basolateral membranes face the interstitial space. (**B**) Illustration of a simulation with basolateral receptor localization. ExE cells secrete BMP4 ligands from

their apical (green) or basolateral (blue) membranes, while epiblast cells have BMP receptors (red) on their basolateral membranes. Ligands diffuse from the epiblast edge (black arrow) through interstitial space to approach and bind basolateral receptors. From[219]

1.3 Objectives of the project

Recent studies have shed light on the direct impact of interstitial fluid accumulations in modulating various developmental processes (reviewed in Chapter 1.2.3) either by acting as signaling hubs or by exerting mechanical forces to shape the developing embryo. One such process that occurs either within or in coordination with an interstitial fluid accumulation happens during gastrulation when the initial segregation of germ layers occurs. Gastrulation is a highly conserved developmental process, but it comes in different flavors (reviewed in Chapter 1.2.1), exhibiting distinct coordination between fluid accumulations and germ layer positioning in different species. These interstitial fluid accumulations have long been speculated to play a role in tissue morphogenesis during gastrulation as they are thought to play a role in compartmentalizing the developing embryo, thereby preventing heterotypic cells from prematurely interacting with each other. On the other hand, such stereotypical fluid accumulations lead to assumptions of their functional role in enabling cell migration at the onset of gastrulation. However, experimental evidence demonstrating such function is still sparse, leaving many fundamental questions open.

Therefore, as a part of this Thesis, we sought to systematically characterize the functional relevance of interstitial fluid accumulations during gastrulation movements using zebrafish as a model system, specifically to experimentally address the functional correlation between fluid localization and its function. Also, we tackled the mechanism of interstitial fluid formation and maintenance, allowing us to tune the amount of interstitial fluid during zebrafish gastrulation. Finally, we sought to functionally analyze the feedback mechanism between axial mesendoderm internalization and interstitial fluid relocalization and elucidate the principles of interstitial fluid relocalization.

2 MATERIALS AND METHODS

2.1 Key Resources

Reagent type	Designation	Reference	Identifiers	Additional info
Strain, strain background (*D.rerio*)	Zebrafish: wildtype ABxTL	MPI-CBG Dresden		
Strain, strain background (*D.rerio*)	Zebrafish: Tg(gsc::EGFP-CAAX)	Smutny et al., 2017[89]	ZFINID:ZDB-ALT-170811-2	
Strain, strain background (*D.rerio*)	Zebrafish: Tg(actb2::HRAS-EGFP)	Cooper et al., 2005[220]	ZDB-ALT-061107-2	
Strain, strain background (*D.rerio*)	Zebrafish: *MZ*oep	Gritsman et al., 1999[33]	ZFINID:ZDB-ALT-980203-1256	
Strain, strain background (*D.rerio*)	Zebrafish: *MZ*oep;Tg(gsc::EGFP-CAAX)			
Recombinant DNA reagent	pCS2-Membrane-RFP plasmid for mRNA synthesis	Iioka et al., 2004		80pg (1-cell injection)
Recombinant DNA reagent	pCS2^{+}-H2A-mCherry plasmid for mRNA synthesis	Arboleda-Estrudillo et al., 2010[22]		50pg (1-cell injection)
Recombinant DNA reagent	pCS2-LifeAct-RFP plasmid for mRNA synthesis	Behrndt et al., 2012[221]		50pg (1-cell injection)
Recombinant DNA reagent	pCS2^{+}-Cyclops plasmid for mRNA synthesis	Rebagliati et al., 1998[39]		100pg (1-cell injection)
Recombinant DNA reagent	pT7-TS-Oep plasmid for mRNA synthesis	Zhang et al. 1998[70]		100pg (1-cell injection)
Sequence-based reagent	Human ß-Globin Morpholino: 5′-CCTCTTACCTCAGTTACAATTTATA-3′	Gene Tools		4 ng (1-cell injection)
Sequence-based reagent	cyc Morpholino: 5`-GCGACTCCGAGCGTGTGCATGATG-3′	Gene Tools		4 ng (1-cell injection)
Antibody	α_1-Na^{+}/K^{+}-ATPase antibody produced in rabbit	Gift from Dr. Nobuhiro Nakamura, Tokyo Tech Mistry et al. (2001)		

Antibody	aPKC antibody produced in rabbit	Santa Cruz Biotechnology	SC-216	
Antibody	ß-Catenin antibody produced in mouse	Sigma-Aldrich	C7207	
Antibody	ZO-1 antibody (ZO1-1A12) produced in mouse	Thermo Fisher Scientific	33-9100	
Antibody	Alexa Fluor 488 goat anti-rabbit IgG (H+L)	Thermo Fischer Scientific	A-11008	
Antibody	Alexa Fluor 647 goat anti-mouse IgG (H+L)	Thermo Fischer Scientific	A-21235	
Chemical compound	Universal agarose	VWR	732-2789	
Chemical compound	Ouabain octahydrate	Sigma-Aldrich	O3125	
Chemical compound	D-Mannitol	Sigma-Aldrich	M4125	
Chemical compound	Dextran, Alexa Fluor™ 647, 10000 MW	Invitrogen	D22914	
Chemical compound	Dextran, Tetramethylrhodamine, 10000 MW	Invitrogen	D1868	
Chemical compound	Dextran, DMNB-caged fluorescein, 10000 MW	Molecular Probes	D3310	
Chemical compound	Dextran, Fluorescein, 10,000 MW	Invitrogen	D1820	
Chemical compound	Atto 488-Biotin	Sigma-Aldrich	30574	
Chemical compound	Nile Red	Sigma-Aldrich	19123	
Cell culture reagent	Dulbecco's Modified Eagle Medium/Nutrient Mixture F-12	Sigma-Aldrich	D6434	
Cell culture reagent	Fibronectin bovine plasma	Sigma-Aldrich	F1141	
Cell culture reagent	GlutaMAX™ Supplement	Thermo Fischer Scientific	35050061	
Cell Culture Dishes	Glass-bottom dish 35 mm, Uncoated	MatTek Life Sciences	P35G-1.5-14-C	
Cell Culture Dishes	Cellview™ Cell Culture Dishes, Glass Bottom, Sterile, No. of Compartments=4	Greiner Bio One	627975	

Technical equipment	P-97 Micropipette Puller	Sutter Instrument		
Technical equipment	Microinjection capillaries 1.0 0Dx0.58 IDx 150LM	Harvard Apparatus	30-0020	
SPIM imaging materials	Glass capillaries (size 4, ID 2.15 mm) with corresponding Teflon-coated plungers		701910	
SPIM imaging materials	FEP Tubing			OD/ID 2.15/1.58 mm
SPIM imaging materials	FluoSpheres™ Carboxylate-Modified Microspheres, 0.5 µm, red fluorescent (580/605), 2% solids	Invitrogen	F8812	
Microscope	Zeiss Axio Examiner Z1 Upright LSM880 confocal microscope+ Airyscan (incubation chamber)	Zeiss		W Plan-Apochromat 20x/1,0 DIC D=0,17 M27 75mm (421452-9880-000)
Microscope	Zeiss Axio Observer Z1 Inverted LSM880 confocal microscope + Fast Airyscan (incubation chamber)	Zeiss		LD C-Apochromat 40x / NA 1.1 Water
Microscope	Zeiss Axio Imager Z2 Upright LSM900 confocal microscope + Airyscan 2 (incubation chamber)	Zeiss		W Plan-Apochromat 20x/1,0 DIC D=0,17 M27 75mm (421452-9880-000)
Microscope	Leica SP5 Inverted confocal microscope	Leica		HC PLAN APO 10x/0.4 0.17/A2.2 (11506165), WD=2.2 mm, D=0.17 mm
Microscope	Nikon Eclipse Ti2E inverted (incubation chamber)	Nikon		Plan Apo λ 20x/0.75 DIC 1 air PFS
Microscope	Zeiss Z1 SPIM	Zeiss		Plan Apochromat 10x/0.5 water immersion detection and two 5x/0.1 air illumination objectives

Software	Fiji	Schindelin et al., 2012[222]	https://fiji.sc/	
Software	Imaris	Bitplane	https://imaris.oxinst.com/packages	
Software	Excel	Microsoft	https://products.office.com/en-us/?rtc=1	
Software	GraphPad Prism	GraphPad Software	https://www.graphpad.com/scientific-software/prism/	
Software	MATLAB	MATLAB Software	https://www.mathworks.com/products/matlab.html	
Software	Ilastik	Sommer et al., 2011[223]	https://www.ilastik.org/	
Software	Illustrator	Adobe	https://www.adobe.com/products/illustrator.html	

2.2 Fish maintenance and embryo collection

Zebrafish (*Danio Rerio*) maintenance was performed as previously described[224]. The embryos were grown in E3 medium at 28-31°C and staged according to (Kimmel et al., 1995)[7]. Wildtype, transgenic and mutant fish lines used in this study are detailed in the key resource table. Zebrafish were bread in the fish facility at IST Austria, and all experimental methods are in line with the Ethics Committee of IST Austria ensuring animal welfare.

2.3 Interstitial fluid labelling and manipulation of interstitial fluid amount

Interstitial fluid (IF) was labelled by injecting 0.5 nL of 1 mg/mL of Dextran Alexa Fluor 647 between the deep cells (DCs) of high to sphere stage embryos (3.3-4 hours post fertilization, hpf), as previously described[78]. In order to increase the IF amount, or rescue the IF interface in Ouabain treated embryos, 0.5 nL of 400 mM D-Mannitol was co-injected with the IF label in high to sphere stage embryos.

2.4 Ouabain treatments

For inhibiting interstitial fluid (IF) formation, chorionated embryos were exposed to a specific Na^+/K^+-ATPase inhibitor Ouabain (1 mM in standard embryo medium, E3) from 0.5-3.3 hpf, after which the inhibitor was washed off, and embryos were dechorionated in standard embryo medium, E3.

2.5 Dextran, mRNA and Morpholino injections

Embryos at the 1-cell stage were injected as previously described[224]. Microinjection needles (30-0020, Harvard Apparatus) were pulled using a P-97 needle puller (Sutter Instruments). Injections were performed using a microinjection system (PV820, World Precision Instruments). For blastoderm segmentation, the cell cytoplasm was labelled by injection of 1 nL of 1 mg/mL of Dextran-FITC or Dextran Alexa Fluor 647 at the 1-cell stage in *wildtype* and *MZ*oep embryos. mRNA transcription was performed using the mMESSAGE mMACHINE Kit (Ambion) and used plasmids are detailed in the key resources table. For time-lapse imaging of the interstitial fluid relocalization during gastrulation, Tg(gsc::EGFP-CAAX) embryos at 1-cell stage were also injected with 50 pg of H2A-mCherry to visualize the nuclei. For analysing the effects of axial mesendoderm internalization on interstitial fluid relocalization *MZ*oep;Tg(gsc::EGFP-CAAX) embryos injected with 50 pg of H2A-mCherry at 1-cell stage and Dextran Alexa Fluor 647 at sphere stage to label the IF and compared with the embryos rescued with 100 pg of *oep* mRNA at 1-cell stage[33]. YSL injections were performed right after its formation, between 1-k and high stage (3-3.3 hpf). For visualizing the protrusive activity of the prechordal plate (*ppl*) leading edge, YSL was injected with 0.5 nL of 1 mg/mL of Dextran TMR in Tg(gsc::EGFP-CAAX) embryos. To generate embryos with smaller prechordal plates, *cyc* morpholino antisense oligonucleotide, MO (4 ng) was injected into 1-cell stage Tg(gsc::EGFP-CAAX) embryos, together with 50 pg of H2B-mCherry mRNA. Human β-globin MO (4 ng) was used as a standard negative control MO.

2.6 Sample preparation for live imaging

For upright imaging dechorionated embryos were mounted in 2% agarose molds on petri dishes and immobilized in 0.5% low melting point agarose. For inverted imaging dechorionated embryos were mounted in 0.7% low melting point (LMP) agarose on a glass-bottom dish (Glass-bottom dish 35 mm, Uncoated, MatTek Life Sciences).

2.7 Imaging setups for live and fixed sample imaging

Interstitial fluid relocalization imaging was performed using Zeiss LSM880 and LSM900 upright confocal microscopes equipped with a Zeiss Plan-Apochromat 20x/1.0 water immersion objective. Fixed samples were imaged using a Zeiss LSM880 upright confocal microscope equipped with a Zeiss Plan-Apochromat 20x/1.0 water immersion objective was used. Whole-embryo time-lapse bright-field/fluorescence imaging was performed using a Nikon Eclipse inverted wide-field microscope equipped with CFI Plan Fluor ×10/0.3 objective (Nikon) and a fluorescent light source (Lumencor). For high-magnification confocal imaging of prechordal plate, *ppl* protrusions, a Zeiss LSM880 inverted microscope, equipped with a Plan-Apochromat ×40/NA 1.2 water-immersion objective (Zeiss), was used. *In vitro* cell cultures were imaged using a Nikon Ti2E inverted wide-field microscope equipped with Plan Apo λ 20x/0.75 DIC air objective (Nikon) and a fluorescent light source (Lumencor). Magnetic tweezer experiments were imaged using a Leica SP5 inverted microscope equipped

with a resonant scanner and a HC Plan-Apochromat ×10/NA 0.4 objective (Leica) was used.

2.8 *In toto* live imaging for measuring interstitial fluid volume

2.8.1 Sample preparation

For measuring the interstitial fluid (IF) volume throughout gastrulation Tg(actb2:HRAS-EGFP) embryos, labelling the plasma membrane and cytosol, were developed until 64-cell stage, dechorionated and stained with 60 µM Nile Red in E3 (20 min at 28°C) to label the yolk cell (YC) and thoroughly washed. IF was labelled by injection of 0.5 nL of 1 mg/mL of Dextran Alexa Fluor 647 to high stage embryos. Samples were mounted in Glass capillaries (size 4, inner diameter ~2.15 mm) with corresponding Teflon-coated plungers. Matching FEP tube (OD/ID 2.15/1.58 mm) was tightly inserted into the glass capillary. For mounting the sample, a similar strategy as (Kaufmann et al., 2012)[225] was used in order to ensure uninterrupted development during imaging. Initially ~150 µL of 0.5% LMP agarose containing 1:2000 dilution of fluorescent beads (500 nm, red) was aspirated into the FEP tube using a plunger, after which an embryo was aspirated together with ~300 µM of E3 media, resulting in final LMP agarose concentration of ~0.1–0.2%. The sample was held vertically until the embryo sediment at the lower portion of the FEP tube.

2.8.2 3D live imaging

Volumentric imaging of gastrulating zebrafish embryos labelling cell membranes, interstitial fluid (IF) and the yolk cell (YC) was performed using a Zeiss Lightsheet Z.1 light-sheet microscope equipped with Plan Apochromat 10x/0.5 water immersion detection and two 5x/0.1 air illumination objectives. The heating chamber ensured the imaging at 28.5°C. Two views (0° and 180°) were acquired as image stacks of 100 to 120 *z*-planes at 3–4 µm spacing. The frame rate of the multi-view recording was 3–5 min.

2.8.3 Multi-view reconstruction of time-lapse data

For each timepoint and channel, the embryo was illuminated from both sides (dual illumination) and the emitted light was collected at a perpendicular angle. Next, the capillary containing the sample was turned by 180° and the illumination was repeated. Hence, for each timepoint and channel, the dataset consists of 4 views, representing the same embryo from different orientations. The 4 views were reconstructed using the BigStitcher plugin in Fiji[222] as previously described[226]. Briefly, Zeiss .czi files were converted and saved to hdf5. Next, fluorescent beads contained in the sample capillary were localized and used as interest points for estimating the relative shift between the 4 views. Multi-view reconstruction was performed using these interest points (precise descriptor-based method, default parameters). To exclude imaging artefacts caused by light diffraction due to the opaque yolk structure, we implemented a 2x2 tiling approach resulting in 4 equally sized blocks spanning the embryo. When fusing the 4 views together into one new 3D image stack, for each view we included

only those tiles that had sufficient image quality (i.e. the areas of the embryo having the best orientation relative to illumination and detection objective for the selected view). By selecting tiles for fusion specifically for each view, we excluded image slices showing increased light diffraction due to an obstructed light path. Excluded image slices were then compensated for by selecting the corresponding tiles in another view, thereby including only tiles with good image quality. This approach resulted in enhanced overall image quality of the embryo for all timepoints and channels. The fused dataset comprising all channels and timepoints was downsampled 4x and saved as .tiff file.

2.9 Whole mount fluorescent immunohistochemistry

Embryos were fixed in 4% paraformaldehyde overnight at 4°C. After fixation, they were washed in 0.1% Triton X-100 in 1xPBS (PBT) and dechorionated. Embryos were permeabilized by 1h incubation in 0.5% PBT after which they were incubated in blocking solution (0.5% Triton X-100, 1% dimethylsulfoxide (DMSO) and 10% goat serum in 1×PBS) for 3 h at RT. Embryos were then incubated with the primary antibody (rabbit anti-α_1-Na^+/K^+-ATPase [1:1000] or rabbit anti-aPKC and mouse anti-ß-Catenin [1:200 and 1:500]) diluted in the blocking solution overnight at 4 °C. Afterwards embryos were washed 3 x 15 min in 0.1% PBT at RT and incubated with the secondary antibody (Alexa Fluor 488 goat anti-rabbit or Alexa Fluor 488 goat anti-rabbit and Alexa Fluor 647 goat anti-mouse; 1:1000) diluted in the blocking solution for 3 hours at RT. Finally, embryos were washed 3 × 15 min in 0.1% PBT and imaged in 2% agarose molds in PBS using a Zeiss LSM880 upright confocal microscope equipped with a Zeiss Plan-Apochromat 20x/1.0 water immersion objective.

2.10 Whole mount in situ hybridization

Whole mount in situ hybridization (WMISH) was performed as previously described[227]. Antisense RNA probes for Goosecoid (*gsc)* were synthesized using T7 RNA polymerase from mMessage mMachine kits (ThermoFisher, AM1344) with Roche digoxigenin (DIG)-modified nucleotides from partial cDNA sequences. WMISHs were imaged on a stereo-microscope (Olympus SZX 12) equipped with a QImaging Micropublisher 5.0 camera.

2.11 *In vitro* prechordal plate (*ppl*) cell spreading assay

For *in vitro* cell spreading assay prechordal plate (*ppl*) progenitors were induced by injecting 100 pg of *cyc* mRNA in combination with 50 pg of H2A-mCherry at 1-cell stage of Tg(gsc::EGFP-CAAX) embryos. Glass bottom dishes were plasma-cleaned for 2 min and coated with 30 µl of Fibronectin (1:4 in dH_2O) per well. When control embryos were at dome stage, the *ppl*-induced embryos were transferred and dechorionated in glass dishes with Danieau's medium (58 mM, 0.7 mM KCl, 0.4 mM $MgSO_4$, 0.6 mM $Ca(NO_3)_2$, 5 mM HEPES, pH 7.6). *Ppl* explants were prepared from *ppl*-induced embryos by removing the blastoderm from the yolk cell (YC). After YC removal explants were transferred to glass dishes with pre-warmed DMEM/F12 cell culture medium (stock was diluted with 10% dH_2O) and cut into pieces consisting of

~50 cells. The explants were then mounted on Fibronectin-coated glass bottom dishes, incubated in culture medium at 28°C for 2 hrs and imaged in respective media using a Nikon Ti2E inverted wide-field microscope equipped with Plan Apo λ 20x/0.75 DIC air objective (Nikon) and a fluorescent light source (Lumencor).

2.12 Prechordal plate (*ppl*) cell transplantations

To assess the sufficiency of the prechordal plate (*ppl*) to relocalize the interstitial fluid (IF) autonomously within the embryo and provide control experiments for pharmacological treatments, we turned to a host-donor system. To this end, we took use of the transgenic mutant *MZ*oep;Tg(gsc::EGFP-CAAX) embryos, lacking all mesendoderm specification and marking the dorsal side of the gastrula. As *ppl* donors, transgenic wildtype Tg(gsc::EGFP-CAAX) embryos expressing the EGFP in the *ppl* cells were used. At the 1-cell stage, donor embryos were injected with either 50 pg of H2A-mCherry or LifeAct-RFP mRNA to label the nuclei and actin-rich protrusions, respectively. Depending on the experiment, 0.5 hours post-fertilization (hpf), either only host embryos or a combination of host and donor embryos was treated with a specific Na^+/K^+-ATPase inhibitor Ouabain (1 mM in standard embryo medium, E3) until high stage (3.3 hpf), as described above for treatment of wildtype embryos. After the inhibitor removal, embryos were dechorionated with forceps, and IF was labelled in the host embryos, as described above. At 50% epiboly (5.7 hpf), embryos were transferred to Danieau's buffer and prepared for transplantation. Using a custom-made transplantation setup (a 20 mL syringe connected to a transplantation needle (ID 20 um) via silicone tubing), a cluster of *ppl* cells (10-20 cells) was taken from the *ppl* of the donor embryos and placed at the yolk cell-deep cell (YC-DC) interface, near the germ margin at the dorsal side of the host embryos. Transplanted host embryos were mounted for upright and inverted imaging, depending on the experimental assay.

2.13 Light activation of caged FITC in the interstitial fluid

To assess the mechanism of interstitial fluid (IF) relocalization at the onset of gastrulation, we took advantage of a local, UV laser-induced activation of a caged fluorophore within the IF. Thereby, we probed the IF relocalization mechanism in transgenic wildtype Tg(gsc::EGFP-CAAX) and mesendoderm-specification deficient transgenic mutant *MZ*oep;Tg(gsc::EGFP-CAAX) embryos to assess the effect of mesendoderm (prechordal plate, *ppl*) on the efficiency of the IF relocalization. Embryos were developed as described above, and at 3.3-4 hpf, they were co-injected with the 0.5 nL of a solution containing Dextran Alexa Fluor 647, 1 mg/ml (uniform IF labelling) and caged-FITC, 1 mg/ml (non-fluorescent before local activation) between the deep cells (DCs), targeting the IF. Embryos were developed until 50% epiboly (5.7 hpf) and mounted for upright imaging with lateral orientation. Embryos were imaged on a Zeiss Axio Imager Z2 Upright LSM900 confocal microscope using a custom-designed pattern for continuous UV activation within the IF accumulation at the EVL-DC interface, above the *ppl*. The local accumulation of uncaged-FITC from the source

at the EVL-DC interface and IF area measurements were performed at the YC-DC interface, ahead of the migrating *ppl*.

2.14 Mimicking *ppl*-induced IF relocalization by a magnetic bead

To assess the mechanical effect of *ppl* migration on the interstitial fluid (IF) relocalization, we sought to mimic the *ppl*-induced DC/epiblast displacement by radially pulling a *ppl*-size bead via a locally applied magnetic field. To this end, mesendoderm-specification mutant *MZ*oep embryos were used and developed in standard embryo medium (E3) until high stage (3.3 hpf), after which they were dechorionated and transferred to Danieau's buffer. Magnetic bead (OD 40 um), conjugated with Streptavidin, was coated with Atto488 – biotin for precise localization within the tissue. Bead implantation was performed at the oblong stage (3.7 hpf). Coated beads were placed within a mineral oil droplet on a glass coverslip for easier access during implantation. Embryos were lined in a large transplantation mold and oriented laterally. Using a custom-made transplantation setup (a 20 mL syringe connected to a transplantation needle (ID 40 um) via silicone tubing), several magnetic beads were aspirated and individually implanted into host *MZ*oep embryos. Embryos were incubated at RT for 30 min post-implantation to heal the wound, after which the interstitial fluid (IF) was labelled, as described above. At 50% epiboly, embryos with correct localization of the magnetic bead (at the yolk cell-deep cell, YC-DC interface) were selected for the experiment. The experiment was performed on an inverted Leica SP5 confocal microscope equipped with a micropipettes aspiration and magnetic tweezer systems. To prevent it from moving towards the magnetic coil when the magnetic field was switched on, the embryo was held on the yolk cell (YC) side by a blunt micropipette (OD 80 um/30°), applying a slight aspiration without deforming the surface of the YC. The magnetic bead was pulled orthogonally to the animal-vegetal (AV) axis via a locally applied magnetic field during continuous imaging.

2.15 Data analysis and statistics

For characterization of the interstitial fluid (IF) relocalization as a function of morphogenetic movements, blastoderm and IF segmentation was performed using the Pixel and Object classification paradigm in Ilastik followed by a custom developed Matlab script for mapping the position of the IF along the animal-vegetal axis. For quantification of IF distribution on the dorsal side, relative to the prechordal plate (ppl) position, region-of-interest (ROI) analysis in Fiji was used. Initially, the binary masks were generated by doing a segmentation in Ilastik, and the curvature of the embryo was compensated for using a macro "Straighten" in Fiji. IF distribution profiles on the EVL-DC and YC-DC interface were plotted relative to the position of the *ppl.* Surface cell, DC, and *ppl* cell volume were quantified using the Cells algorithm in Imaris. Pairwise comparisons of not normally distributed data were performed using Mann-Whitney statistical test. For measuring the degree of *ppl* cell spreading *in vitro,* a previously published Fiji script was used[91]. *Ppl* cell clusters were segmented, and binary masks were generated using Ilastik. The binary masks were used to compare the actual perimeter length of the cluster to the perimeter of an ellipse fitted to the

same area. For analysis of the radial DC/epiblast displacement relative to the *ppl* migration, DC and *ppl* nuclei were tracked using the Spots algorithm in Imaris for wildtype and *MZ*oep embryos. Tracks were corrected for the embryo curvature, and radial DC velocity heatmaps were generated relative to the position of the *ppl* (or superimposed wildtype *ppl* in case of *MZ*oep embryos) and IF. Average radial velocities in the area around the *ppl* were plotted for wildtype and *MZ*oep embryos. The porosity of the DCs/epiblast and *ppl* was quantified within the ROI of $4•10^3$ um^2 by measuring the fraction of IF within the region. IF relocalization from the localized source at the EVL-DC to the YC-DC interface, ahead of the *ppl* leading edge, was quantified by correlating the increase in the IF area to the rate of accumulation of the uncaged FITC at the YC-DC interface. To quantify the FITC accumulation rate at the YC-DC interface, kymographs along the radial axis (from the EVL-DC to the YC-DC interface) were generated using a plugin in Fiji, and the rate was quantified by measuring the FITC intensity as a function of time at the YC-DC interface.

3 RESULTS

This study was designed by Carl-Philipp Heisenberg and myself. Presented data is a result of collaborative work, in which I was the leading scientist. Collaborators, together with their specific contribution, are referenced in each figure legend.

3.1 Interstitial fluid bathes the embryonic cells throughout early development in zebrafish

Accumulation of interstitial fluid (IF) between embryonic cells is a common phenomenon in vertebrate embryogenesis. Across different species, a hallmark of such accumulations in early embryonic development is the formation of the blastocoel[1] [98,133,136,228–230]. Unlike other model systems, where the blastocoel occupies the central position within the embryo, in zebrafish, we have previously detected the presence of small, fluid-filled interstitial gaps within the blastoderm[2] of pre-gastrula stage embryos[18,78]. Such IF distribution could likely be due to a specific geometry of the zebrafish embryo, where the blastoderm sits atop of a large yolk cell (YC), which seemingly occupies the position of the blastocoel. Moreover, in dissection experiments, where the YC has been mechanically removed, the blastoderm formed a central, fluid-filled cavity[231].

The blastocoel has long been speculated to play a role in embryo morphogenesis[3], explicitly supporting gastrulation[4] movements, but experimental evidence showing its direct involvement is still sparse. To shed light on the impact of IF accumulations in early embryonic development, we initially sought to characterize the process of IF formation and distribution within the blastoderm.

To visualize the onset of IF formation between the embryonic cells, we used a transgenic line ubiquitously expressing membrane-bound EGFP (*actb2::HRAS-EGFP*) and additionally labelled the cytosol with a fluorescent dextran (Dextran, Alexa Fluor™ 647). The resulting labelling allowed us to detect the forming interstitial spaces as label-free negatives (Fig. 3.1.1.A). During early development, the embryonic cells are continuous with the YC on their basal side due to the incomplete, meroblastic[5] cleavages and organized in a single layer atop of the YC[8]. The initial interstitial spaces formed as little pockets, specifically under the basolateral membranes of the surface cells, (Fig. 3.1.1.A), in coordination with the change in the cell division plane[7] and

[1] Also termed the blastocyst or cleavage cavity is a fluid-filled cavity that forms in the blastula stages of embryonic development.

[2] Or the embryo-proper. These are the cells that will give rise to the future animal.

[3] A biological process that causes a cell, tissue, or organism to develop its shape.

[4] A milestone of early embryogenesis that marks the formation of the primary germ layers from which all the embryonic tissues will be generated.

[5] Incomplete or partial cleavage. Due to the presence of a large yolk cell the cleavage furrows have a hard time to cleave or split a cell all the way through.

formation of fully enclosed cells on the surface of the embryo. These pockets increased in size and number during the following cell cleavages (Fig. 3.1.1.A). To better visualize the interstitial pockets' morphology during their expansion, we injected a fluorescent dextran (Dextran, Alexa Fluor™ 647) into the interstitium, aiming for the initial pockets, in *actb2::HRAS-EGFP* embryos, schematised in (Fig. 3.1.1.B).

Although injected before the YC membrane was formed, the IF labelling never intermixed with the YC content and stayed specifically restricted to the blastoderm portion of the embryo, unable to diffuse out of the embryo due to the barrier properties of the squamous epithelial layer on the embryo surface – the enveloping layer (EVL). Upon labelling, we detected a dynamic redistribution of the IF – from the spatially restricted initial pockets at 128-cell stage to a relatively uniform interface, bathing the embryonic cells, as the embryo developed to sphere stage (2.25-4 hours-post-fertilization, hpf) (Fig. 3.1.1.B').

Morphogenetic events which occur throughout gastrulation are orchestrated around the YC. At the onset of epiboly[6] (dome stage), when the YC bulges up and invades the blastoderm portion of the embryo, consequently, the blastoderm thins and spreads, eventually completely engulfing the YC at the end of gastrulation[7]. When the tissue has spread past the equator of the embryo the most marginal cells, all around the circumference, undergone the first cell fate specification event and committed to meso- and/or endoderm cell fates with mesenchymal[7] morphology. These cells actively migrated towards the animal pole[8], confined between the YC and overlying deep cells (epiblast), forming a layered embryo with a defined body plan by the end of gastrulation[7,19].

We detected a major reorganization of the IF during this process, which appeared to be developmentally orchestrated, compartmentalizing the IF within different embryo regions (Fig. 3.1.1.B'). Such characteristic IF accumulation pattern during gastrulation raised questions about its potential direct involvement in this process.

[6] A conserved gastrulation movement which describes thinning and spreading of a sheet or multi-layer of cells.

[7] Morphology of cells where they exhibit migratory polarization, extending protrusions towards the direction of movement. It enables cells to travel to specific targets within the embryo.

[8] In terms of the embryonic axis, animal-vegetal is up-down, and dorsal-ventral is left-right.

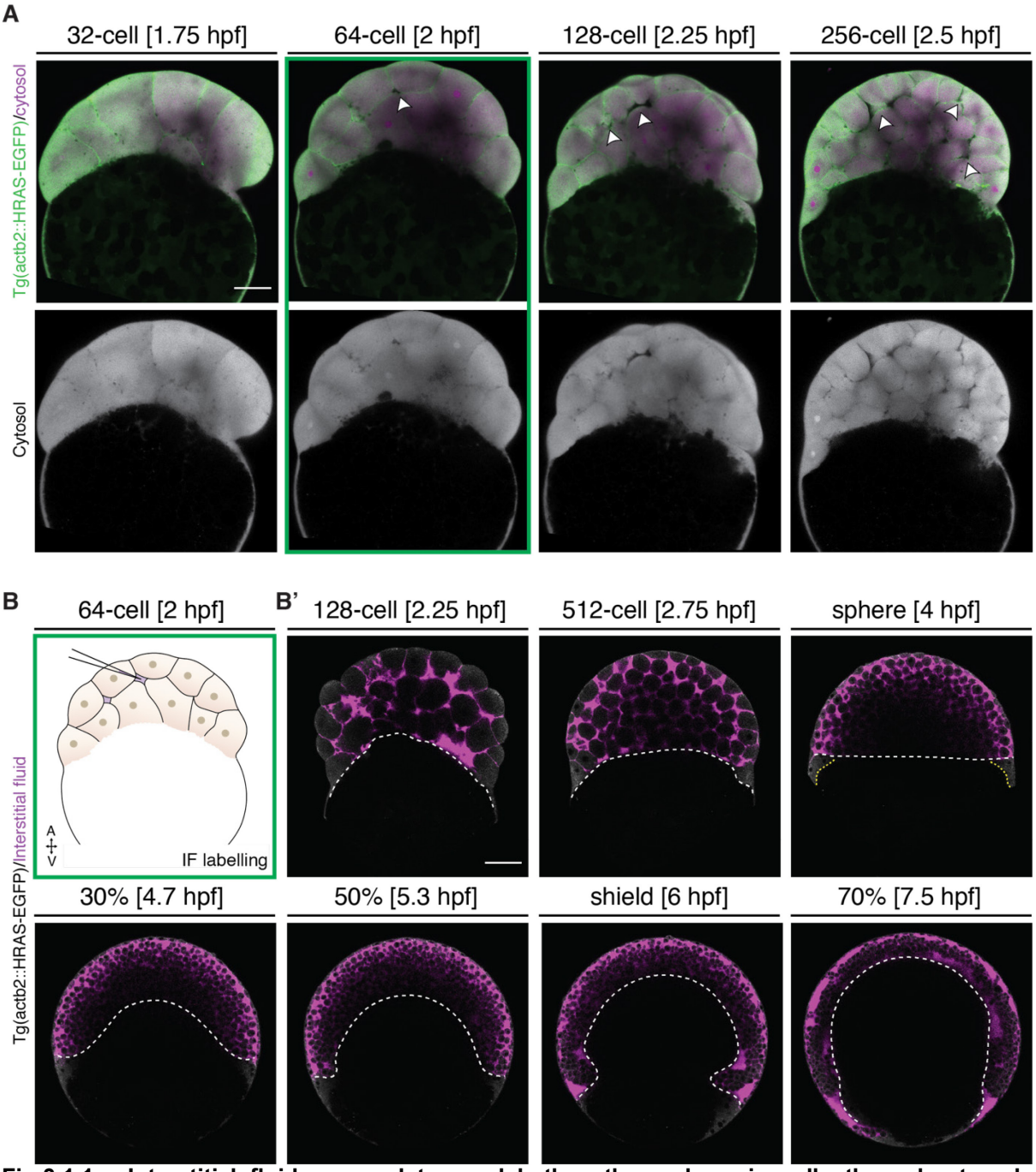

Fig.3.1.1 - Interstitial fluid accumulates and bathes the embryonic cells throughout early development in zebrafish. (**A**) Representative confocal cross-section images of transgenic zebrafish embryos expressing actb2::HRAS-EGFP to label cell outlines injected with fluorescent dextran to label the cytosol (top row) and cytosol only (bottom row) from 1.75–2.5 hours post fertilization (hpf). Arrowheads highlight the emergence of interstitial spaces. Scale bar, 100 um. (**B**) Schematic illustrating the interstitial fluid (IF) labelling by injection of extracellular fluorescent tracers at 2 hpf. A-V, animal-vegetal axis. (**B'**) Representative confocal cross-section images of transgenic zebrafish embryos expressing actb2::HRAS-EGFP to label cell outlines injected with fluorescent dextran to label the IF from 2.25–7.5 hpf. White dashed line outlines the blastoderm-yolk cell interface. Yellow dashed line highlights the yolk syncytial layer. Scale bar, 100 um.

3.2 IF undergoes a developmentally coordinated relocalization during gastrulation

To investigate the potential role of interstitial fluid (IF) accumulations within the blastoderm during gastrulation, we first systematically determined how the distribution of IF changes during this period.

We labelled the blastoderm by cytosolic injection of fluorescent dextran (Dextran, Fluorescein, 10,000 MW) into 1-cell stage *wildtype* embryos and labelled the IF by injection of fluorescent dextran (Dextran, Alexa Fluor™ 647) between the deep cells (DCs) at high stage (3.3 hours-post-fertilization, hpf), schematised in (Fig. 3.2.1.A). Next, we quantified the IF distribution relative to its position within the blastoderm (Fig. 3.2.1.A-B'').

During pre-gastrula stages (4-6 hpf), the IF localization gradually changed from initially even distribution of fluid-filled gaps between DCs to a preferential accumulation at the interface under the surface enveloping layer (EVL) cells (EVL-DC IF accumulation) (Fig. 3.2.1.A'-B'', 4-6 hpf). This was followed by a spatiotemporally highly coordinated IF relocalization from the EVL-DC interface towards the yolk cell (YC) underneath the DC layer (YC-DC IF accumulation) (Fig. 3.2.1.A'-B'', 6-8 hpf), schematised in (Fig. 3.2.1.B). Notably, this relocalization became first apparent at the blastoderm margin (germ margin) at the time when mesendoderm[9] progenitors began internalizing there (Fig. 3.3.1.B-B', 6 hpf), and then spread from the margin to the animal pole of the embryo (Fig. 3.3.1.B-B', 8 hpf), continuous with the animal-directed migration of the mesendoderm progenitors.

[9] Refers to the cells which have the ability to further differentiate into mesoderm and endoderm, respectively.

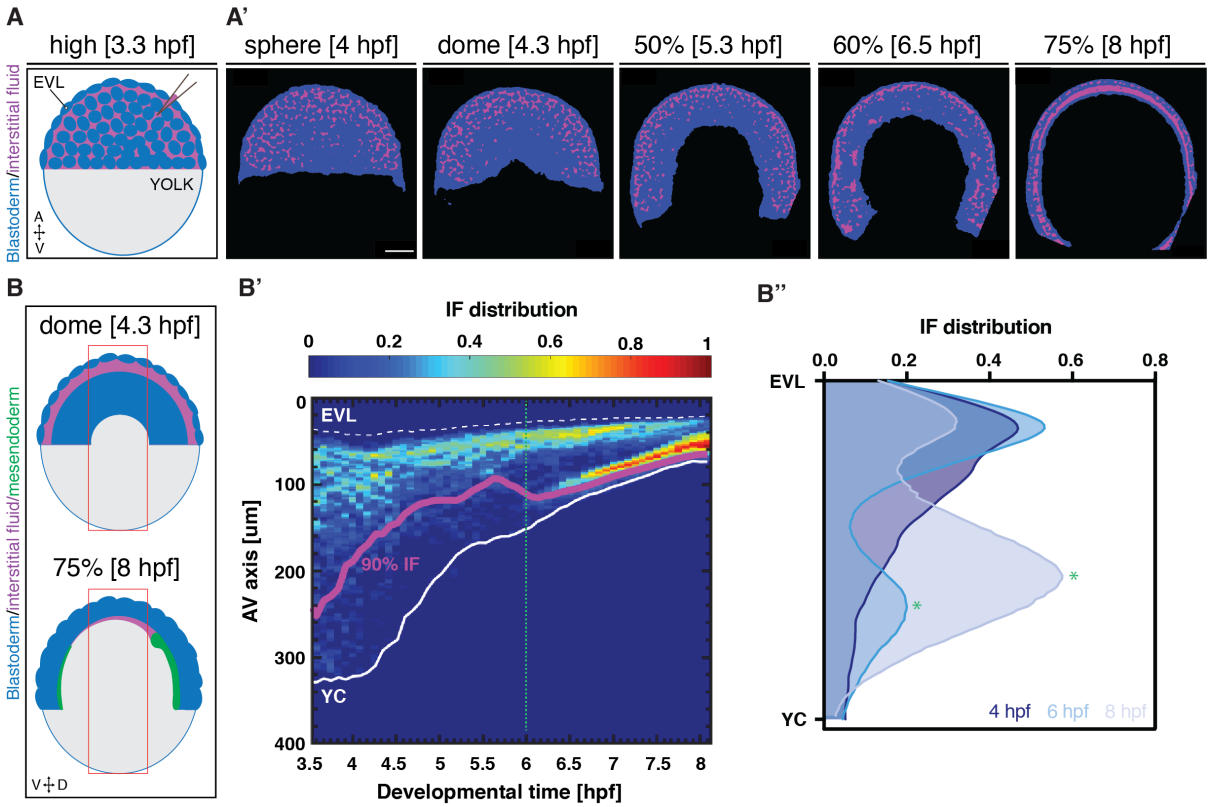

Fig.3.2.1 - IF undergoes a developmentally coordinated relocalization during gastrulation. Enveloping layer, EVL. Yolk cell, YC. (**A**) Schematic illustrating the interstitial fluid (IF) labelling at 3.3 hpf. A-V, animal-vegetal axis. (**A'**) Blastoderm and interstitial fluid (IF) binary masks generated using Pixel Classification workflow in ilastik from 4–8 hours post fertilization (hpf). Scale bar, 100 um. (**B**) Schematic illustrating the developmentally orchestrated IF reorganization at 4.3 and 8 hpf. The red rectangle demarcates the region within which the analysis in (**B'-B''**) was performed. V-D, dorsoventral axis. (**B'**) Representative kymograph of IF distribution along the animal-vegetal (AV axis) of the embryo as a function of developmental time. IF distribution is color-coded. The 90% IF (magenta line) indicates the distribution of 90% of the IF along the AV axis at a given time point. The line at 6 hpf (dashed, green) marks the onset of mesendoderm internalization at the germ margin. (**B''**) Average IF distribution within the blastoderm along the AV axis at 4, 6 and 8 hpf (N = 4, n = 8). Stars (green) indicate the emergence of the second IF accumulation within the blastoderm. n, number of embryos. Generating the code and assisting in the design of the analysis was performed by Shayan Shamipour.

Moreover, IF volume within the blastoderm stayed relatively constant during this relocalization (Fig. 3.2.2.A-B'), arguing in favour of IF redistribution within the blastoderm rather than a *de-novo* accumulation at the YC-DC interface.

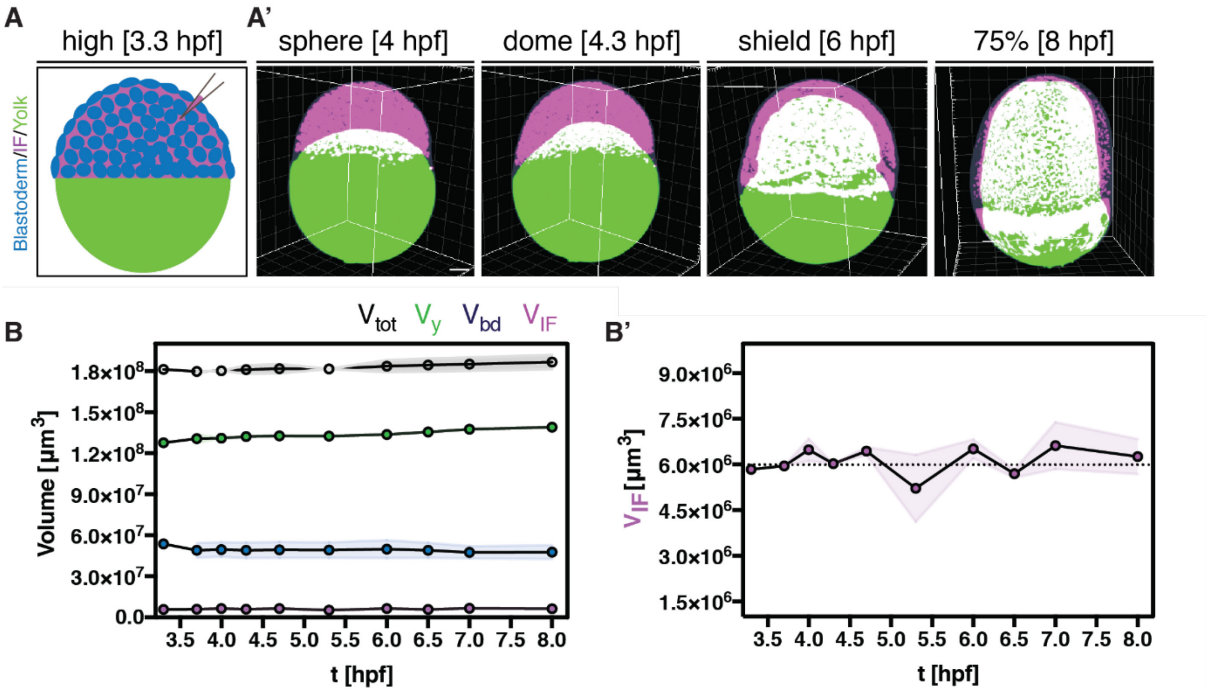

Fig.3.2.2 – IF volume stays relatively constant throughout gastrulation. (**A**) Schematic illustrating the blastoderm (BD), yolk cell (YC) and interstitial fluid (IF) labelling for Selective plane illumination microscopy (SPIM). (**A'**) 3D reconstructed images of dual-illumination, multi-view SPIM from 4–8 hours post fertilization (hpf). Scale bar, 100 um. (**B**) Quantification of total embryo volume (V_T), yolk cell volume (V_{YC}), blastoderm volume (V_{BD}), and interstitial fluid volume (V_{IF}) from 3–8 hpf. Mean + SEM. (**B'**) Close up quantification of IF volume from 3–8 hpf. Mean + SEM. (N = 2). N, number of independent embryo replicates. 3D reconstruction of raw data was performed by Friedrich Preusser. V_T, V_{YC}, V_{BD} was segmented by Christoph Sommer.

3.3 IF relocalization coincides with axial mesendoderm internalization and migration

IF distribution analysis revealed a local bias in IF relocalization. Importantly, this highly orchestrated relocalization of IF was most clearly recognizable at the dorsal side of the gastrula (Fig. 3.3.1.A-C'), where a compact cluster of anterior axial mesendoderm (prechordal plate, *ppl*) and posterior axial mesendoderm (*pam*) progenitors internalizes and migrates in a straight path towards the animal pole[7,19,22]. Unlike the rest of the internalizing mesendoderm, *ppl* and *pam* progenitors are composed of several cell layers, eventually giving rise to the head and spinal cord structures, respectively, of the future animal[7,19,21].

To characterize the IF relocalization in relation to *ppl* internalization at the dorsal side, we labelled the IF in a transgenic fish embryo expressing membrane-bound EGFP under the control of the *goosecoid* (*gsc*) promotor – a specific marker of *ppl* cell fate (Fig. 3.3.1.A-C'). Analysing the IF distribution above and below the DCs, relative to the *ppl* position, we detected a local depletion of the IF above the DCs, on top of *ppl,* (Fig. 3.3.1.B-B', 6 hpf, blue outline) and *ppl*/*pam* (Fig. 3.3.1.C-C', 8 hpf, blue outline). Interestingly, below the DCs, we detected a stable IF accumulation ahead of the *ppl*, that increased in amount relative to *ppl/pam* migration and surface IF depletion (Fig. 3.3.1.B-C', pink outline).

In contrast, in lateral and ventral regions of the gastrula, where mesendoderm progenitors internalize and migrate as loosely aggregated cells[7,19], the relocalization of IF was much less pronounced. Collectively, these findings point at the possibility that there might be a functional link between the relocalization of IF from the EVL-DC to YC-DC interface with the internalization and animal-directed migration of axial mesendoderm progenitors at the onset of gastrulation.

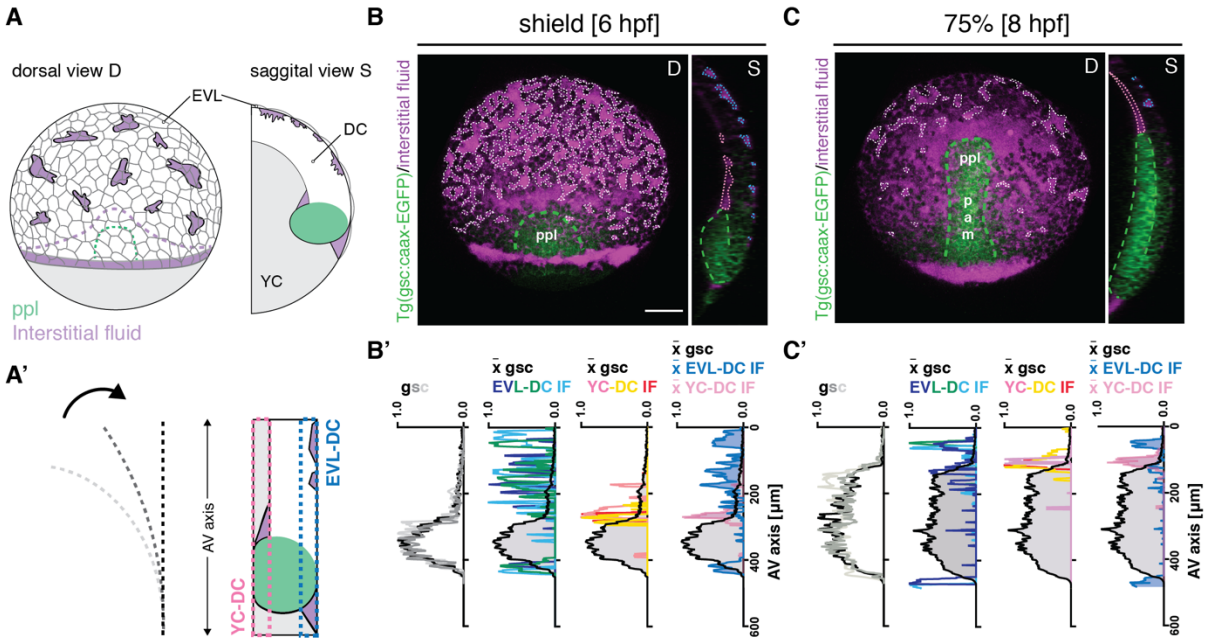

Fig.3.3.1 - Interstitial fluid relocalization coincides with axial mesendoderm internalization and migration. Enveloping layer, EVL. Yolk cell, YC. Deep cells (epiblast), DC. *Ppl*, prechordal plate. (**A**) Schematic illustrating the dorsal, D and sagittal, S view of the zebrafish embryo at the onset of mesendoderm (ppl/pam) internalization. (**A'**) Schematic illustrating the principle of interstitial fluid (IF) distribution analysis. AV, animal-vegetal axis. The pink rectangle indicates the region of IF accumulation analysis at the yolk cell-deep cell, YC-DC interface. The blue rectangle indicates the region of IF accumulation analysis at the enveloping layer-deep cell, EVL-DC interface. (**B, C**) Maximum intensity projections (dorsal view, D) and single cross-sections (sagittal view, S) of a transgenic zebrafish embryo expressing gsc::caax-EGFP to label the prechordal plate, *ppl/pam*, injected with dextran to label the interstitial fluid (IF) at (**B**) 6 hours post fertilization (hpf) and (**C**) 8 hpf. Dashed outlines (green) indicate the *ppl*. In D, dashed outlines (white) indicate the IF at the EVL-DC interface. In S, dashed outlines (blue) indicate the IF at the EVL-DC, and (pink) indicate the IF at the YC-DC interface. Scale bar, 100 um. (**B', C'**) IF distribution profiles along the AV axis relative to the position of ppl/pam, indicated by the expression of *goosecoid* (*gsc*) at (**B'**) 6 hpf and (**C'**) 8 hpf. Multi-color curves show N=3 representative replicates of IF distribution at the EVL-DC (cold colors) and YC-DC (warm colors) interface, averaged in the last panel.

3.4 Transient inactivation of Na^+/K^+ ATPases results in strongly reduced IF accumulation during the formation phase

To address the functional relevance of the IF accumulation at the YC-DC interface for *ppl* progenitor cell migration, we sought to interfere with the overall IF accumulation within the blastoderm and analyse how this affects *ppl* cell migration.

To this end, we asked how IF accumulation is regulated within the blastoderm. We found that the occurrence of first interstitial pockets coincides with the apicobasal[10] polarization of the surface cells (Fig. 3.4.1.A). Surface cell polarization was accompanied by the restricted localization Na^+/K^+-ATPases[11] - key regulators of IF accumulation in other organisms[156] - to the basolateral side of surface cells (Fig. 3.4.1.A), pointing at the possibility that Na^+/K^+-ATPases are involved in IF accumulation into the blastoderm. To test this possibility, we blocked Na^+/K^+-ATPase activity at the onset of IF formation by exposing embryos to 1 mM of the specific Na^+/K^+-ATPase inhibitor Ouabain[12][159,161] from 1-3 hpf, schematised in (Fig. 3.4.1.C).

The occurrence of initial interstitial pockets in treated embryos was undetectable compared to the control embryos (Fig. 3.4.1.B). This reduced accumulation of IF was accompanied by a transient swelling of blastoderm cells (Fig. 3.4.1.D) which, however, normalized before the onset of gastrulation (Fig. 3.4.1.D'-D'').

[10] Cell polarity specific to epithelial cells. Apical membranes face the body`s outside surface, while the basolateral enclose the rest of the cell. The two domains are often physically separated by adherens junction complexes.

[11] An enzyme found in the membrane of all animal cells. For every ATP molecule that it uses, 3 Na^+ ions are exported, and 2 K^+ ions are imported, thereby increasing extracellular Na^+ concentration.

[12] A steroid hormone that binds to the catalytic α-subunit of the plasma membrane Na^+/K^+-ATPase and inhibits the ion transport activity.

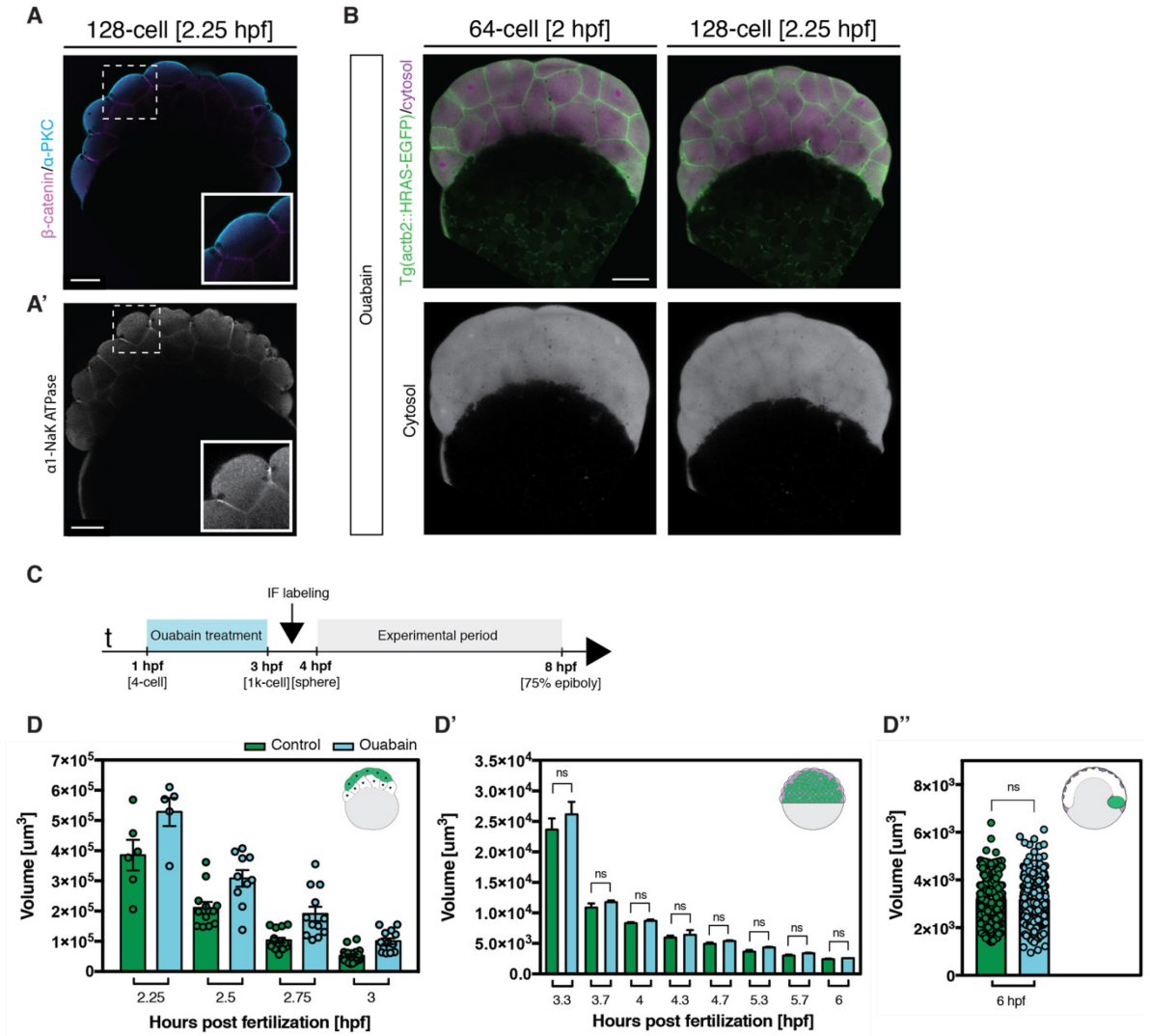

Fig.3.4.1. - Transient inactivation of Na^+/K^+-ATPases results in strongly reduced IF accumulation during the formation phase. (**A**) Cross-section confocal images of ß-catenin, α-PKC and (**A'**) α1-Na^+/K^+-ATPase enriched in the surface cells at 2.25 hours post fertilization (hpf). Scale bar, 100 um. (**B**) Confocal cross-section images of Ouabain treated transgenic zebrafish embryos expressing actb2::HRAS-EGFP to label cell outlines injected with dextran to label the cytosol (top row) and cytosol only (bottom row) at 2 and 2.5 hpf. Scale bar, 100 um. (**C**) Schematic illustrating the experimental design. (**D**) Surface cell, (**D'**) deep cell and **(D'')** *goosecoid* positive (*ppl*) cell volume quantification in control and Ouabain treated embryos. (**D**) Control (N=1), Ouabain (N = 2). (**D'**) Control at 3.3 hpf (N = 3), 3.7 hpf (N = 3), 4 hpf (N = 7), 4.3 hpf (N = 6), 4.7 hpf (N = 5), 5.3 hpf (N = 2), 5.7 hpf (N = 2), 6 hpf (N = 2). (**D''**) Control (N = 4), Ouabain (N = 4). Individually plotted values represent volume quantifications of each individual cell. ns, not significant. N, number of embryos. Data are mean ± SEM. Mann-Whitney test.

3.5 Extracellular osmolarity controls the amount of IF accumulation within the blastoderm

The ability to interfere with the IF accumulation served as a valuable tool to further understand how the IF amount correlates with its distribution within the gastrulating embryo. For this reason, we designed the experimental assay such that we exposed the embryos to 1 mM of Ouabain in E3 medium[13] around the time of IF formation (1-3

[13] Standard zebrafish embryo husbandry medium.

hpf) after which we removed the inhibitor from the medium and labelled the IF with fluorescent dextran (Dextran, Alexa Fluor™ 647), schematised in (Fig. 3.5.1.A).

We performed the same analysis as in *Chapter 3.2* and observed that, despite being significantly reduced, IF accumulations in treated embryos displayed similar initial distribution as found in control embryos (Fig. 3.5.1.B-B'). First, the IF accumulated to the interface between EVL and DCs and then from there to the YC-DC interface, although the localization to any of these interfaces in strongly affected embryos was often hardly recognizable (Fig. 3.5.1.B-B') and (Fig. 3.5.2.A-B'). This suggests that Ouabain treatment predominantly interferes with IF accumulation *per se*, but not necessarily with the processes regulating the relocalization within the blastoderm.

To determine whether Na^+/K^+-ATPases function in IF accumulation by regulating intra- to extracellular fluid osmolarity[14], as found in other organisms[156,159,161], we injected 0.5 nL of 400 mM Mannitol[15] into the extracellular space of Ouabain-treated embryos at 3.5 hpf to increase extracellular osmolarity and, consequently, IF accumulation in those embryos. Mannitol-injection efficiently rescued IF accumulation in Ouabain-treated embryos (Fig. 3.5.1.C-C') and (Fig. 3.5.2.C-D'), suggesting that Ouabain inhibits IF accumulation within the blastoderm by unbalancing the ratio of extra- to intracellular osmolarity.

Moreover, injection of 0.5 nL of 400 mM Mannitol into the extracellular space of control embryos increased the total amount of IF in those embryos but did not abolish the general pattern of IF relocalization observed in control embryos (Fig. 3.5.1.D-D') and (Fig. 3.5.2.E-F'). Together, these findings suggest that regulating extracellular osmolarity represents an effective tool for tuning the amount of IF accumulation in early blastula and gastrula stage embryos.

[14] Osmotic concentration is the measure of solute concentration, defined as the number of osmoles of solute per litre of solution (Osm/L).

[15] Mannitol is a type of sugar alcohol.

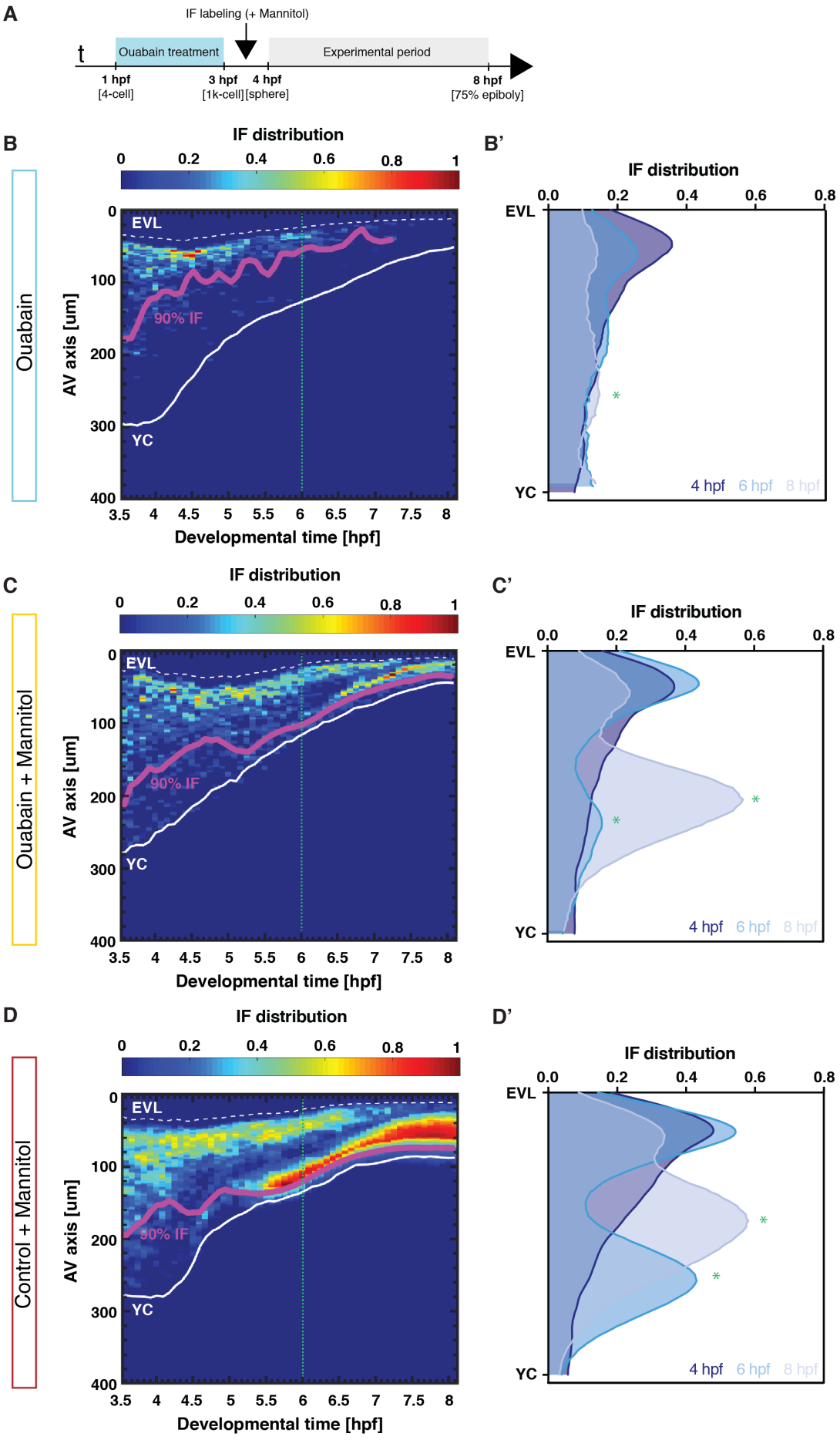
A
IF labeling (+ Mannitol)
t
Ouabain treatment
Experimental period
1 hpf
[4-cell]
3 hpf
[1k-cell]
4 hpf
[sphere]
8 hpf
[75% epiboly]
B
Ouabain
IF distribution
0
0.2
0.4
0.6
0.8
1
EVL
90% IF
YC
AV axis [um]
0
100
200
300
400
3.5
4
4.5
5
5.5
6
6.5
7
7.5
8
Developmental time [hpf]
B'
IF distribution
0.0
0.2
0.4
0.6
0.8
EVL
YC
4 hpf
6 hpf
8 hpf
*
C
Ouabain + Mannitol
C'
D
Control + Mannitol
D'

Fig.3.5.1 - Extracellular osmolarity controls the amount of IF accumulation within the blastoderm. Enveloping layer, EVL. Yolk cell, YC. (**A**) Schematic illustrating the experimental design. (**B**) Representative kymograph of IF distribution along the animal-vegetal (AV axis) as a function of developmental time in Ouabain treated (N = 4, n = 8) (**B-B'**), Mannitol rescue (N = 4, n = 6) (**C-C'**), and Mannitol-injected control embryos (N = 4, n = 9) (**D-D'**). (**B'**, **C'**, **D'**) Average IF distribution within the blastoderm along the AV axis at 4, 6 and 8 hpf. n, number of embryos. Analysis as in *Fig.3.2.1*.

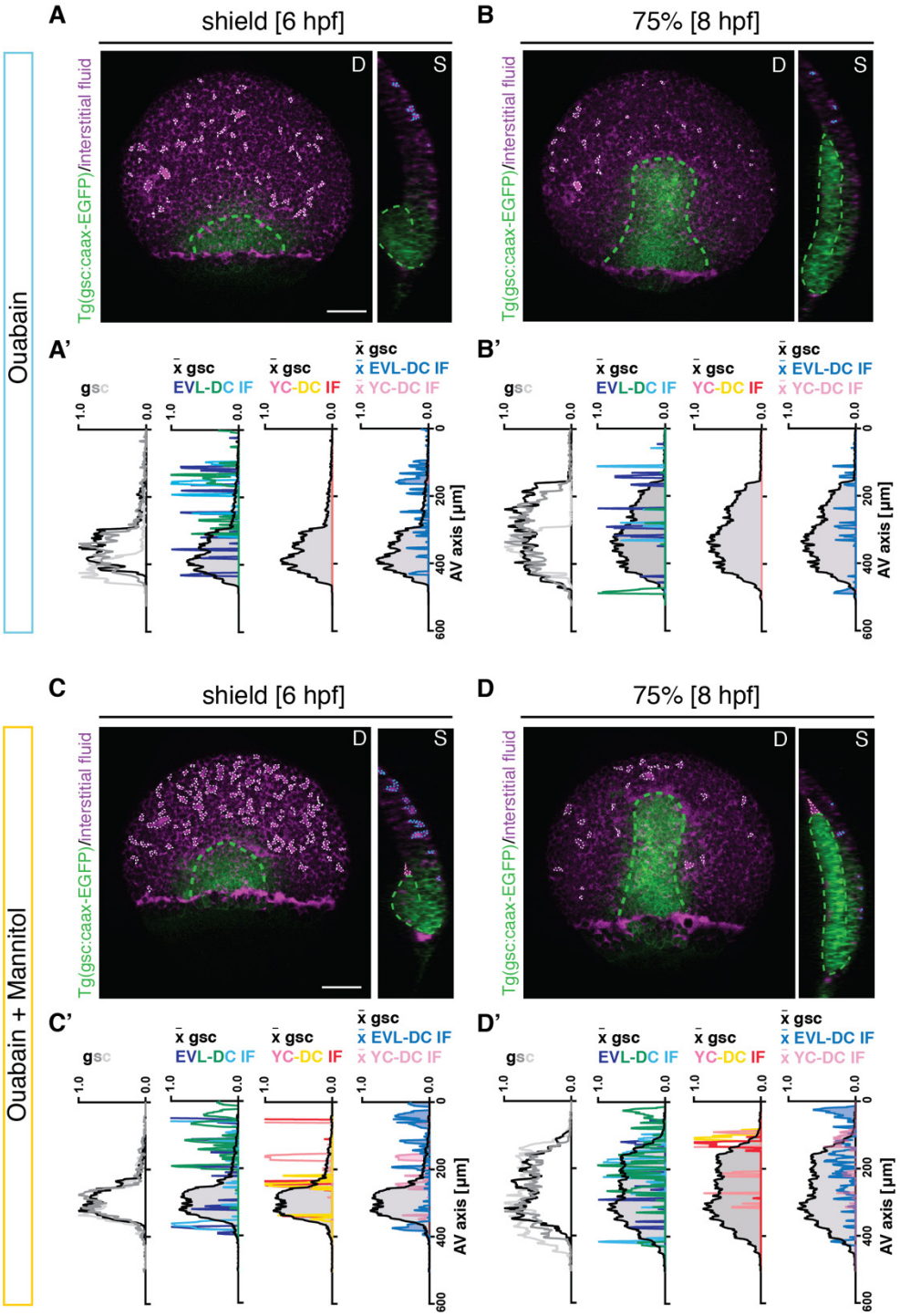

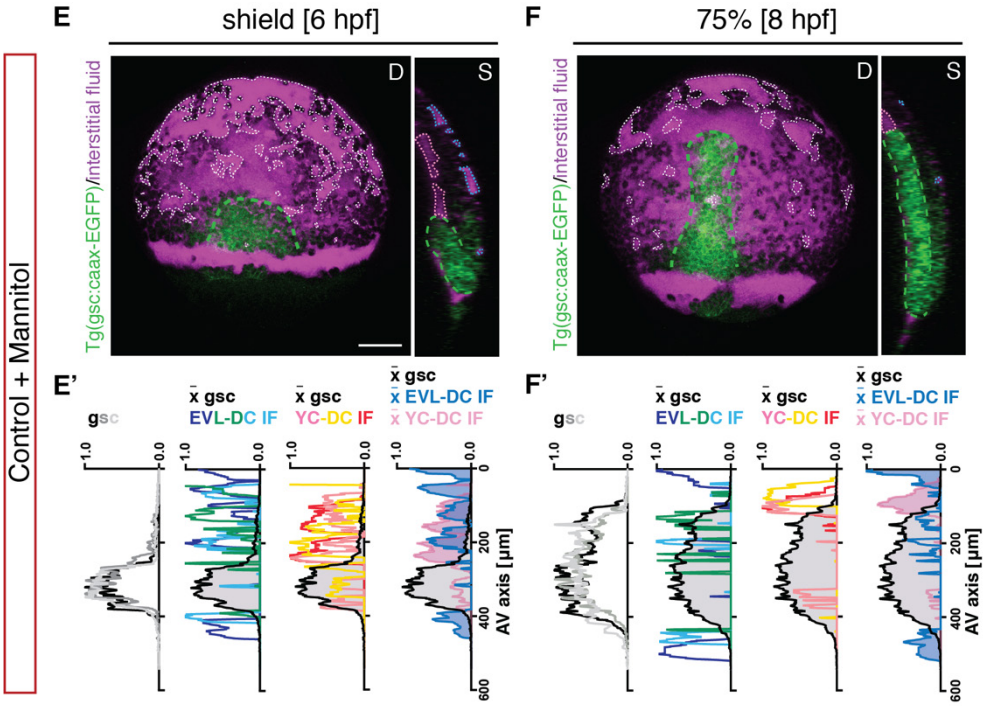

Fig.3.5.2 – Characteristic relocalization pattern depends on the available interstitial fluid amount. Maximum intensity projections (dorsal view, D) and single cross-sections (sagittal view, S) of a transgenic zebrafish embryo expressing gsc::caax-EGFP injected with dextran to label the interstitial fluid (IF) at 6 hpf and 8 hpf in Ouabain treated (**A, B**), Mannitol rescue (**C, D**), and Mannitol-injected control embryos (**E, F**). Scale bar, 100 um. IF distribution profiles along the AV axis relative to the position of *ppl*/*pam*, indicated by the expression of *goosecoid* (*gsc*) at 6 hpf and 8 hpf in Ouabain treated (**A'**, **B'**), Mannitol rescue (**C'**, **D**), and Mannitol-injected control embryos (**E'**, **F'**). Multi-color curves show 3 representative replicates of IF distribution at the EVL-DC (cold colors) and YC-DC (warm colors) interface, averaged in the last panel. Analysis as in *Fig.3.3.1*.

3.6 IF accumulations are required for enabling *ppl* migration

Being able to modulate IF accumulations within the blastoderm, we next asked whether and how IF accumulation in front of the advancing *ppl* progenitors affects their migration towards the animal pole of the gastrula. Prior to internalization, marginal tissue at the dorsal side slightly thickens, forming a characteristic structure – the embryonic shield, one of the first signs of dorsoventral[16] polarity in the zebrafish embryo, followed by the animal-directed migration of *ppl* progenitors and establishment of the body axis[7,19]. Embryos exposed to 1 mM Ouabain from 1-3 hpf to block IF accumulation within the blastoderm showed a pronounced thickening at the position of the embryonic shield (Fig. 3.6.1.A, B, B''). Morphogenetic events preceding internalization, such as EVL epiboly and blastoderm thinning, were unaffected by Ouabain treatments (Fig. 3.6.1.A-A'). This local thickening of the germ ring was due to internalizing *ppl* progenitors failing to migrate away and, consequently, piling up at the margin where internalization occurs (Fig. 3.6.1.B', blue).

To test whether this failure in *ppl* progenitor cell migration is due to Ouabain blocking IF accumulation within the blastoderm, we restored IF accumulation by injecting 0.5

[16] An axis defining the front and the back of the future animal.

nL of 400 mM Mannitol into the extracellular space in Ouabain-treated embryos. Mannitol injection not only restored IF accumulation ahead of the advancing *ppl* progenitors (Fig. 3.6.1.B) but also their migration away from the germ margin (Fig. 3.6.1.B', yellow)

In contrast, increasing IF accumulations within the blastoderm above control levels by injecting Mannitol in untreated embryos had no recognizable effect of germ ring morphology or *ppl* progenitor cell migration (Fig. 3.6.1.A-B'', red). This suggests a permissive function of IF accumulation in front of the internalized *ppl* progenitors for their migration away from the germ ring margin towards the animal pole.

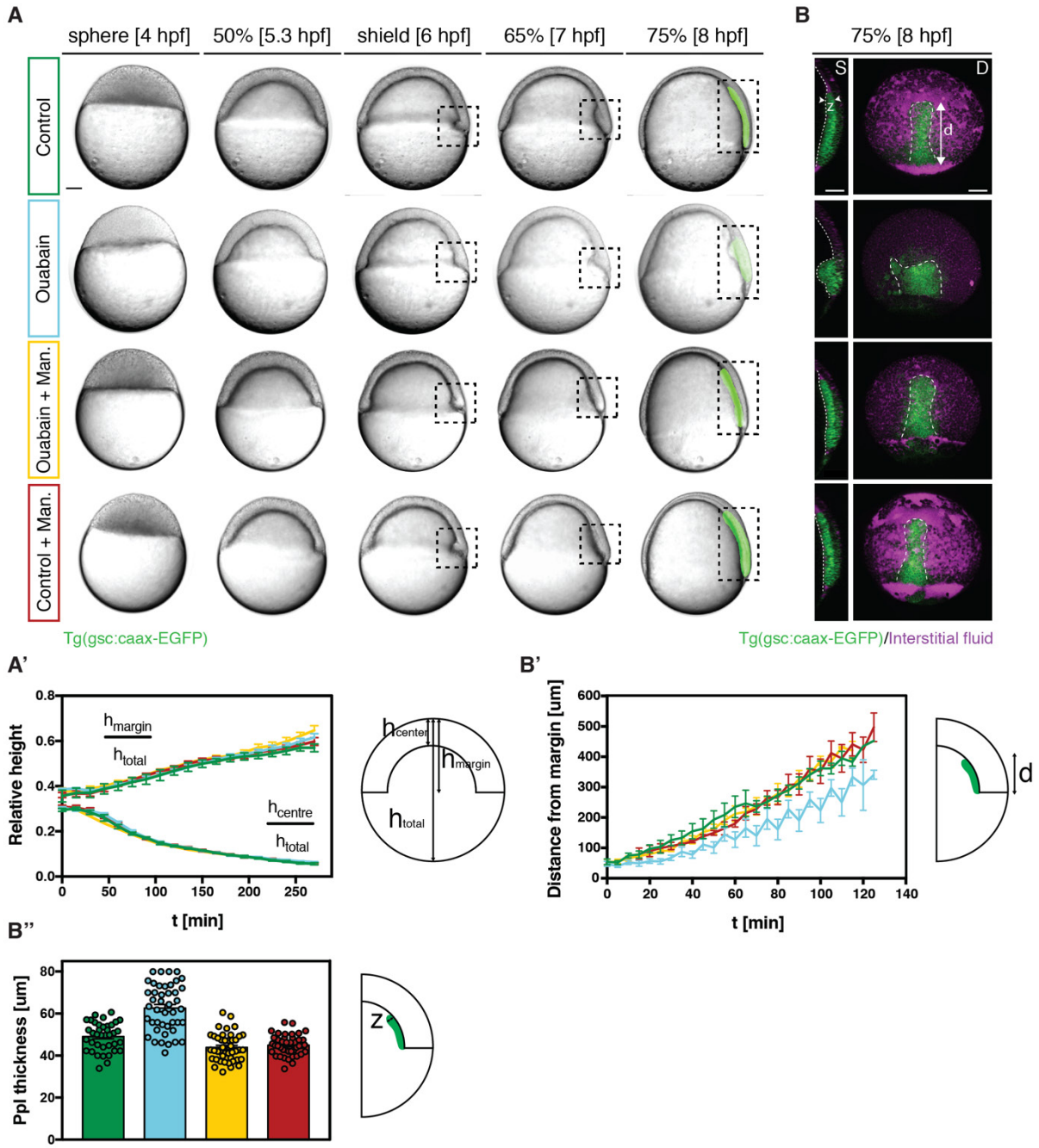

Fig.3.6.1 – Interstitial fluid accumulations are required for enabling *ppl* migration. (**A**) Bright-field (4–8 hpf) and fluorescence (8 hpf) images of transgenic zebrafish embryos expressing gsc::caax-EGFP

in 4 experimental conditions: control (green), Ouabain treated (blue), Mannitol rescue (yellow), and Mannitol-injected control embryos (red). Dashed rectangle highlights the zone of axial mesendoderm internalization. Scale bar, 100 um. (**A'**) Quantification of blastoderm thinning and EVL spreading in control (n = 4), Ouabain treated (n = 6), Mannitol rescue (n = 7), and Mannitol-injected control embryos (n = 6). (**B**) Single cross-section (sagittal view, S) and maximum intensity projections (dorsal view, D) of a transgenic zebrafish embryo expressing gsc::caax-EGFP injected with dextran to label the interstitial fluid (IF) at 6 hpf and 8 hpf in control (green), Ouabain treated (blue), Mannitol rescue (yellow), and Mannitol-injected control embryos (red). Scale bar, 100 um. *d* indicates the distance from the germ margin, quantified in (**B'**), and *z* indicates the *ppl* thickness, quantified in (**B''**). (**B'**) Distance of the *ppl* leading edge from the germ margin from the onset of internalization (0' is 6 hpf) for control (N = 9, n = 9), Ouabain treated (N = 8, n = 9), Mannitol rescue (N = 5, n = 6), and Mannitol-injected control embryos (N = 4, n = 4). (**B''**) *Ppl* thickness quantification from 6–8 hpf in control (N = 2, n = 4), Ouabain treated (N = 2, n = 4), Mannitol rescue (N = 2, n = 4), and Mannitol-injected control embryos (N = 2, n = 4). n, number of embryos. Data are mean ± SEM.

3.7 IF accumulations at the leading edge enable *ppl* polarization

To understand why IF accumulation ahead of the advancing *ppl* progenitors is required for their normal migration, we analysed *ppl* cell morphology and movement in Ouabain-treated versus control embryos. Once internalized, the leading *ppl* progenitors typically elongate in the direction of the animal pole and form various types of cell protrusions [17] at their leading-edge, including lamellipodia, filopodia and blebbs[21,91] (Fig. 3.7.1.A-D).

Initially, when the yolk cell and the overlying DCs are still adjacent, and no IF accumulation can be detected ahead, the leading-edge of the *ppl* progenitors is smooth with occasional blebs (Fig. 3.7.1.B-C, 0-20'), schematised in Fig. 3.7.1.A. Coinciding with the IF accumulation at this interface, the leading-edge increase in roughness and frequent filopodia and lamellipodia were detected extending in the direction of the animal pole (Fig. 3.7.1.B-C, >20', D). The formation of these protrusions precisely coincided with the accumulation of IF in front of the internalized *ppl* progenitors and was strongly reduced in Ouabain-treated embryos (Fig. 3.7.1.B-D).

[17] Cellular extensions used e.g. for cell adhesion, mechanically probing the environment and/or generating contacts in order to displace the cell body.

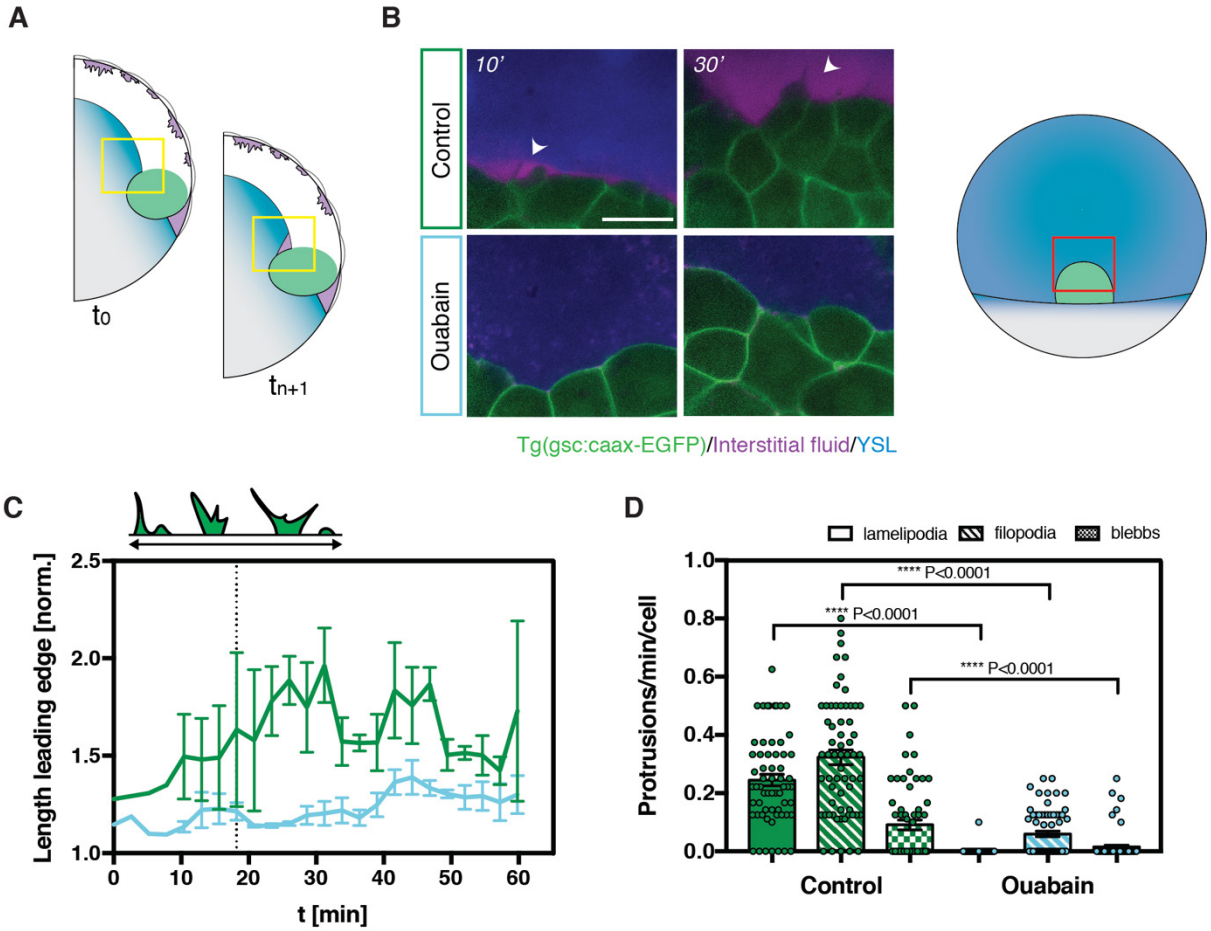

Fig.3.7.1 - IF accumulations at the leading edge enable *ppl* polarization. (**A**) Schematic illustrating the sagittal section of the yolk syncytial layer (YSL) labelled (blue) zebrafish embryo at the onset of mesendoderm internalization. The yellow rectangle highlights the accumulation of interstitial fluid (IF) between the yolk cell/YSL and the overlying deep cells/epiblast, ahead of the prechordal plate (*ppl*) leading edge at the onset of internalization. (**B**) High resolution imaging of the *ppl* leading edge from the dorsal view (the orientation of imaging highlighted by the red rectangle) at the onset of *ppl* internalization in control and Ouabain treated embryos. Arrowhead highlights the extrusion of a long filopodium and lamellipodium in a direction of cell migration. Scale bar, 20 um. (**C**) Quantification of the *ppl* leading edge length in control (N = 3) and Ouabain treated (N = 3) embryos. (**D**) Filopodia, lamellipodia, and blebb count per time frame, normalized for the number of cells in control (N = 3) and Ouabain treated (N = 3) embryos. Individually plotted values represent individual protrusion count per minute and per cell. N, number of embryos. Data are mean ± SEM. Mann-Whitney test.

To test whether this reduction of *ppl* cell protrusion formation in Ouabain-treated embryos was due to Ouabain blocking IF accumulations and not other, potentially more direct effects, we dissected primary *ppl* cells from Ouabain-treated embryos (1-3 hpf), plated them on Fibronectin-coated substrate, and compared their spreading ability to control *ppl* cells, schematised in (Fig. 3.7.2.A).

Thereby, we tested if the Ouabain treatment renders the cells incapable of polarizing and spreading in culture, unconstrained by the embryonic environment. Despite the large variability of cellular behaviors in such artificial conditions, Ouabain-treated cells still managed to polarize and spread, resembling the non-treated cells (Fig. 3.7.2.A'-A''), suggesting that Ouabain does not directly interfere with *ppl* cell protrusion formation.

Finally, to test whether Ouabain treatment might affect *ppl* cell migration by affecting *ppl* cell fate specification, we analysed the expression of *goosecoid* (*gsc*), a characteristic marker gene of *ppl* cell fate specification[232], in Ouabain-treated and control embryos. The expression of *gsc* in *ppl* progenitor cells was unchanged in Ouabain-treated embryos (Fig. 3.7.2.B-B''), suggesting that Ouabain does not affect *ppl* cell fate specification. Collectively, these results suggest that the IF accumulation in front of migrating *ppl* cells is required for their protrusion formation and migration away from the germ ring margin towards the animal pole.

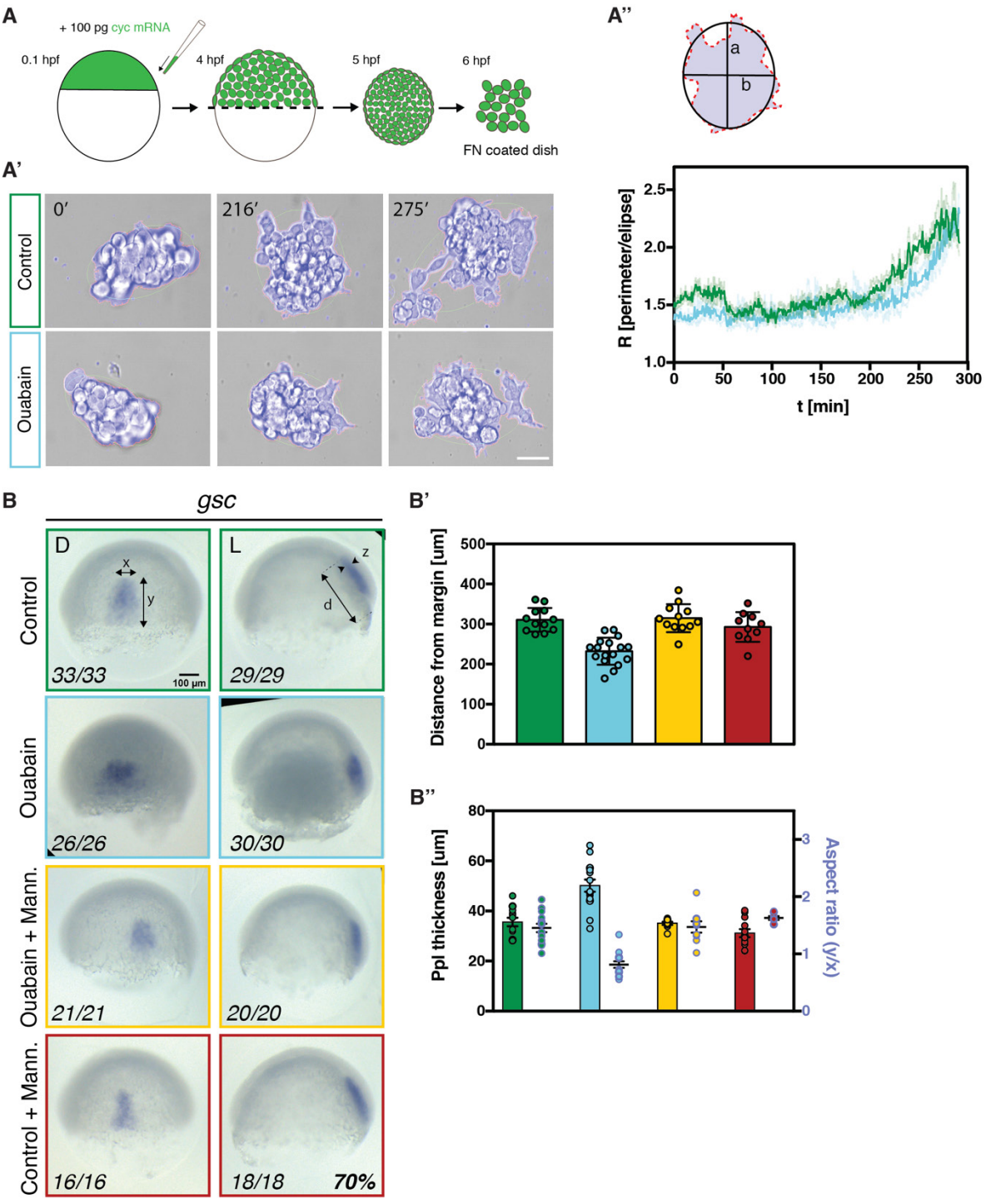

Fig.3.7.2 – Ouabain treatments do no directly inhibit cell spreading and *ppl* cell fate specification. (**A**) Schematic illustrating the steps of the *in vitro* cell spreading assay. (**A'**) Representative bright-field images of control and Ouabain treated *ppl* cell clusters on the fibronectin (FN) coated glass coverslip, before (0'), at the onset (216'), and during cell spreading (275'). Cell perimeter (red line) was measured and the ellipse (green line) was fitted to the same area (purple). Scale bar, 50 um. (**A''**) Quantification of *ppl* cell spreading of control (N = 6) and Ouabain treated (N = 5) *ppl* cell clusters by normalizing the cell cluster perimeter to the fitted ellipse. Data are mean ± SEM. (**B**) Whole mount in situ hybridization (WMISH) with RNA antisense probe against the *ppl* cell fate specification marker *goosecoid* (*gsc*) in 4 experimental conditions at ~7 hpf. The left column is the dorsal view, D, highlighting the aspect ratio of the *gsc* positive domain, quantified in (**B''**). The right column is the lateral view, L, highlighting the distance from the margin, *d*, quantified in (**B'**) and *ppl* thickness, *z*, quantified in (**B''**). (**B'-B''**) Control (N=12), Ouabain (N=17), Ouabain+Mann. (N=12), Control+Mann. (N=10). Scale bar, 100 um. Data are mean ± SEM. WMISH was performed by Alexandra Schauer.

3.8 Axial mesendodem is required for IF relocalization from the EVL-DC to YC-DC interface

The observation that IF relocalization from the EVL-DC to the YC-DC interface ahead of the *ppl* leading edge is required for proper *ppl* progenitor cell protrusion formation and migration raises questions about the mechanism underlying this IF relocalization. One possibility is that *ppl* internalization and animal-directed migration locally triggers this IF relocalization by squeezing in between the YC and DC layer (epiblast), thereby pushing the epiblast up against the EVL. This would eventually squeeze out the IF from the EVL-DC interface, resulting in IF flowing through the DC layer towards the YC-DC interface.

To test this hypothesis, we asked whether this IF relocalization would occur when *ppl* progenitor cell internalization and animal-directed migration are impaired. To this end, we first turned to maternal-zygotic *one-eyed pinhead* mutant embryos (*MZ*oep*)*, which are defective in mesendoderm specification and germ layer formation[33]. In *MZ*oep mutants, IF largely remained at the EVL-DC interface, and only small IF fragments appeared at the YC-DC interface at the time when spatially restricted IF relocalization was observed in wildtype and rescued embryos (Fig. 3.8.1A-E', 6-7.5 hpf).

At later stages of gastrulation (7-8 hpf), however, some IF accumulation at the YC-DC interface was observed in *MZ*oep mutants, but unlike wildtype embryos where IF specifically accumulated from the margin, in *MZ*oep mutants, the accumulation was detected only at the animal pole (Fig. 3.8.1F). This suggests that mesendoderm specification and internalization is required for proper IF relocalization at the dorsal side at the onset of gastrulation.

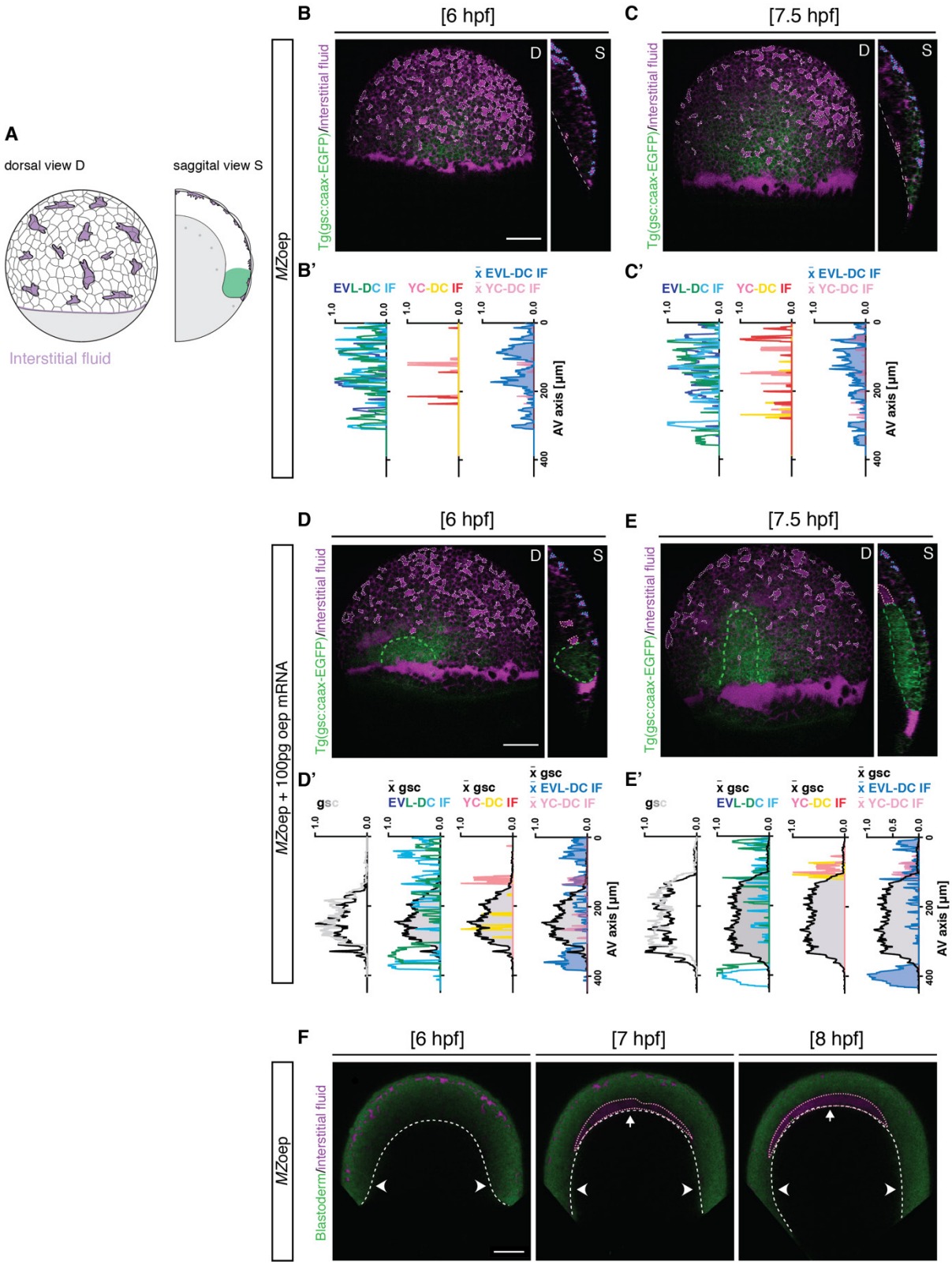

Fig.3.8.1 - Axial mesendodem is required for interstitial fluid relocalization from the EVL-DC to YC-DC interface. (**A**) Schematic illustrating the morphology of an *MZ*oep mutant embryo. Together with the absence of mesendoderm internalization, no interstitial fluid (IF) can be detected at the YC-DC interface, and residual IF can be found at the EVL-DC interface. (**B, C**) Maximum intensity projections (dorsal view, D) and single cross-sections (sagittal view, S) of an *MZ*oep mutant transgenic zebrafish embryo expressing gsc::caax-EGFP, and (**D, E**) oep mRNA rescued embryos injected with dextran to label the IF at 6 hpf and 7.5 hpf. Scale bar, 100 um. (**B'**, **C'**) IF distribution profiles along the AV axis on the dorsal side, where the *ppl*/*pam* is positioned in the rescue embryos, indicated by the expression of

goosecoid (*gsc*) at 6 hpf and 7.5 hpf (**D'**, **E'**). Multi-color curves show 3 representative replicates of IF distribution at the EVL-DC (cold colors) and YC-DC (warm colors) interface, averaged in the last panel. Analysis as in *Fig.3.3.1*. (**F**) Characteristic IF relocalization pattern in *MZ*oep mutant embryos from 6–8 hpf, absent from the germ margin (arrowhead) and accumulating directly at the animal pole (arrow). Scale bar, 100 um.

3.9 Axial mesendoderm thickness controls the efficiency of IF relocalization

To further test whether the amount of axial mesendoderm internalization determines the extent of IF relocalization, as expected if mesendoderm would mechanically trigger this relocalization, we analysed IF relocalization in *cyclops (cyc)* morphant[18] embryos, where the amount of internalizing *ppl* progenitors is reduced[59].

In *cyc* morphant embryos, IF relocalization from the EVL-DC interface to the YC-DC interface ahead of the *ppl* leading edge was still detectable (Fig. 3.9.1B-C'). However, the extent to which this relocalization occurred was greatly diminished, closely matching the reduction in internalizing *ppl* progenitors found in *cyc* morphant embryos (Fig. 3.9.1C-C'). Interestingly, variable *ppl* and posterior axial mesendoderm (pam) morphology in *cyc* morphants additionally supported the hypothesis of *ppl* induced IF relocalization, as locally fragmented *ppl*/pam failed to efficiently relocalize the IF from EVL-DC interface (Fig. 3.9.1D-D'). Collectively, these observations suggest that *ppl/pam* specification and internalization are causatively linked to the IF relocalization from the EVL-DC to the YC-DC interface, ahead of the internalizing cells.

[18] An organism which has been injected with a morpholino antisense oligo (MO) to temporarily knock down expression of a targeted gene.

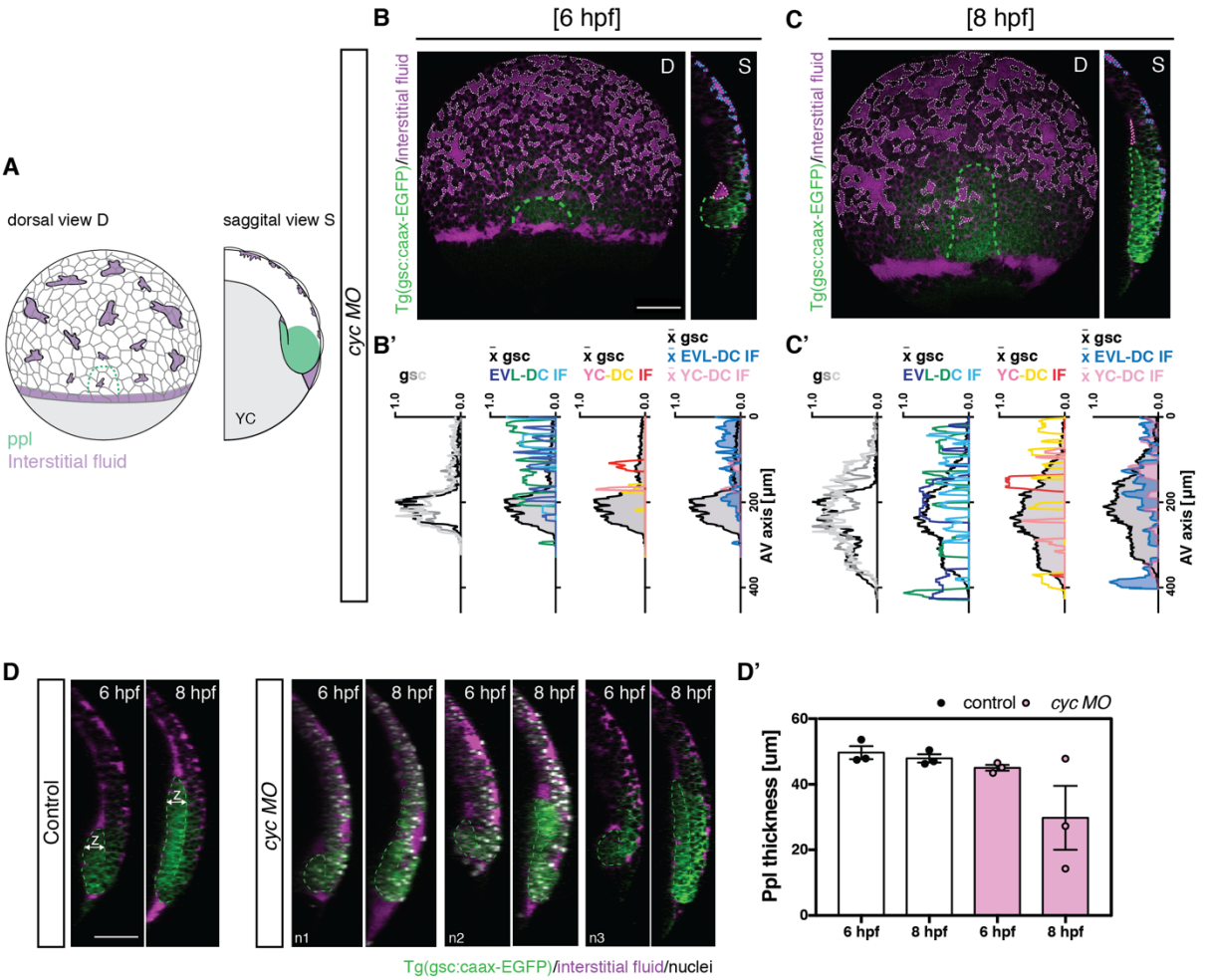

Fig.3.9.1 - Axial mesendoderm thickness controls the efficiency of IF relocalization. (**A**) Schematic illustrating the morphology of a *cyclops* (*cyc*) morphant embryo. Due to decreased amount of internalizing *ppl* cells residual IF can be found at the EVL-DC interface. (**B, C**) Maximum intensity projections (dorsal view, D) and single cross-sections (sagittal view, S) of a *cyc* morphant transgenic zebrafish embryo expressing gsc::caax-EGFP injected with dextran to label the IF at 6 hpf and 8 hpf. Scale bar, 100 um. (**B'**, **C'**) IF distribution profiles along the AV axis relative to the position of *ppl*/*pam*, indicated by the expression of *goosecoid* (*gsc*) at 6 hpf and 8 hpf. Multi-color curves show 3 representative replicates of IF distribution at the EVL-DC (cold colors) and YC-DC (warm colors) interface, averaged in the last panel. Analysis as in *Fig.3.3.1*. (**D**) A sagittal cross-section of a transgenic zebrafish embryo expressing gsc::caax-EGFP and 3 representative replicates of the variable *ppl* morphology in *cyc* morphant embryos injected with dextran to label the IF at 6 hpf and 8 hpf. *z* highlights the thickness of the *ppl*. Scale bar, 100 um. (**D''**) Quantification of the *ppl* thickness at 6 and 8 hpf in control (n = 3) and *cyc* morphant (n = 3) embryos. Data are mean ± SEM.

3.10 *Ppl* is sufficient to induce IF relocalization required for its animal pole-directed migration

Next, we asked whether *ppl* cell internalization is not only required but also sufficient for IF relocalization from the EVL-DC to the YC-DC interface. To that end, we sought to rescue IF relocalization in *MZ*oep mutant embryos, lacking mesendoderm specification and internalization[33], by transplanting a cluster of *ppl* cells (~15-20 cells) from a wildtype donor embryo to the YC-DC interface, close to the germ margin, of an *MZ*oep host embryo, schematised in (Fig. 3.10.1A). In transplanted *MZ*oep embryos, IF accumulated at the YC-DC interface surrounding the transplanted *ppl* cell cluster,

accompanied by a local IF depletion from the EVL-DC interface, directly above the transplanted cluster (Fig. 3.10.1B-C').

Notably, the transplanted *ppl* cell cluster, while being uniformly surrounded by IF at the YC-DC interface, still displayed directed migration away from the germ margin towards the animal pole (Fig.3.10.1B, C, F). This suggests that *ppl* cell internalization is sufficient to trigger IF relocalization from the EVL-DC to the YC-DC interface, but also that this relocalization does not provide positional cues required for directed *ppl* cell migration.

To further test whether IF accumulation around the transplanted cluster is required for animal-directed *ppl* cell migration, as found in wildtype (wt) embryos, we inhibited IF accumulation in host *MZ*oep embryos by exposing them to 1mM Ouabain during IF formation (1-3 hpf). When a *ppl* cell cluster from an untreated wt embryo was transplanted to the YC-DC interface of a Ouabain-treated *MZ*oep host, no clear IF relocalization to the YC-DC interface around the transplanted cell cluster was observed at shield and mid-gastrulation stages (Fig.3.10.1D-E'). This lack of proper IF accumulation was accompanied by transplanted *ppl* cells failing to efficiently migrate away from the germ margin towards the animal pole (Fig.3.10.1F, dark blue).

To exclude that the inability of *ppl* cells to undergo directed migration in Ouabain-treated *MZ*oep embryos is not due to Ouabain directly affecting the migratory capability of the transplanted *ppl* cells, we asked whether *ppl* cells can undergo directed migration when transplanted from a Ouabain-treated wt donor embryo into an untreated *MZ*oep host embryo. We found that *ppl* clusters from Ouabain-treated donors migrated towards the animal pole similar to non-treated transplanted *ppl* cells (Fig.3.10.1F, light green). In contrast, when *ppl* cells from Ouabain-treated donors were transplanted into Ouabain-treated *MZ*oep hosts, transplanted cells failed to efficiently migrate towards the animal pole (Fig.3.10.1F, light blue). This suggests that Ouabain treatment does not directly interfere with the ability of *ppl* cells to migrate towards the animal pole.

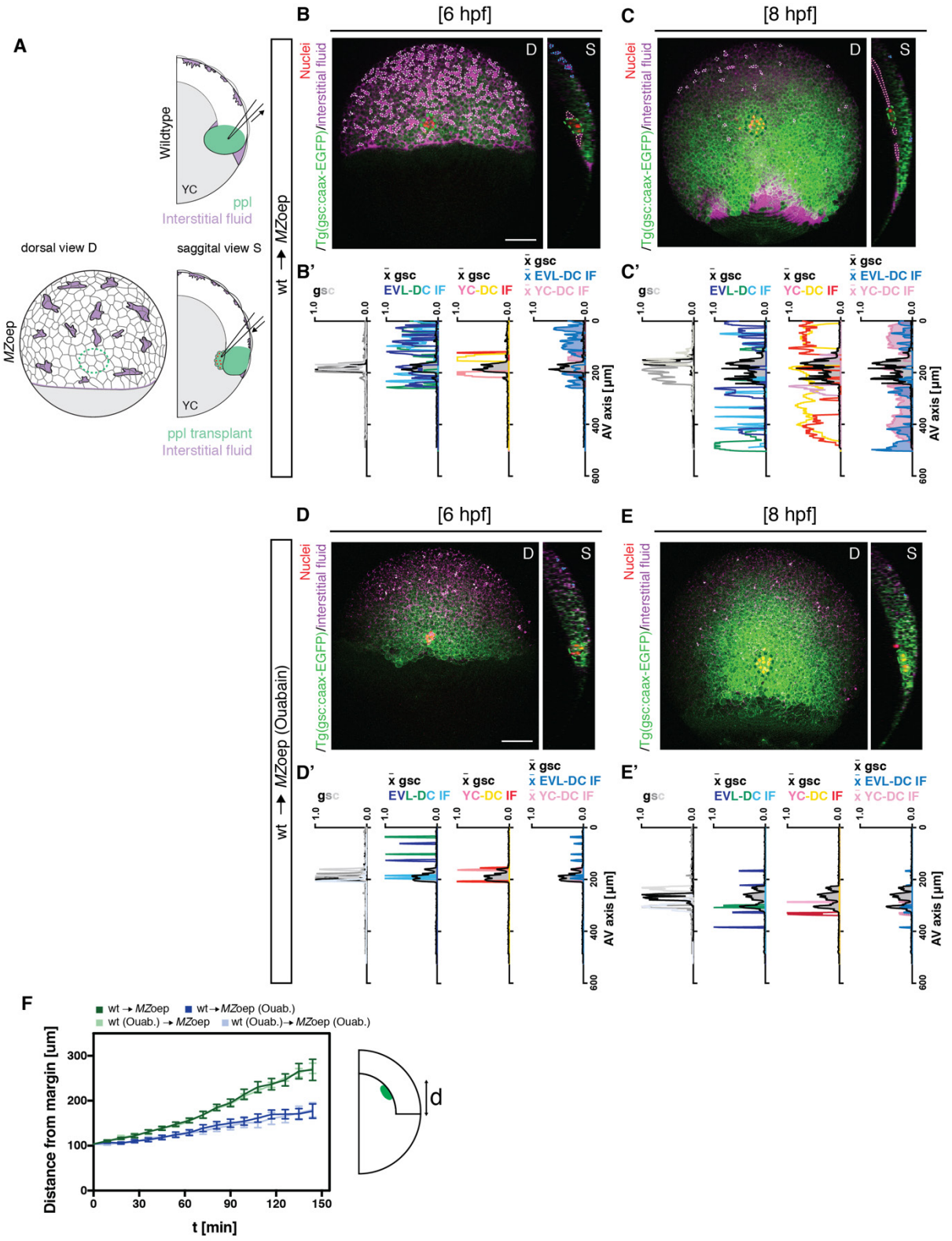

Fig.3.10.1 - *Ppl* is sufficient to induce interstitial fluid relocalization required for its animal pole-directed migration. (**A**) Schematic illustrating the principle of the *ppl* transplantation assay. A cluster of *ppl* cells was aspirated from the margin of a wildtype embryo and transplanted at the yolk cell - deep cell (YC-DC) interface of a control or Ouabain treated *MZ*oep embryo. (**B, C**) Maximum intensity projections (dorsal view, D) and single cross-sections (sagittal view, S) of a control, and Ouabain treated (**D, E**) *MZ*oep mutant transgenic zebrafish embryo expressing gsc::caax-EGFP implanted with a wildtype *ppl* cell cluster and injected with dextran to label the IF at 6 hpf and 8 hpf. The position of the transplant is highlighted by a dashed line (green). Scale bar, 100 um. (**B'**, **C'**) IF distribution profiles

along the AV axis relative to the position of the transplanted *goosecoid* (*gsc*) expressing *ppl* cell cluster at 6 hpf and 8 hpf in control and Ouabain treated (**D', E'**) *MZ*oep host embryos. Multi-color curves show 3 representative replicates of IF distribution at the EVL-DC (cold colors) and YC-DC (warm colors) interface, averaged in the last panel. Analysis as in *Fig.3.3.1*. (**F**) Distance of the *ppl* transplant leading edge from the germ margin as a function of developmental time (0' is 6 hpf) for control *ppl* donors into control *MZ*oep hosts (wt→*MZ*oep) (N = 6, n = 6), control *ppl* donors into Ouabain treated *MZ*oep hosts (wt→*MZ*oep (Ouab.) (N = 6, n = 9), Ouabain treated *ppl* donors into control *MZ*oep hosts (wt (Ouab.)→*MZ*oep (N = 4, n = 4), and Ouabain treated *ppl* donors into Ouabain treated *MZ*oep hosts (wt (Ouab.)→*MZ*oep (Ouab.) (N = 2, n = 2). Data are mean ± SEM. *Ppl* transplantation was performed by Diana Pinhero.

3.11 Defective *ppl* cell polarization results from the absence of environmental IF accumulation

Finally, to determine whether the inability of transplanted *ppl* cells in Ouabain-treated *MZ*oep host embryos to undergo directed migration was due to defective IF relocalization to the YC-DC interface affecting *ppl* cell protrusion formation, as found in wildtype embryos (Fig.3.7.1A-D), we analyzed protrusion formation of the transplanted cells. While *ppl* cells transplanted into untreated control, *MZ*oep host embryos formed filopodia and lamellipodia preferentially oriented towards the free, IF-filled space, no such oriented protrusion was detectable in *ppl* cells transplanted into Ouabain-treated host embryos lacking IF relocalization (Fig.3.11.1A, B', C').

In addition, the total number of filopodia and lamellipodia formed by transplanted *ppl* cells was clearly reduced in treated compared to untreated *MZ*oep host embryos (Fig.3.11.1A-B, C), suggesting that, similar to the situation in wildtype embryos, defective IF relocalization in Ouabain-treated *MZ*oep host embryos interferes with the directed migration of transplanted *ppl* cells by impairing both protrusion formation and orientation.

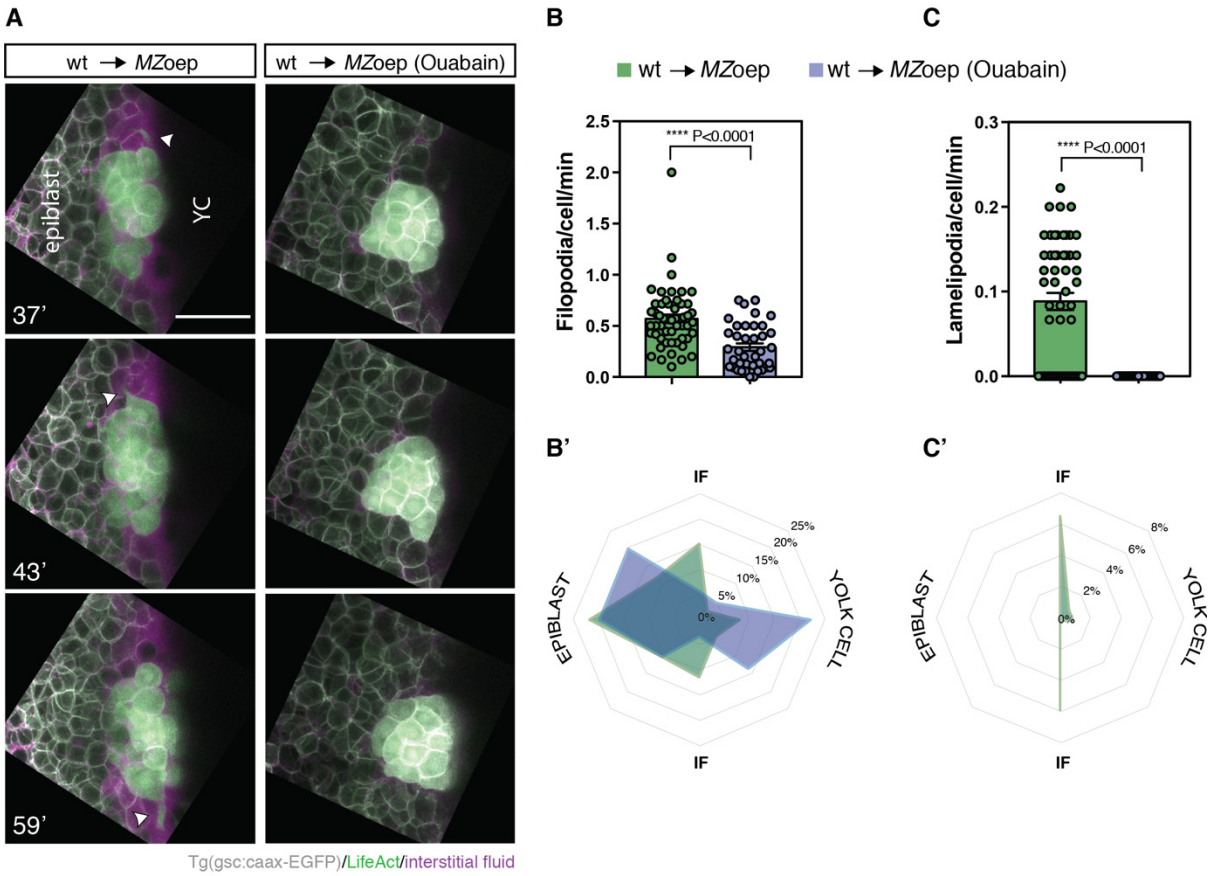

Fig.3.11.1 - Defective *ppl* cell polarization results from the absence of interstitial fluid accumulation. (**A**) High resolution images of transplanted *ppl* cell clusters expressing LifeAct-RFP to characterize their protrusive activity in control and Ouabain treated *MZ*oep host embryos. Arrowheads highlight the extrusions of large protrusions towards the free, interstitial fluid-filled space around the transplant. Scale bar, 50 um. (**B-B'**) Quantification of the number and orientation of filopodia and lamellipodia (**C-C'**) in control (N = 3) and Ouabain treated (N = 3) host embryos. Individually plotted values represent individual protrusion count per minute and per cell. N, number of embryos. Data are mean ± SEM. Mann-Whitney test. *Ppl* transplantation was performed by Diana Pinhero.

3.12 *Ppl* cells exert a mechanical push onto the overlying epiblast to efficiently relocalize the interstitial fluid

Our finding that the *ppl* cell cluster can itself trigger IF relocalization from the EVL-DC to the YC-DC interface raises questions about the mechanism(s) by which this highly orchestrated IF relocalization is achieved. One possibility is that the *ppl*, by squeezing in between the YC and DCs (epiblast), pushes up and compacts the overlying DC layer, thereby triggering the IF flow in the opposite direction – from the EVL-DC to the YC-DC interface.

To address this hypothesis, we analyzed the extent of DC movements along the radial axis within the epiblast adjacent to the *ppl*, schematised in (Fig.3.12.1A). We detected a pronounced outward radial movement of DCs above the *ppl*, which gradually propagated in direction to the animal pole as the *ppl* moved in that direction (Fig.3.12.1B-B', D, dotted line, top - *ppl* leading-edge; bottom – pam trailing edge). This outward radial movement of DC was accompanied by IF accumulating in front of

the migrating *ppl* (Fig,3.12.1B', magenta dashed line), suggesting that these processes are spatiotemporally linked.

To test whether they are also causatively linked, we turned to *MZ*oep mutants lacking *ppl* cell specification/migration and proper IF accumulation at the YC-DC interface (Fig. 3.8.1A-C'). No clearly recognizable radial movement of DCs was detected in *MZ*oep embryos (Fig.3.12.1C-C', D), suggesting that *ppl* cells moving in between the YC and the DCs (epiblast) push the epiblast upwards and, consequently, relocalize the IF from the EVL-DC to the YC-DC interface.

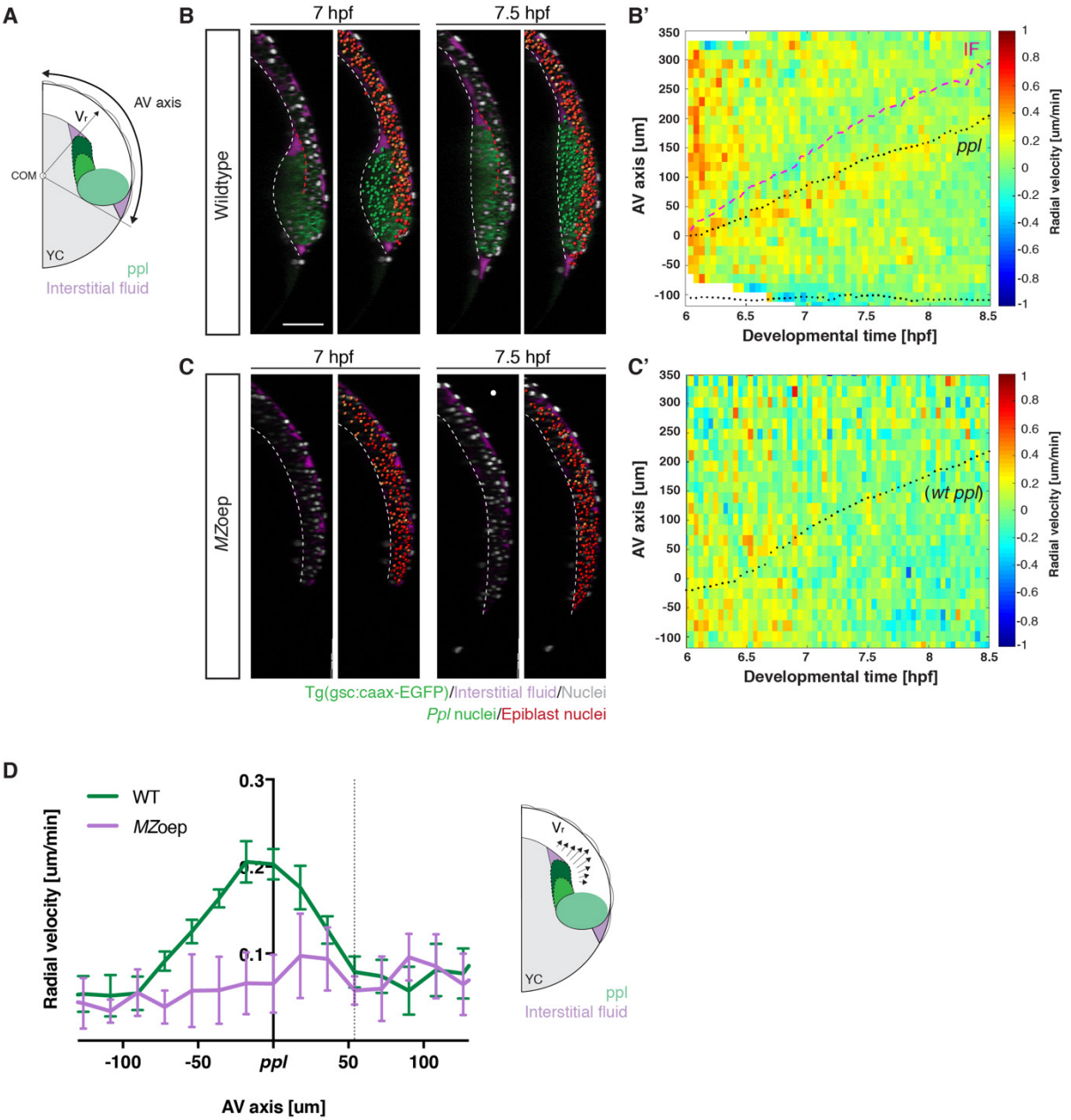

Fig.3.12.1 - *Ppl* cells exert a mechanical push onto the overlying epiblast to efficiently relocalize the interstitial fluid. (**A**) Schematic illustrating the analysis of radial displacement of the deep cell/epiblast (DC) as a function of *ppl* cell migration. (**B**) A sagittal cross-section of a transgenic zebrafish embryo expressing gsc::caax-EGFP, raw data (left panel) and 3D rendering and tracking of *ppl* (green spheres) and DC/epiblast (red spheres) at 7 and 7.5 hpf. Red dashed line highlights the deformation in

the DC/epiblast induced by the *ppl* leading edge. Scale bar, 100 um. (**B'**) Representative heatmap of radial displacement of the DC/epiblast along the animal-vegetal (AV) axis as a function of developmental time in wildtype embryos. The extent of radial velocity is color-coded. Dotted black lines indicate the *ppl* leading edge (top) and the position of axial mesendoderm internalization (bottom). Dashed magenta line indicates the position of the interstitial fluid (IF) ahead of the *ppl* leading edge. (**C**) A sagittal cross-section of an MZoep mutant transgenic zebrafish embryo expressing gsc::caax-EGFP, raw data (left panel) and 3D rendering and tracking of the DC/epiblast (red spheres) at 7 and 7.5 hpf. (**C'**) Representative heatmap of radial displacement of the DC/epiblast along the animal-vegetal (AV) axis as a function of developmental time in *MZ*oep embryos. The extent of radial velocity is color-coded. Dotted black line indicates the position of *ppl* leading edge superimposed from an average value of *ppl* position in wildtype embryos. (**D**) Average radial velocity of DC/epiblast relative to the *ppl* position in wildtype (N = 4) and *MZ*oep embryos (N = 3). Dashed line at ~50um indicated a propagation of the pushing force up to 50 um ahead of the *ppl* leading edge. Data are mean ± SEM. Analysis was performed in collaboration with Shayan Shamipour.

3.13 IF relocalization occurs as a flow through the epiblast induced by a mechanical push from the underlying *ppl*

For the *ppl*-triggered IF flow from the EVL-DC to the YC-DC interface, the DC layer must remain sufficiently porous during the relocalization process to allow for such flows to happen. To address this requirement, we analyzed spatiotemporal changes in DC layer compaction and porosity during *ppl* cell movement by measuring the fraction of IF between the DC, schematised in (Fig.3.13.1A). We found that the DC layer (epiblast) adjacent to the *ppl* is devoid of IF, to a similar extent as the *ppl* itself, while the epiblast layer ahead of the *ppl* is considerably more porous (Fig.3.13.1A'). This suggests that the epiblast layer ahead of the advancing *ppl* meets the requirement for allowing the potential flow-through during IF relocalization.

To directly monitor whether the IF flows through the DC/epiblast layer in order to relocalize from the EVL-DC to the YC-DC interface, we labelled the IF with a photoactivatable dye (DMNB-caged fluorescein) and locally uncaged it with a UV laser, generating a source at the EVL-DC interface above and ahead of the *ppl* at the onset of internalization, schematised in (Fig.3.13.1B). We then followed the redistribution of those locally generated fluorescent tracers during *ppl* animal-directed migration (Fig.3.13.1B'). As a control, we performed the same experiment in *MZ*oep mutant embryos, lacking *ppl* specification/migration and proper IF relocalization. With the onset of *ppl* internalization and animal-directed migration in wildtype embryos, the fluorescent tracer relocalized from the source at the EVL-DC interface to the place of IF accumulation at the YC-DC interface directly ahead of the migrating *ppl* (Fig.1.13.1B-B'). No such pronounced relocalization of the fluorescent tracer was observed in *MZ*oep embryos (Fig.1.13.1B-B', $\alpha_{wt}=0.0134 > \alpha_{MZoep}=0.0066$), lacking IF relocalization, suggesting that the relocalization of IF and fluorescent tracer accumulation are coupled processes. Together, these findings support the notion that IF is relocalized from the EVL-DC to the YC-DC interface as a result of *ppl* internalization and migration.

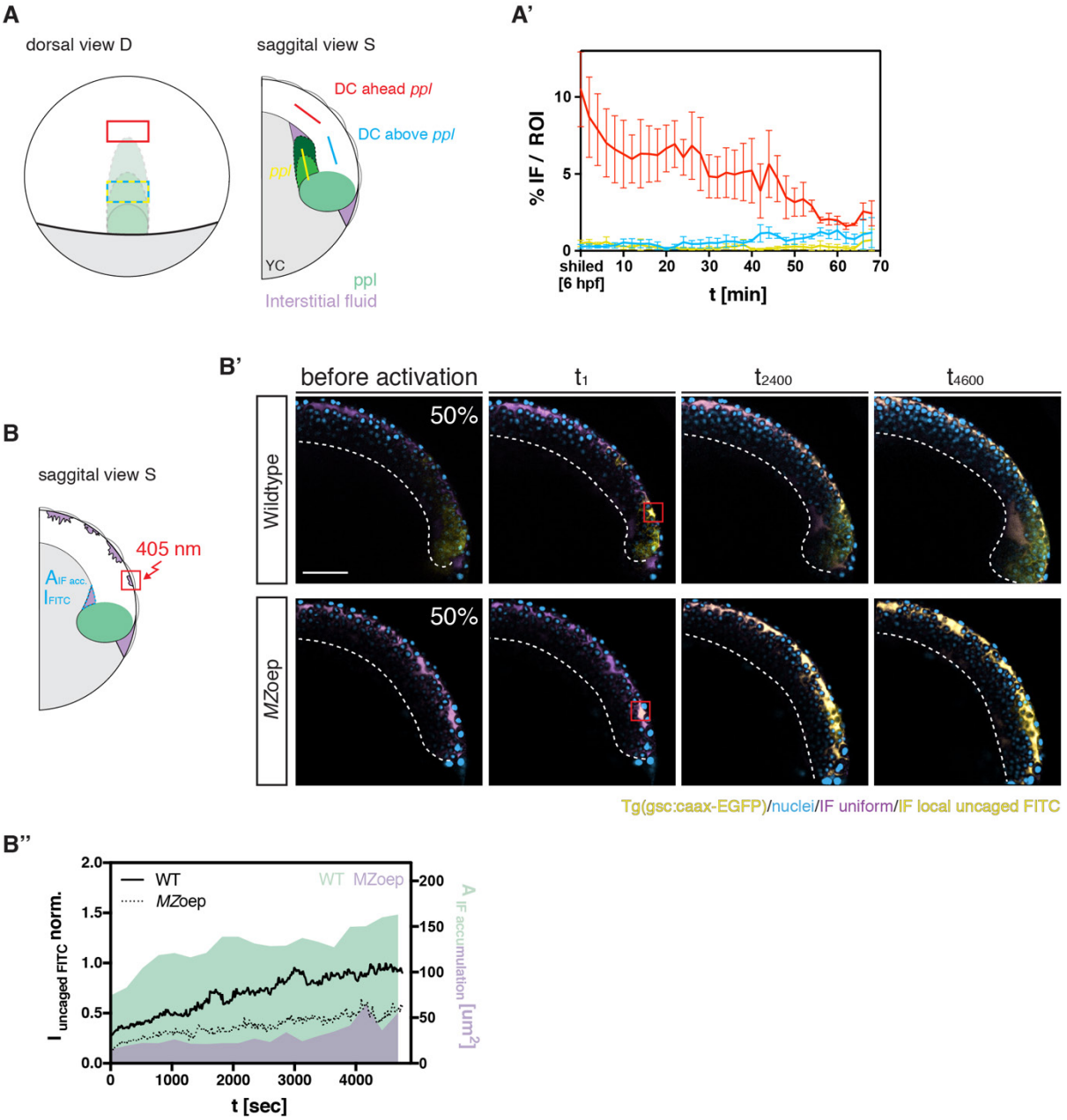

Fig.3.13.1 – Interstitial fluid relocalization occurs as a flow through the epiblast induced by a mechanical push from the underlying *ppl*. (**A**) Schematic illustrating the principle of interstitial fluid (IF) fraction analysis within the DCs ahead of the *ppl* (red), DCs above the *ppl* (blue) and within the *ppl* (yellow), quantified in a region of interest (ROI) of 4000 um^2 (**A'**). (**B**) Schematic illustrating the principle of local photoactivation of a caged fluorescent dye within the IF at the EVL-DC interface (red rectangle) and measuring the rate of IF accumulation at the YC-DC interface (blue outline). (**B'**) Lateral view of the wildtype and *MZ*oep transgenic embryos expressing gsc::caax-EGFP injected with Alexa647 conjugated dextran to uniformly label the IF and caged-FITC to induce a local source within the IF at the onset of internalization in wildtype embryos. The red rectangle highlights the ROI of local FITC activation. Scale bar, 100 um. (**B''**) Quantification of the IF accumulation rate at the YC-DC interface by measuring the IF accumulation area (right y axis) and the rate of uncaged FITC accumulation (left y axis) in wildtype (N = 3) and *MZ*oep (N = 2) embryos.

4 CONCLUSIONS AND DISCUSSION

Our results propose a feedback mechanism between the prechordal plate (*ppl*) induced interstitial fluid relocalization required for proper polarization of leading-edge *ppl* cells and subsequent migration and positioning of axial mesendoderm during gastrulation.

Interstitial fluid accumulations, namely the blastocoel, have long been speculated to play a critical role in gastrulation movements across different species where the onset of gastrulation occurs either within the blastocoel or around it, as seen in, e.g., avian and amphibian embryos, respectively[125,133]. By definition, the blastocoel is a relatively large (often comprising more than 50% of the total embryo volume) central fluid-filled cavity, and it is a frequently seen form of fluid compartmentalization within the early developing organism[98,133,136,228–230]. Due to its significant structural role, interfering with the blastocoel to discriminate the function of the fluid is nearly impossible without interfering with the embryo geometry[125]. Additionally, components of the extracellular matrix (ECM) within the blastocoel were shown to be indispensable for proper gastrulation movements, making it difficult to study the direct impact of interstitial fluid in the context of gastrulation[121].

In zebrafish, due to the presence of a large yolk cell (YC) at the position where the blastocoel would be found in other model systems, no centralized fluid accumulation can be observed. However, some small, irregular fluid-filled pockets have previously been detected within the embryo proper or the blastoderm[18,78]. Furthermore, no ECM components, namely fibronectin, and integrin were found to be expressed at the onset and early progression of gastrulation in the zebrafish embryo[89,94,95]. Together with the necessity of observing live development when studying the function of fluid, zebrafish gastrulation was shown to be an ideal system, circumventing the aforementioned shortcomings.

In this study, we first sought to characterize the spatiotemporal distribution of the interstitial fluid during pre-gastrula and gastrula stages of zebrafish embryonic development, and we found that relocalization of fluid within the blastoderm is highly developmentally orchestrated. With the morphogenetic movements at the onset of epiboly, interstitial fluid preferentially compartmentalized from a relatively uniform distribution within the deep cells (DCs) towards the interface under the enveloping cell layer (EVL) at the surface of the embryo (DC-EVL interface). The exact mechanism of how this relocalization is achieved is unclear but could likely be driven by compaction of the DCs during doming and subsequent accumulation of the interstitial fluid at the lowest adhesion site, namely at the zone of heterotypic cell-cell contacts between the DCs and EVL cells. Strikingly, coinciding with the onset of mesendoderm progenitor internalization at the germ margin, we detected a second, expanding interstitial fluid accumulation as the progenitors internalized and migrated within the region between the yolk cell (YC) and the overlying DCs. Due to relatively constant interstitial fluid

volume throughout gastrulation, we reasoned that this accumulation at the YC-DC interface is merely a redistribution rather than a de-novo interstitial fluid accumulation from external sources. More specifically, we noticed that this highly orchestrated interstitial fluid relocalization is most pronounced at the dorsal side of the gastrula, where the anterior (prechordal plate, *ppl*) and posterior (notochord) axial mesendoderm progenitors internalize as a compact, multilayered tissue and migrate directly towards the animal pole of the gastrula. Such a stereotypical interstitial fluid accumulation ahead of the migrating *ppl* cells leads us to hypothesize its involvement in enabling the directed migration of axial mesendoderm.

To test this, we first sought to find ways to deplete the interstitial fluid and interfere with its formation. Mechanical aspiration was shown to be impossible due to the dispersed nature of interstitial fluid within the blastoderm during the early stages. During later stages, attempts of local fluid aspiration from the YC-DC interface were unsuccessful.

We found that the interstitial fluid forms specifically under the surface cells at 2 hours post-fertilization (hpf), coinciding with the establishment of their basolateral membranes and apicobasal polarization. Together with epithelial polarization, we found a basolateral enrichment of Na^+/K^+-ATPases in the surface cells, as previously seen in mouse trophectoderm (TE), where the activity of those pumps increases the interstitial Na^+ concentration in order to drive the blastocyst expansion[156]. Additionally, water was shown to flow into the blastocyst cavity down the concentration gradient via the aquaporins expressed in the TE[156]. Genetically interfering with the expression or activity of the Na^+/K^+-ATPases and aquaporins was not feasible due to the multiple isoforms of each expressed in early development, but most notably due to the involvement of these components in the oocyte development prior to fertilization[233]. The experimental setup we decided to pursue was to pharmacologically interfere with the Na^+/K^+-ATPase activity in a transient manner by exposing the embryos to 1 mM of Ouabain in a standard embryo medium during the stages of interstitial fluid formation (1-3 hpf). Ouabain is a specific Na^+/K^+-ATPase inhibitor commonly used for preventing the expansion of mouse blastocysts[159,161]. This window of inhibition (1-3 hpf) resulted in a sufficient reduction of interstitial fluid within the blastoderm without affecting the development and morphogenetic movements prior to the onset of gastrulation. Moreover, Ouabain acted by shifting the equilibrium between intra- and extracellular osmolarity, as seen from the rescue experiments, by increasing the extracellular osmolarity with Mannitol injections (referred to as Ouabain rescue experiments). In turn, cells responded to that shift by volume regulation, resulting in cell swelling. Therefore, removing the drug made this effect transient and cellular volume normalized prior to the onset of internalization.
The characteristic phenotype of interstitial fluid depletion became apparent at the onset of mesendoderm progenitor internalization, specifically at the dorsal side, where a prominent interstitial fluid accumulation precedes the internalizing cells. In the absence of such accumulation, an excessive thickening of the so-called embryonic

shield was observed as the internalizing cells failed to adequately polarize and migrate away from the germ margin towards the animal pole. The overall volume of the interstitial fluid is relatively small and comprises about 10% of the total blastoderm volume. Still, it is strategically relocalized and functionally critical for enabling the polarization of the leader *ppl* cells required for proper migration and positioning of the axial mesendoderm. Additionally, Ouabain rescue experiments, where the interstitial fluid amount is only partially restored, hint at a minimal interstitial fluid volume requirement for enabling proper mesendoderm migration. Further supporting that idea, an increase in baseline interstitial fluid amount did not affect the efficiency of mesendoderm migration.

Global pharmacological treatments, such as our transient Ouabain-mediated inhibition of interstitial fluid accumulation, hold a risk of potentially directly causing the observed phenotypes. To control for such, we tested if the Ouabain treatment renders the cells incapable of polarizing and spreading in culture, unconstrained by the embryonic environment. To this end, we assayed the cell-cluster spreading on fibronectin-coated glass coverslips. Despite the large variability of cellular behaviors in such artificial conditions, Ouabain-treated cells still managed to polarize and spread, resembling the non-treated cells. Additionally, we examined the potential impact of Ouabain treatments on induction of mesendoderm cell fate, which could affect the migratory capacity of the internalizing cells. The expression of the characteristic *ppl* marker gene, Goosecoid (*gsc*), was not affected by Ouabain treatments nor by tuning the interstitial fluid amount.

To circumvent the direct pharmacological treatments of migratory cells but still ask questions of the functional relevance of interstitial fluid in their migration during gastrulation, we turned to a host-donor system where we transplanted a cluster of *ppl* cells onto the margin of either control or fluid depleted host embryos, mutant for mesendoderm induction. Additionally, we assayed the effect of pharmacological treatments in this context by examining the behavior of treated donor cells. Our observation that the absence of environmental fluid hindered effective migration of *ppl* transplants away from the germ margin compared to uninterrupted migration in the presence of fluid, regardless of the pharmacological treatment of *ppl* cells *per se*, further supported the direct impact of interstitial fluid in this process. Moreover, *ppl* transplants actively induced interstitial fluid relocalization in mesendoderm-deficient *MZ*oep mutant host embryos suggesting that *ppl* is sufficient to trigger the characteristic interstitial fluid relocalization, as seen in intact control embryos.
Unlike the intact embryo, where the *ppl* is accompanied by the trailing posterior axial mesendoderm (*pam*), and the interstitial fluid preferentially accumulates only at the leading edge, the *ppl* transplants are entirely surrounded by the interstitial fluid. We examined the polarization of these transplants and detected a significant decrease in protrusive activity in the absence of local interstitial fluid accumulation. Specifically, no large, lamellipodia-like protrusions towards the free, interstitial fluid-filled space were

observed. Moreover, in the absence of fluid, *ppl* transplants exerted only small, filopodia-like protrusions directed primarily towards the yolk cell and the deep cells/epiblast. Interestingly, the portion of filopodia directed towards the yolk cell was more significant in the absence of interstitial fluid. As migratory cells commonly use these protrusions for probing their environment, it could be that the *ppl* cells are searching for lower resistance areas to initiate their migration[234]. Despite the ability to move in any direction due to a uniform accumulation of fluid around them, *ppl* transplants always migrated directly towards the animal pole, demonstrating that the fluid accumulations function more permissively rather than instructively.

Similarly, in Cyclops (*cyc*) morphant embryos, we observed a correlation between axial mesendoderm thickness and efficiency of interstitial fluid relocalization, with fluid remnants left behind at the DC-EVL interface when the *ppl* and *pam* size was reduced. Interestingly, *cyc* morphants exhibited variable axial mesendoderm morphologies, sometimes resulting in *ppl*/*pam* fragmentation. Consistent with the observation from *ppl* transplants in *MZ*oep embryos, *ppl*/*pam* fragmentation locally affected the interstitial fluid relocalization in *cyc* morphant embryos.

We have shown that the characteristic interstitial fluid relocalization at the dorsal side depends on the presence and animal-directed migration of the axial mesendoderm as in mesendoderm-deficient *MZ*oep embryos such relocalization was not detectable. Moreover, *ppl* transplants into *MZ*oep embryos were sufficient to locally rescue the interstitial fluid relocalization. Therefore, we reasoned that *ppl* cells exert an active push on the overlying deep cells/epiblast as they migrate.

By mapping radial ectoderm displacement, we have observed increased local velocities in the proximity of the migrating *ppl*, which propagated from the leading edge towards the animal pole with a characteristic length scale (~ 50 um ahead) occupied by the interstitial fluid. These results suggest that as it migrates towards the animal pole, the *ppl* gradually displaces the epiblast radially towards the EVL on the surface of the embryo. Furthermore, such coordinated radial movement was not seen in the DCs/epiblast of *MZ*oep embryos.

Finally, in coordination with the local epiblast displacement, we hypothesized that the interstitial fluid percolates through the epiblast tissue in order to accumulate ahead of the *ppl* leading edge. Generating a local source of fluorescent tracers within the interstitial fluid at the EVL-DC interface, above the *ppl*, showed that that the interstitial fluid relocalization, as was seen by the accumulation of tracers at the YC-DC interface, is indeed facilitated by the *ppl* as the rate of fluorescent tracer accumulation at that interface was notably reduced in *MZ*oep embryos. Additionally, quantification of interstitial fluid distribution within the DCs/epiblast relative to the position of the *ppl* revealed lower porosity of the epiblast in close proximity to the *ppl*, in agreement with the idea that the fluid is being squeezed out of the porous tissue by the mechanical push from the *ppl*.

If the IF relocalization is directly induced by the *ppl* mechanically pushing up and thus compacting the adjacent DC/epiblast layer, then such process should also be inducible by a mechanical signal alone. To test this possibility, we designed a minimal system, where we transplanted a magnetic bead roughly mimicking the *ppl* in size (40 um) below the DC layer in *MZoep* embryos, lacking *ppl* specification (Fig.4.1.1A). Even before the pull, around the bead, at the YC-DC interface, we observed an accumulation of interstitial fluid as seen in *ppl* transplants. Our preliminary data from radially pulled magnetic bead suggest that the bead is sufficient to induce the interstitial fluid relocalization and accumulation at the YC-DC interface (Fig.4.1.1B) arguing in favour of a purely mechanical process driving the interstitial fluid relocalization during gastrulation.

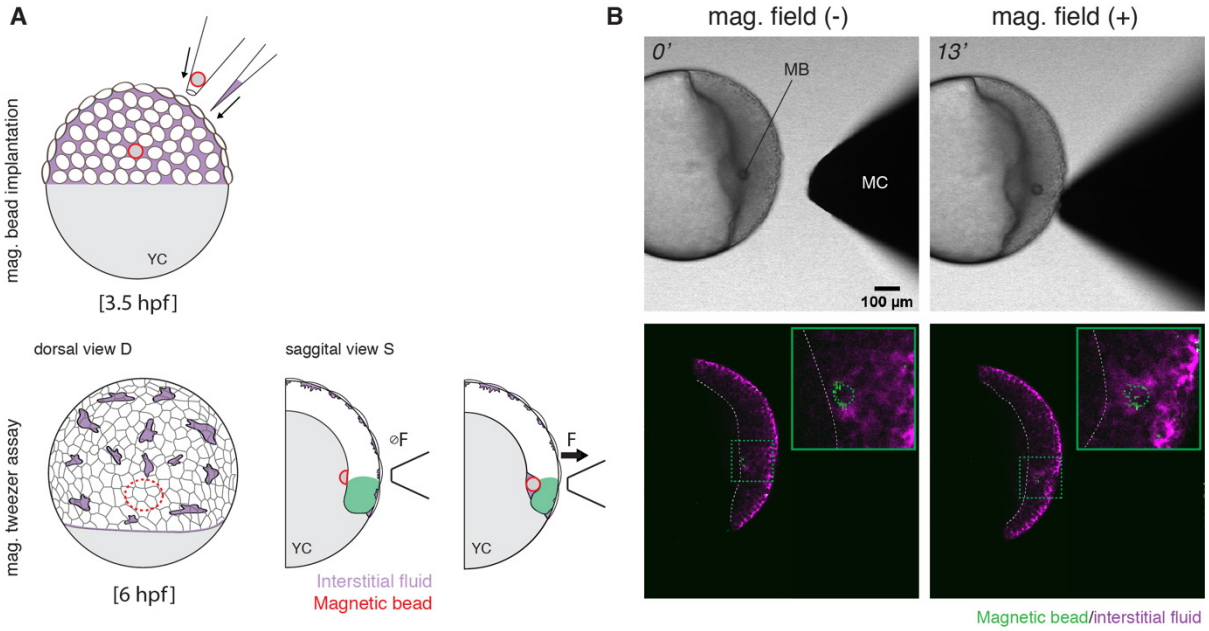

Fig.4.1.1 - Mimicking *ppl*-induced interstitial fluid relocalization by a magnetic bead. (**A**) Schematic illustrating the experimental design. Magnetic bead was implanted into the oblong stage (3.5 hours post fertilization, hpf) zebrafish embryo followed by interstitial fluid (IF) labelling. Embryos in which the magnetic bead localized near the margin at the yolk cell-deep cell, YC-DC interface were selected for the experiment. Magnetic bead was pulled radially by the localized magnetic field. (**B**) Bright-field (upper panel) and confocal (lower panel) images of *MZ*oep embryos with implanted magnetic bead at the YC-DC interface before (0') and after (13') the pull. YC-DC interface is highlighted (white dashed line). Insert shows a close-up of magnetic bead relocalization towards the magnetic coil (green rectangle) and subsequent IF accumulation at the YC-DC interface. Magnetic bead (MB), Magnetic coil (MC). Scale bar, 100 um.

REFERENCES

1. Hadjantonakis, K. & Solnica-Krezel, L. Developmental biology 50 years-investigating the emergence of shape. *Dev. Biol.* **341**, 2–4 (2010).
2. Heisenberg, C. P. & Bellaïche, Y. XForces in tissue morphogenesis and patterning. *Cell* **153**, 948 (2013).
3. Selman, K., Wallace, R. A., Sarka, A. & Qi, X. Stages of oocyte development in the zebrafish, Brachydanio rerio. *J. Morphol.* **218**, 203–224 (1993).
4. Yanagimachi, R. *et al.* Sperm attractant in the micropyle region of fish and insect eggs. *Biol. Reprod.* **88**, 1–11 (2013).
5. Xia, P., Gütl, D., Zheden, V. & Heisenberg, C. P. Lateral Inhibition in Cell Specification Mediated by Mechanical Signals Modulating TAZ Activity. *Cell* **176**, 1379-1392.e14 (2019).
6. Shamipour, S. *et al.* Bulk Actin Dynamics Drive Phase Segregation in Zebrafish Oocytes. *Cell* **177**, 1463-1479.e18 (2019).
7. Kimmel, C. B., Ballard, W. W., Kimmel, S. R., Ullmann, B. & Schilling, T. F. Stages of embryonic development of the zebrafish. *Dev. Dyn.* **203**, 253–310 (1995).
8. Kimmel, C. B. & Law, R. D. Cell lineage of zebrafish blastomeres. I. Cleavage pattern and cytoplasmic bridges between cells. *Dev. Biol.* **108**, 78–85 (1985).
9. Kiener, T. K., Selptsova-Friedrich, I. & Hunziker, W. Tjp3/zo-3 is critical for epidermal barrier function in zebrafish embryos. *Dev. Biol.* **316**, 36–49 (2008).
10. Moriwaki, K., Tsukita, S. & Furuse, M. Tight junctions containing claudin 4 and 6 are essential for blastocyst formation in preimplantation mouse embryos. *Dev. Biol.* **312**, 509–522 (2007).
11. Wang, F., Kooistra, M., Lee, M., Liu, L. & Baltz, J. M. Mouse embryos stressed by physiological levels of osmolarity become arrested in the late 2-cell stage before entry into M phase. *Biol. Reprod.* **85**, 702–713 (2011).
12. Kane, D. A. & Kimmel, C. B. The zebrafish midblastula transition. *Development* **119**, 447–456 (1993).
13. Carvalho, L. & Heisenberg, C. P. The yolk syncytial layer in early zebrafish development. *Trends Cell Biol.* **20**, 586–592 (2010).
14. Kimmel, C. B. & Law, R. D. Cell lineage of zebrafish blastomeres. II. Formation of the yolk syncytial layer. *Dev. Biol.* **108**, 86–93 (1985).
15. Lepage, S. E. & Bruce, A. E. E. Zebrafish epiboly: Mechanics and mechanisms. *Int. J. Dev. Biol.* **54**, 1213–1228 (2010).
16. Warga, R. M. & Kimmel, C. B. Cell movements during epiboly and gastrulation in zebrafish. *Development* **108**, 569–580 (1990).
17. Morita, H. *et al.* The Physical Basis of Coordinated Tissue Spreading in Zebrafish Gastrulation. *Dev. Cell* **40**, 354-366.e4 (2017).

18. Petridou, N. I., Grigolon, S., Salbreux, G., Hannezo, E. & Heisenberg, C. P. Fluidization-mediated tissue spreading by mitotic cell rounding and non-canonical Wnt signalling. *Nat. Cell Biol.* **21**, 169–178 (2019).

19. Keller, P. J., Schmidt, A. D., Wittbrodt, J. & Stelzer, E. H. K. Reconstruction of zebrafish early embryonic development by scanned light sheet microscopy. *Science (80-.).* **322**, 1065–1069 (2008).

20. Montero, J. A. *et al.* Shield formation at the onset of zebrafish gastrulation. *Development* **132**, 1187–1198 (2005).

21. Dumortier, J. G., Martin, S., Meyer, D., Rosa, F. M. & David, N. B. Collective mesendoderm migration relies on an intrinsic directionality signal transmitted through cell contacts. *Proc. Natl. Acad. Sci. U. S. A.* **109**, 16945–16950 (2012).

22. Arboleda-Estudillo, Y. *et al.* Movement Directionality in Collective Migration of Germ Layer Progenitors. *Curr. Biol.* **20**, 161–169 (2010).

23. Chng, S. C., Ho, L., Tian, J. & Reversade, B. ELABELA: A hormone essential for heart development signals via the apelin receptor. *Dev. Cell* **27**, 672–680 (2013).

24. Sepich, D. S., Calmelet, C., Kiskowski, M. & Solnica-Krezel, L. Initiation of convergence and extension movements of lateral mesoderm during zebrafish gastrulation. *Dev. Dyn.* **234**, 279–292 (2005).

25. Myers, D. C., Sepich, D. S. & Solnica-Krezel, L. Bmp activity gradient regulates convergent extension during zebrafish gastrulation. *Dev. Biol.* **243**, 81–98 (2002).

26. Gore, A. V. *et al.* The zebrafish dorsal axis is apparent at the four-cell stage. *Nature* **438**, 1030–1035 (2005).

27. Tran, L. D. *et al.* Dynamic microtubules at the vegetal cortex predict the embryonic axis in zebrafish. *Dev.* **139**, 3644–3652 (2012).

28. Shao, M. *et al.* Vegetally localised vrtn functions as a novel repressor to modulate bmp2b transcription during dorsoventral patterning in zebrafish. *Dev.* **144**, 3361–3374 (2017).

29. Marlow, F. L. *Setting up for gastrulation in zebrafish*. *Current Topics in Developmental Biology* vol. 136 (Elsevier Inc., 2020).

30. Yan, L. *et al.* Maternal Huluwa dictates the embryonic body axis through b-catenin in vertebrates. *Science (80-.).* **362**, (2018).

31. Schneider, S., Steinbeisser, H., Warga, R. M. & Hausen, P. B-Catenin Translocation Into Nuclei Demarcates the Dorsalizing Centers in Frog and Fish Embryos. *Mech. Dev.* **57**, 191–198 (1996).

32. Feldman B, Gates MA, Egan ES, Dougan ST, Rennebeck G, Sirotkin HI, Schier AF, T. W. Zebrafish organizer development and germ-layer formation require nodal-related signals. *Nature* **246**, 170 (1998).

33. Gritsman, K. *et al.* The EGF-CFC protein one-eyed pinhead is essential for nodal signaling. *Cell* **97**, 121–132 (1999).

34. Schulte-Merker S, Lee KJ, McMahon AP, H. M. The zebrafish organizer requires chordino. *Nature* (1997) doi:10.1038/43092.

35. Leung, T. C. *et al.* Bozozok Directly Represses Bmp2B Transcription and Mediates the Earliest Dorsoventral Asymmetry of Bmp2B Expression in Zebrafish. *Development* **130**, 3639–3649 (2003).

36. Ryu, S. L. *et al.* Regulation of dharma/bozozok by the Wnt pathway. *Dev. Biol.* **231**, 397–409 (2001).

37. Shimizu, T. *et al.* Cooperative roles of Bozozok/Dharma and Nodal-related proteins in the formation of the dorsal organizer in zebrafish. *Mech. Dev.* **91**, 293–303 (2000).

38. Yamanaka, Y. *et al.* A novel homeobox gene, dharma, can induce the organizer in a non-cell- autonomous manner. *Genes Dev.* **12**, 2345–2353 (1998).

39. Rebagliati, M. R., Toyama, R., Haffter, P. & Dawid, I. B. Cyclops Encodes a Nodal-Related Factor Involved in Midline Signaling. *Proc. Natl. Acad. Sci. U. S. A.* **95**, 9932–9937 (1998).

40. Bisgrove, B. W., Su, Y. C. & Yost, H. J. Maternal Gdf3 is an obligatory cofactor in nodal signaling for embryonic axis formation in zebrafish. *Elife* **6**, 1–19 (2017).

41. Montague, T. G. & Schier, A. F. Vg1-nodal heterodimers are the endogenous inducers of mesendoderm. *Elife* **6**, 1–24 (2017).

42. Pelliccia, J. L., Jindal, G. A. & Burdine, R. D. Gdf3 is required for robust nodal signaling during germ layer formation and left-right patterning. *Elife* **6**, 1–23 (2017).

43. Pinheiro, D. & Heisenberg, C. P. *Zebrafish gastrulation: Putting fate in motion*. *Current Topics in Developmental Biology* vol. 136 (Elsevier Inc., 2020).

44. Hill, C. S. Spatial and temporal control of NODAL signaling. *Curr. Opin. Cell Biol.* **51**, 50–57 (2018).

45. Bennett, J. T. *et al.* Nodal signaling activates differentiation genes during zebrafish gastrulation. *Dev. Biol.* **304**, 525–540 (2007).

46. Dickmeis, T. *et al.* Identification of Nodal signaling targets by array analysis of induced complex probes. *Dev. Dyn.* **222**, 571–580 (2001).

47. Aoki, T. O. *et al.* Molecular integration of casanova in the Nodal signalling pathway controlling endoderm formation. *Development* **129**, 275–286 (2002).

48. Dougan, S. T., Warga, R. M., Kene, D. A., Schier, A. F. & Talbot, W. S. The role of the zebrafish nodal-related genes squint and cyclops in patterning of mesendoderm. *Development* **130**, 1837–1851 (2003).

49. Dubrulle, J. *et al.* Response to Nodal morphogen gradient is determined by the kinetics of target gene induction. *Elife* **4**, 1–27 (2015).

50. Hagos, E. G. & Dougan, S. T. Time-dependent patterning of the mesoderm and endoderm by Nodal signals in zebrafish. *BMC Dev. Biol.* **7**, 1–18 (2007).

51. Sako, K. *et al.* Optogenetic Control of Nodal Signaling Reveals a Temporal

Pattern of Nodal Signaling Regulating Cell Fate Specification during Gastrulation. *Cell Rep.* **16**, 866–877 (2016).

52. Bisgrove, B. W., Essner, J. J. & Yost, H. J. Regulation of midline development by antagonism of lefty and nodal signaling. *Development* **126**, 3253–3262 (1999).

53. Meno, C. *et al.* Mouse lefty2 and zebrafish antivin are feedback inhibitors of nodal signaling during vertebrate gastrulation. *Mol. Cell* **4**, 287–298 (1999).

54. Chen, Y. & Schler, A. F. The zebrafish nodal signal Squint functions as a morphogen. *Nature* **411**, 607–610 (2001).

55. Chen, Y. & Schier, A. F. Lefty proteins are long-range inhibitors of Squint-mediated Nodal signaling. *Curr. Biol.* **12**, 2124–2128 (2002).

56. Müller, P. *et al.* Differential diffusivity of nodal and lefty underlies a reaction-diffusion patterning system. *Science (80-.).* **336**, 721–724 (2012).

57. Tian, J., Andrée, B., Jones, C. M. & Sampath, K. The pro-domain of the zebrafish Nodal-related protein cyclops regulates its signaling activities. *Development* **135**, 2649–2658 (2008).

58. Hong, S. K., Jang, M. K., Brown, J. L., McBride, A. A. & Feldman, B. Embryonic mesoderm and endoderm induction requires the actions of non-embryonic Nodal-related ligands and Mxtx2. *Development* **138**, 787–795 (2011).

59. Fan, X. *et al.* Nodal signals mediate interactions between the extra-embryonic and embryonic tissues in zebrafish. *Dev. Biol.* **310**, 363–378 (2007).

60. van Boxtel, A. L. *et al.* A Temporal Window for Signal Activation Dictates the Dimensions of a Nodal Signaling Domain. *Dev. Cell* **35**, 175–185 (2015).

61. Rogers, K. W. *et al.* Nodal patterning without Lefty inhibitory feedback is functional but fragile. *Elife* **6**, 1–20 (2017).

62. van Boxtel, A. L., Economou, A. D., Heliot, C. & Hill, C. S. Long-Range Signaling Activation and Local Inhibition Separate the Mesoderm and Endoderm Lineages. *Dev. Cell* **44**, 179-191.e5 (2018).

63. Mathieu, J. *et al.* Nodal and Fgf pathways interact through a positive regulatory loop and synergize to maintain mesodermal cell populations. *Development* **131**, 629–641 (2004).

64. Rodaway, A. *et al.* Induction of the mesendoderm in the zebrafish germ ring by yolk cell-derived TGF-β family signals and discrimination of mesoderm and endoderm by FGF. *Development* **126**, 3067–3078 (1999).

65. Scholpp S, B. M. Endocytosis controls spreading and effective signaling range of Fgf8 protein. *Curr Biol.* (2004) doi:10.1016/j.cub.2004.09.084.

66. Ho RK, K. C. Commitment of cell fate in the early zebrafish embryo. *Science (80-.).* (1993) doi:10.1126/science.8316841.

67. Kiecker, C., Bates, T. & Bell, E. Molecular specification of germ layers in vertebrate embryos. *Cell. Mol. Life Sci.* **73**, 923–947 (2016).

68. Thisse, B., Wright, C. V. E. & Thisse, C. Activin- and nodal-related factors control antero-posterior patterning of the zebrafish embryo. *Nature* **403**, 425–428 (2000).

69. Vopalensky, P., Pralow, S. & Vastenhouw, N. L. Reduced expression of the nodal co-receptor Oep causes loss of mesendodermal competence in zebrafish. *Dev.* **145**, (2018).

70. Zhang, J., Talbot, W. S. & Schier, A. F. Positional cloning identifies zebrafish one-eyed pinhead as a permissive EGF-related ligand required during gastrulation. *Cell* **92**, 241–251 (1998).

71. Babb, S. G. & Marrs, J. A. E-cadherin regulates cell movements and tissue formation in early zebrafish embryos. *Dev. Dyn.* **230**, 263–277 (2004).

72. Carmany-Rampey, A. & Schier, A. F. Single-cell internalization during zebrafish gastrulation. *Curr. Biol.* **11**, 1261–1265 (2001).

73. David, N. B. & Rosa, F. M. Cell autonomous commitment to an endodermal fate and behaviour by activation of Nodal signalling. *Development* **128**, 3937–3947 (2001).

74. STEINBERG, M. S. On the mechanism of tissue reconstruction by dissociated cells. I. Population kinetics, differential adhesiveness. and the absence of directed migration. *Proc. Natl. Acad. Sci. U. S. A.* **48**, 1577–1582 (1962).

75. Krieg, M. *et al.* Tensile forces govern germ-layer organization in zebrafish. *Nat. Cell Biol.* **10**, 429–436 (2008).

76. Maître, J. L. *et al.* Adhesion functions in cell sorting by mechanically coupling the cortices of adhering cells. *Science (80-.).* **338**, 253–256 (2012).

77. Schötz, E. M. *et al.* Quantitative differences in tissue surface tension influence zebrafish germ layer positioning. *HFSP J.* **2**, 42–56 (2008).

78. Krens, S. F. G. *et al.* Interstitial fluid osmolarity modulates the action of differential tissue surface tension in progenitor cell segregation during gastrulation. *Dev.* **144**, 1798–1806 (2017).

79. Ninomiya, H. *et al.* Cadherin-dependent differential cell adhesion in xenopus causes cell sorting in vitro but not in the embryo. *J. Cell Sci.* **125**, 1877–1883 (2012).

80. Giger, F. A. & David, N. B. Endodermal germ-layer formation through active actin-driven migration triggered by N-cadherin. *Proc. Natl. Acad. Sci. U. S. A.* **114**, 10143–10148 (2017).

81. Liu, Z., Woo, S. & Weiner, O. D. Nodal signaling has dual roles in fate specification and directed migration during germ layer segregation in zebrafish. *Dev.* **145**, 1–12 (2018).

82. Barone, V. *et al.* An Effective Feedback Loop between Cell-Cell Contact Duration and Morphogen Signaling Determines Cell Fate. *Dev. Cell* **43**, 198-211.e12 (2017).

83. Pinheiro, D. & Bellaïche, Y. Mechanical Force-Driven Adherens Junction

Remodeling and Epithelial Dynamics. *Dev. Cell* **47**, 3–19 (2018).

84. Lele, Z. *et al.* Parachute/ n-cadherin is required for morphogenesis and maintained integrity of the zebrafish neural tube. *Development* **129**, 3281–3294 (2002).

85. Warga, R. M. & Kane, D. A. A role for N-cadherin in mesodermal morphogenesis during gastrulation. *Dev. Biol.* **310**, 211–225 (2007).

86. Pauli, A. *et al.* Toddler: An embryonic signal that promotes cell movement via apelin receptors. *Science (80-.).* **343**, (2014).

87. Norris, M. L. *et al.* Toddler signaling regulates mesodermal cell migration downstream of nodal signaling. *Elife* **6**, 1–18 (2017).

88. Bosze, B. *et al.* Pcdh18a regulates endocytosis of E-cadherin during axial mesoderm development in zebrafish. *Histochem. Cell Biol.* **154**, 463–480 (2020).

89. Smutny, M. *et al.* Friction forces position the neural anlage. *Nat. Cell Biol.* **19**, 306–317 (2017).

90. Heisenberg, C., Tada, M., Rauch, È., Smith, J. C. & Wilson, S. W. Silberblick / Wnt11 mediates convergent extension movements during zebrafish gastrulation. **405**, (2000).

91. Čapek, D. *et al.* Light-activated Frizzled7 reveals a permissive role of non-canonical wnt signaling in mesendoderm cell migration. *Elife* **8**, 1–24 (2019).

92. Ulrich, F. *et al.* Slb/Wnt11 controls hypoblast cell migration and morphogenesis at the onset of zebrafish gastrulation. *Development* **130**, 5375–5384 (2003).

93. Boucaut, J.-C. *et al.* Fibronectin-rich fibrillar extracellular cell migration during amphibian matrix controls gastrulation. *Scanning* **147**, 139–147.

94. Latimer, A. & Jessen, J. R. Extracellular matrix assembly and organization during zebrafish gastrulation. *Matrix Biol.* **29**, 89–96 (2010).

95. Jülich, D. *et al.* Integrinα5 and delta/notch signaling have complementary spatiotemporal requirements during zebrafish somitogenesis. *Dev. Cell* **8**, 575–586 (2005).

96. Dumortier, J. G. & David, N. B. The TORC2 component, sin1, controls migration of anterior mesendoderm during zebrafish gastrulation. *PLoS One* **10**, 1–16 (2015).

97. Hill, M. A. Embryology Book - The Frog Its Reproduction and Development. https://embryology.med.unsw.edu.au/embryology/index.php/Book_-_The_Frog_Its_Reproduction_and_Development_7.

98. Kalt, M. R. The relationship between cleavage and blastocoel formation in Xenopus laevis. I. Light microscopic observations. *J. Embryol. Exp. Morphol.* **26**, 51–66 (1971).

99. Discover Development. http://www.discoverdevelopment.com/PHP/SlidesFrogEarlyDev.php.

100. TUFT, P. H. The uptake and distribution of water in the embryo of Xenopus laevis (Daudin). *J. Exp. Biol.* **39**, 1–19 (1962).

101. Müllegger, J. & Lepperdinger, G. Hyaluronan is an abundant constituent of the extracellular matrix of Xenopus embryos. *Mol. Reprod. Dev.* **61**, 312–316 (2002).

102. Johnson, K. E. Glycoconjugate synthesis during gastrulation in Xenopus laevis. *Integr. Comp. Biol.* **24**, 605–614 (1984).

103. Müllegger, J. & Lepperdinger, G. Degradation of hyaluronan by a Hyal2-type hyaluronidase affects pattern formation of vitelline vessels during embryogenesis of Xenopus laevis. *Mech. Dev.* **111**, 25–35 (2002).

104. Barua, D., Parent, S. E. & Winklbauer, R. Mechanics of Fluid-Filled Interstitial Gaps. II. Gap Characteristics in Xenopus Embryonic Ectoderm. *Biophys. J.* **113**, 923–936 (2017).

105. Gillespie, J. The distribution of small ions during the early development of Xenopus laevis and Ambystoma mexicanum embryos. *J Physiol* 359–377 (1983).

106. Keller, R. E. Vital dye mapping of the gastrula and neurula of Xenopus laevis. II. Prospective areas and morphogenetic movements of the deep layer. *Dev. Biol.* **51**, 118–137 (1976).

107. Shook, D. R. & Keller, R. Epithelial type, ingression, blastopore architecture and the evolution of chordate mesoderm morphogenesis. *J. Exp. Zool. Part B Mol. Dev. Evol.* **310**, 85–110 (2008).

108. Huang, Y. & Winklbauer, R. Cell migration in the Xenopus gastrula. *Wiley Interdiscip. Rev. Dev. Biol.* **7**, 1–21 (2018).

109. Beetschen, J. C. Amphibian gastrulation: History and evolution of a 125 year-old concept. *Int. J. Dev. Biol.* **45**, 771–795 (2001).

110. Evren, S. *et al.* EphA4-dependent Brachyury expression is required for dorsal mesoderm involution in the Xenopus gastrula. *Dev.* **141**, 3649–3661 (2014).

111. Huang, Y. & Winklbauer, R. Cell migration in the Xenopus gastrula. (2018) doi:10.1002/wdev.325.

112. Gorny, A. K. & Steinbeisser, H. Brachet's cleft: A model for the analysis of tissue separation in Xenopus. *Wiley Interdiscip. Rev. Dev. Biol.* **1**, 294–300 (2012).

113. Winklbauer, R. & Schürfeld, M. Vegetal rotation, a new gastrulation movement involved in the internalization of the mesoderm and endoderm in Xenopus. *Development* **126**, 3703–3713 (1999).

114. Wacker, S., Grimm, K., Joos, T. & Winklbauer, R. Development and control of tissue separation at gastrulation in Xenopus. *Dev. Biol.* **224**, 428–439 (2000).

115. Tepass, U., Godt, D. & Winklbauer, R. Cell sorting in animal development: Signalling and adhesive mechanisms in the formation of tissue boundaries. *Curr. Opin. Genet. Dev.* **12**, 572–582 (2002).

116. Medina, A., Swain, R. K., Kuerner, K. M. & Steinbeisser, H. Xenopus paraxial

protocadherin has signaling functions and is involved in tissue separation. *EMBO J.* **23**, 3249–3258 (2004).

117. Köster, I., Jungwirth, M. S. & Steinbeisser, H. XGit2 and xRhoGAP 11A regulate convergent extension and tissue separation in Xenopus gastrulation. *Dev. Biol.* **344**, 26–35 (2010).

118. Luxardi, G., Marchal, L., Thomé, V. & Kodjabachina, L. Distinct Xenopus Nodal ligands sequentially induce mesendoderm and control gastrulation movements in parallel to the Wnt/PCP pathway. *Development* **137**, 417–426 (2010).

119. Park, E. C., Cho, G. S., Kim, G. H., Choi, S. C. & Han, J. K. The involvement of Eph-Ephrin signaling in tissue separation and convergence during Xenopus gastrulation movements. *Dev. Biol.* **350**, 441–450 (2011).

120. Rohani, N., Canty, L., Luu, O., Fagotto, F. & Winklbauer, R. EphrinB/EphB signaling controls embryonic germ layer separation by contact-induced cell detachment. *PLoS Biol.* **9**, 1–18 (2011).

121. Winklbauer, R. & Keller, R. E. Fibronectin, mesoderm migration, and gastrulation in Xenopus. *Dev. Biol.* **177**, 413–426 (1996).

122. Pierschbacher, M. D. & Ruoslahti, E. Cell attachment activity of fibronectin can be duplicated by small synthetic fragments of the molecule. *Nature* 3–6 (1984).

123. Pierschbacher, M. D. & Ruoslahti, E. Variants of the cell recognition site of fibronectin that retain attachment-promoting activity. *Proc. Natl. Acad. Sci. U. S. A.* **81**, 5985–5988 (1984).

124. Yamada, K. M. & Kennedy, D. W. Dualistic nature of adhesive protein function: Fibronectin and its biologically active peptide fragments can autoinhibit fibronectin function. *J. Cell Biol.* **99**, 29–36 (1984).

125. Keller, R. & Jansa, S. Xenopus gastrulation without a blastocoel roof. *Dev. Dyn.* **195**, 162–176 (1992).

126. Keller, R. & Tibbetts, P. Mediolateral cell intercalation in the dorsal, axial mesoderm of Xenopus laevis. *Dev. Biol.* **131**, 539–549 (1989).

127. Winklbauer, R. & Nagel, M. Directional mesoderm cell migration in the Xenopus gastrula. *Dev. Biol.* **148**, 573–589 (1991).

128. Ewald, A. J., Peyrot, S. M., Tyszka, M. J., Fraser, S. E. & Wallingford, J. B. Regional requirements for Dishevelled signalling during Xenopus gastrulation: Separable effects on blastopore closure, mesendoderm internalization and archenteron formation. *Development* **131**, 6195–6209 (2004).

129. SF., G. *Developmental Biology. 6th edition.Early Development in Birds*. (Sunderland (MA): Sinauer Associates, 2000).

130. Bellairs R, Breathnach AS, G. M. Freeze-fracture replication of junctionsl complexes in unincubated and incubated chick embryos. *Cell Tissue Res* **17**, 235–52 (1975).

131. New, D. A. T. The Formation of Sub-blastodermic Fluid in Hens' Eggs. *Development* **4**, 221–227 (1956).

132. Eyal-Giladi, H., Debby, A. & Harel, N. The posterior section of the chick's area pellucida and its involvement in hypoblast and primitive streak formation. *Development* **116**, 819–830 (1992).

133. Schoenwolf, G. C., Garcia-Martinez, V. & Dias, M. S. Mesoderm movement and fate during avian gastrulation and neurulation. *Dev. Dyn.* **193**, 235–248 (1992).

134. Stern, C. D. *et al.* Epithelial scatter factor and development of the chick embryonic axis. *Development* **110**, 1271–1284 (1990).

135. DeLuca, S. M. *et al.* Hepatocyte growth factor/scatter factor promotes a switch from E- to N- cadherin in chick embryo epiblast cells. *Exp. Cell Res.* **251**, 3–15 (1999).

136. Frankenberg, S. R., de Barros, F. R. O., Rossant, J. & Renfree, M. B. The mammalian blastocyst. *Wiley Interdiscip. Rev. Dev. Biol.* **5**, 210–232 (2016).

137. Sheng, G. Day-1 chick development. *Dev. Dyn.* **243**, 357–367 (2014).

138. Selwood, L. Mechanisms underlying the development of pattern in marsupial embryos. *Curr Top Dev Biol.* **27**, 175–233 (1992).

139. Menkhorst, E., Nation, A., Cui, S. & Selwood, L. Evolution of the shell coat and yolk in amniotes: A marsupial perspective. *J. Exp. Zool. Part B Mol. Dev. Evol.* **312**, 625–638 (2009).

140. JP., F. T. and H. The development of the monotremata Part IV. Growth of the ovarian ovum, maturation, fertilisation and early cleavage. *Trans. Zool. Soc. Lond.* 445-623. (1939).

141. Hughes, R. L. & Hall, L. S. Early development and embryology of the platypus. *Philos. Trans. R. Soc. B Biol. Sci.* **353**, 1101–1114 (1998).

142. Menkhorst, E. & Selwood, L. Vertebrate extracellular preovulatory and postovulatory egg coats. *Biol. Reprod.* **79**, 790–797 (2008).

143. Sathananthan H, Selwood L, Douglas I, N. K. Early cleavage to formation of the unilaminar blastocyst in the marsupial Antechinus stuartii: ultrastructure. *Reprod Fertil Dev.* **9(2)**, 201–12 (1997).

144. Selwood L, S. D. Time-lapse analysis and normal stages of development of cleavage and blastocyst formation in the marsupials the brown antechinus and the stripe-faced dunnart. *Mol Reprod Dev.* **26(1)**, 53–62 (1990).

145. Frankenberg, S. & Selwood, L. An ultrastructural study of the role of an extracellular matrix during normal cleavage in a marsupial, the brushtail possum. *Mol. Reprod. Dev.* **50**, 420–433 (1998).

146. Babin, P. J. Conservation of a vitellogenin gene cluster in oviparous vertebrates and identification of its traces in the platypus genome. *Gene* **413**, 76–82 (2008).

147. Larue, L., Ohsugi, M., Hirchenhain, J. & Kemler, R. E-cadherin null mutant embryos fail to form a trophectoderm epithelium. *Dev. Biol.* **91**, 8263–8267 (1994).

148. Shirayoshi, Y., Okada, T. S. & Takeichi, M. The calcium-dependent cell-cell

adhesion system regulates inner cell mass formation and cell surface polarization in early mouse development. *Cell* **35**, 631–638 (1983).

149. Stephenson, R. O., Yamanaka, Y. & Rossant, J. Disorganized epithelial polarity and excess trophectoderm cell fate in preimplantation embryos lacking E-cadherin. *Development* **137**, 3383–3391 (2010).

150. Eakin, G. S. & Behringer, R. R. Diversity of germ layer and axis formation among mammals. *Semin. Cell Dev. Biol.* **15**, 619–629 (2004).

151. Vejlsted, M. *et al.* Ultrastructural and immunohistochemical characterization of the bovine epiblast. *Biol. Reprod.* **72**, 678–686 (2005).

152. Bolmberg, L. A., Hashizume, K. & Viebahn, C. Blastocyst elongation, trophoblastic differentiation, and embryonic pattern formation. *Reproduction* **135**, 181–195 (2008).

153. Pilato, G. *et al.* The problem of the origin of primordial germ cells (PGCs) in vertebrates: Historical review and a possible solution. *Int. J. Dev. Biol.* **57**, 809–819 (2013).

154. Maître, J. L. Mechanics of blastocyst morphogenesis. *Biol. Cell* **109**, 323–338 (2017).

155. Biggers, J. D., Bell, J. E. & Benos, D. J. Mammalian blastocyst: Transport functions in a developing epithelium. *Am. J. Physiol. - Cell Physiol.* **255**, 419–432 (1988).

156. Marikawa, Y. & Alarcon, V. B. Creation of trophectoderm, the first epithelium, in mouse preimplantation development. *Results Probl. Cell Differ.* **55**, 165–184 (2012).

157. Schliffka, M. F. & Maître, J. L. Stay hydrated: basolateral fluids shaping tissues. *Curr. Opin. Genet. Dev.* **57**, 70–77 (2019).

158. Dumortier, J. G. *et al.* Hydraulic fracturing and active coarsening position the lumen of the mouse blastocyst. *Science (80-.).* **365**, 465–468 (2019).

159. Chan, C. J. *et al.* Hydraulic control of mammalian embryo size and cell fate. *Nature* **571**, 112–116 (2019).

160. Motosugi, N., Bauer, T., Polanski, Z., Solter, D. & Hiiragi, T. Polarity of the mouse embryo is established at blastocyst and is not prepatterned. *Genes Dev.* **19**, 1081–1092 (2005).

161. Ryan, A. Q., Chan, C. J., Graner, F. & Hiiragi, T. Lumen Expansion Facilitates Epiblast-Primitive Endoderm Fate Specification during Mouse Blastocyst Formation. *Dev. Cell* **51**, 684-697.e4 (2019).

162. Borland, R. M., Biggers, J. D. & Lechene, C. P. Studies on the composition and formation of mouse blastocoele fluid using electron probe microanalysis. *Dev. Biol.* **55**, 1–8 (1977).

163. Watson, A. J., Natale, D. R. & Barcroft, L. C. Molecular regulation of blastocyst formation. *Anim. Reprod. Sci.* **82**–**83**, 583–592 (2004).

164. Manejwala, F. M., Cragoe, E. J. & Schultz, R. M. Blastocoel expansion in the

preimplantation mouse embryo: Role of extracellular sodium and chloride and possible apical routes of their entry. *Dev. Biol.* **133**, 210–220 (1989).

165. Barcroft, L. C., Moseley, A. E., Lingrel, J. B. & Watson, A. J. Deletion of the Na/K-ATPase α1-subunit gene (Atp1a1) does not prevent cavitation of the preimplantation mouse embryo. *Mech. Dev.* **121**, 417–426 (2004).

166. MacPhee, D. J. *et al.* Differential involvement of Na+,K+-ATPase isozymes in preimplantation development of the mouse. *Dev. Biol.* **222**, 486–498 (2000).

167. Gelber, K., Tamura, A. N., Alarcon, V. B. & Marikawa, Y. A potential use of embryonic stem cell medium for the in vitro culture of preimplantation embryos. *J. Assist. Reprod. Genet.* **28**, 659–668 (2011).

168. Edashige, K., Sakamoto, M. & Kasai, M. Expression of mRNAs of the aquaporin family in mouse oocytes and embryos. *Cryobiology* **40**, 171–175 (2000).

169. Offenberg, H. *et al.* mRNAs encoding aquaporins are present during murine preimplantation development. *Mol. Reprod. Dev.* **57**, 323–330 (2000).

170. Saitou, M. *et al.* Complex phenotype of mice lacking occludin, a component of tight junction strands. *Mol. Biol. Cell* **11**, 4131–4142 (2000).

171. Adachi, M. *et al.* Normal Establishment of Epithelial Tight Junctions in Mice and Cultured Cells Lacking Expression of ZO-3, a Tight-Junction MAGUK Protein. *Mol. Cell. Biol.* **26**, 9003–9015 (2006).

172. Xu, J. *et al.* Early Embryonic Lethality of Mice Lacking ZO-2, but Not ZO-3, Reveals Critical and Nonredundant Roles for Individual Zonula Occludens Proteins in Mammalian Development. *Mol. Cell. Biol.* **28**, 1669–1678 (2008).

173. Eckert, J. J. & Fleming, T. P. Tight junction biogenesis during early development. *Biochim. Biophys. Acta - Biomembr.* **1778**, 717–728 (2008).

174. Wang, H. *et al.* Zonula occludens-1 (ZO-1) is involved in morula to blastocyst transformation in the mouse. *Dev. Biol.* **318**, 112–125 (2008).

175. Sheth, B. *et al.* Tight junction protein ZO-2 expression and relative function of ZO-1 and ZO-2 during mouse blastocyst formation. *Exp. Cell Res.* **314**, 3356–3368 (2008).

176. Leonavicius, K. *et al.* Mechanics of mouse blastocyst hatching revealed by a hydrogel-based microdeformation assay. *Proc. Natl. Acad. Sci. U. S. A.* **115**, 10375–10380 (2018).

177. Pinheiro, D. *et al.* Transmission of cytokinesis forces via E-cadherin dilution and actomyosin flows. *Nature* **545**, 103–107 (2017).

178. Stephenson, R. E. *et al.* Rho Flares Repair Local Tight Junction Leaks. *Dev. Cell* **48**, 445-459.e5 (2019).

179. Latorre, E. *et al.* Active superelasticity in three-dimensional epithelia of controlled shape. *Nature* **563**, 203–208 (2018).

180. Freund, J. B., Goetz, J. G., Hill, K. L. & Vermot, J. Fluid flows and forces in development: Functions, features and biophysical principles (Development, 139, (1229-1245)). *Dev.* **139**, 3063 (2012).

181. Daems, M., Peacock, H. M. & Jones, E. A. V. Fluid flow as a driver of embryonic morphogenesis. *Development* **147**, (2020).

182. Nonaka, S. *et al.* Randomization of left-right asymmetry due to loss of nodal cilia generating leftward flow of extraembryonic fluid in mice lacking KIF3B motor protein. *Cell* **95**, 829–837 (1998).

183. Nonaka, S., Shiratori, H., Saijoh, Y. & Hamada, H. Determination of left-right patterning of the mouse embryo by artificial nodal flow. *Nature* **418**, 96–99 (2002).

184. Okabe, N., Xu, B. & Burdine, R. D. Fluid dynamics in zebrafish Kupffer's vesicle. *Dev. Dyn.* **237**, 3602–3612 (2008).

185. Okada, Y., Takeda, S., Tanaka, Y., Belmonte, J. C. I. & Hirokawa, N. Mechanism of nodal flow: A conserved symmetry breaking event in left-right axis determination. *Cell* **121**, 633–644 (2005).

186. Nonaka, S. *et al.* De novo formation of left-right asymmetry by posterior tilt of nodal cilia. *PLoS Biol.* **3**, (2005).

187. Cartwright, J. H. E., Piro, O. & Tuval, I. Fluid-dynamical basis of the embryonic development of left-right asymmetry in vertebrates. *Proc. Natl. Acad. Sci. U. S. A.* **101**, 7234–7239 (2004).

188. Borovina, A., Superina, S., Voskas, D. & Ciruna, B. Vangl2 directs the posterior tilting and asymmetric localization of motile primary cilia. *Nat. Cell Biol.* **12**, 407–412 (2010).

189. Song, H. *et al.* Planar cell polarity breaks bilateral symmetry by controlling ciliary positioning. *Nature* **466**, 378–382 (2010).

190. Tanaka, Y., Okada, Y. & Hirokawa, N. FGF-induced vesicular release of Sonic hedgehog and retinoic acid in leftward nodal flow is critical for left-right determination. *Nature* **435**, 172–177 (2005).

191. Omori T, Winter K, Shinohara K, Hamada H, I. T. Simulation of the nodal flow of mutant embryos with a small number of cilia: comparison of mechanosensing and vesicle transport hypotheses. *R Soc Open Sci.* **5(8)**, 1–15 (2018).

192. McGrath, K. E., Koniski, A. D., Malik, J. & Palis, J. Circulation is established in a stepwise pattern in the mammalian embryo. *Blood* **101**, 1669–1676 (2003).

193. Sampaio, P. *et al.* Left-right organizer flow dynamics: How much cilia activity reliably yields laterality? *Dev. Cell* **29**, 716–728 (2014).

194. Yoshiba S, Shiratori H, Kuo IY, Kawasumi A, Shinohara K, Nonaka S, Asai Y, Sasaki G, Belo JA, Sasaki H, Nakai J, Dworniczak B, Ehrlich BE, Pennekamp P, H. H. Cilia at the node of mouse embryos sense fluid flow for left-right determination via Pkd2. *Science (80-.).* **338(6104)**, 226–31. (2012).

195. Sharma, N., Berbari, N. F. & Yoder, B. K. *Ciliary Dysfunction in Developmental Abnormalities and Diseases*. *Current Topics in Developmental Biology* vol. 85 (Elesvier Inc., 2008).

196. Vick, P. *et al.* An Early Function of Polycystin-2 for Left-Right Organizer

Induction in Xenopus. *iScience* **2**, 76–85 (2018).

197. WW., B. What is the purpose of the embryonic heart beat? Or how facts can ultimately prevail over physiological dogma. *Physiol Biochem Zool.* **77(3)**, 333–45 (2004).

198. Jones, E. A. V. Mechanical factors in the development of the vascular bed. *Respir. Physiol. Neurobiol.* **178**, 59–65 (2011).

199. Samsa, L. A. *et al.* Cardiac contraction activates endocardial notch signaling to modulate chamber maturation in zebrafish. *Dev.* **142**, 4080–4091 (2015).

200. Duchemin, A. L., Vignes, H. & Vermot, J. Mechanically activated Piezo channels modulate outflow tract valve development through Yap1 and Klf2-Notch signaling axis. *bioRxiv* 1–27 (2019) doi:10.1101/529016.

201. Goddard, L. M. *et al.* Hemodynamic Forces Sculpt Developing Heart Valves through a KLF2-WNT9B Paracrine Signaling Axis. *Dev. Cell* **43**, 274-289.e5 (2017).

202. le Noble, F. *et al.* Flow regulates arterial-venous differentiation in the chick embryo yolk sac. *Development* **131**, 361–375 (2004).

203. Lucitti, J. L. *et al.* Vascular remodeling of the mouse yolk sac requires hemodynamic force. *Development* **134**, 3317–3326 (2007).

204. Melchior, B. & Frangos, J. A. Shear-induced endothelial cell-cell junction inclination. *Am. J. Physiol. - Cell Physiol.* **299**, 621–629 (2010).

205. Yamamoto, K. & Ando, J. Endothelial cell and model membranes respond to shear stress by rapidly decreasing the order of their lipid phases. *J. Cell Sci.* **126**, 1227–1234 (2013).

206. Zenker, J. *et al.* Expanding Actin Rings Zipper the Mouse Embryo for Blastocyst Formation. *Cell* **173**, 776-791.e17 (2018).

207. Imuta, Y. *et al.* Mechanical control of notochord morphogenesis by extra-embryonic tissues in mouse embryos. *Mech. Dev.* **132**, 44–58 (2014).

208. Chan, C. J. & Hiiragi, T. Integration of luminal pressure and signalling in tissue self-organization. *Dev.* **147**, 1–10 (2020).

209. Calera, M. R. *et al.* Connexin43 is required for production of the aqueous humor in the murine eye. *J. Cell Sci.* **119**, 4510–4519 (2006).

210. Gutzmann, J. H. & Sive, H. Epithelial relaxation mediated by the myosin phosphatase regulator Mypt1 is required for brain ventricle lumenexpansion and hindbrain morphogenesis. *Development* **137**, 795–804 (2010).

211. Li, J. *et al.* The Strength of Mechanical Forces Determines the Differentiation of Alveolar Epithelial Cells. *Dev. Cell* **44**, 297-312.e5 (2018).

212. Desmond, M. E., Levitan, M. L. & Haas, A. R. Internal luminal pressure during early chick embryonic brain growth: Descriptive and empirical observations. *Anat. Rec. - Part A Discov. Mol. Cell. Evol. Biol.* **285**, 737–747 (2005).

213. Garcia, K. E., Stewart, W. G., Gabriela Espinosa, M., Gleghorn, J. P. & Taber,

L. A. Molecular and mechanical signals determine morphogenesis of the cerebral hemispheres in the chicken embryo. *Dev.* **146**, (2019).

214. Eisenhoffer, G. T. *et al.* Crowding induces live cell extrusion to maintain homeostatic cell numbers in epithelia. *Nature* **484**, 546–549 (2012).

215. Gudipaty, S. A. *et al.* Mechanical stretch triggers rapid epithelial cell division through Piezo1. *Nature* **543**, 118–121 (2017).

216. Piotrowski-Daspit, A. S., Tien, J. & Nelson, C. M. Interstitial fluid pressure regulates collective invasion in engineered human breast tumors via Snail, vimentin, and E-cadherin. *Integr. Biol. (United Kingdom)* **8**, 319–331 (2016).

217. Durdu, S. *et al.* Luminal signalling links cell communication to tissue architecture during organogenesis. *Nature* **515**, 120–124 (2014).

218. Etoc, F. *et al.* A Balance between Secreted Inhibitors and Edge Sensing Controls Gastruloid Self-Organization. *Dev. Cell* **39**, 302–315 (2016).

219. Zhang, Z., Zwick, S., Loew, E., Grimley, J. S. & Ramanathan, S. Mouse embryo geometry drives formation of robust signaling gradients through receptor localization. *Nat. Commun.* **10**, (2019).

220. Cooper, M. S. *et al.* Visualizing morphogenesis in transgenic zebrafish embryos using BODIPY TR methyl ester dye as a vital counterstain for GFP. *Dev. Dyn.* **232**, 359–368 (2005).

221. Behrndt, M. *et al.* Forces driving epithelial spreading in zebrafish gastrulation. *Science (80-.).* **338**, 257–260 (2012).

222. Schindelin, J. *et al.* Fiji: An open-source platform for biological-image analysis. *Nat. Methods* **9**, 676–682 (2012).

223. Sommer, C., Straehle, C., Kothe, U. & Hamprecht, F. A. Ilastik: Interactive learning and segmentation toolkit. *Proc. - Int. Symp. Biomed. Imaging* 230–233 (2011) doi:10.1109/ISBI.2011.5872394.

224. Westerfield, M. *The Zebrafish Book. A Guide for the Laboratory Use of Zebrafish (Danio rerio)*. (Univeristy of Oregon Press, Eugene, 2007).

225. Kaufmann, A., Mickoleit, M., Weber, M. & Huisken, J. Multilayer mounting enables long-term imaging of zebrafish development in a light sheet microscope. *Dev.* **139**, 3242–3247 (2012).

226. Hörl, D. *et al.* BigStitcher: reconstructing high-resolution image datasets of cleared and expanded samples. *Nat. Methods* **16**, 870–874 (2019).

227. Thisse, C. & Thisse, B. High-resolution in situ hybridization to whole-mount zebrafish embryos. *Nat. Protoc.* **3**, 59–69 (2008).

228. Kominami, T. & Takata, H. Gastrulation in the sea urchin embryo: A model system for analyzing the morphogenesis of a monolayered epithelium. *Dev. Growth Differ.* **46**, 309–326 (2004).

229. Nance, J. & Priess, J. R. Cell polarity and gastrulation in C. elegans. *Development* **129**, 387–397 (2002).

230. Jensen, P. L. *et al.* Proteomic analysis of bovine blastocoel fluid and blastocyst cells. *Syst. Biol. Reprod. Med.* **60**, 127–135 (2014).

231. Schauer, A., Pinheiro, D., Hauschild, R. & Heisenberg, C. P. Zebrafish embryonic explants undergo genetically encoded self-assembly. *Elife* **9**, (2020).

232. Schulte-Merker, S. *et al.* Expression of zebrafish goosecoid and no tail gene products in wild-type and mutant no tail embryos. *Development* **120**, 843–852 (1994).

233. Sullivan, C. V. & Yilmaz, O. *Vitellogenesis and yolk proteins, fish*. *Encyclopedia of Reproduction* (Elsevier Ltd., 2018). doi:10.1016/B978-0-12-809633-8.20567-0.

234. Leithner, A. *et al.* Diversified actin protrusions promote environmental exploration but are dispensable for locomotion of leukocytes. *Nat. Cell Biol.* **18**, 1253–1259 (2016).